Development and application of sequence specific DNA detection through hybridization-induced aggregation

Briony Catherine Strachan
Uddingston, Scotland

Msci 1st Class, University of Huddersfield, England, 2009
BA Upper Second, Stirling University, Scotland, 2005

A Dissertation presented to the Graduate Faculty
of the University of Virginia in Candidacy for the Degree of
Doctor of Philosophy

Department of Chemistry

University of Virginia
August, 2013

Acknowledgements

Few things in life are truly accomplished alone, and this is not one of them. I am here not because of who I am but due to those that got me here. Dr Landers, I cannot express the profound influence your guidance, energy and vision have had on me. For making me the scientist I am I will forever be grateful and appreciative to have worked with you. Our group is a family; we will do anything for each other to bring success whether that be a 2 am coffee run or knowing how to stop frustration tears. To Carmen and Dan, thank you for molding my young analytical mind, enabling me to go it alone. To my amazing undergraduate Daniel, without whom this work would not have been accomplished. Of particular note is the bear family. Brother, Baby and Koala, you made this an experience that I never want to end. You were all there for me when life was hard and science was slow. My best moments were the ones spent with you. My roommate Amanda: you have been a wonderful person to me over this very stressful year, for that I am forever grateful. Then there is Jenny, who was a mentor, a friend, a sister. It's not an exaggeration to say that this would not have been possible without you. To Kristin, without whom I would not be here at all. Infinityillions, always pumpkin. Finally, to my family who were always there even though they are far across the pond. We were raised to believe that we can do anything if we put our minds to it and Russell you are the embodiment of that philosophy. To my Granddad, who's generosity made all of this possible and to Frank for always being there. Finally, to my Mum, my best friend, whom I love more each day. I promise, no more degrees.

Abstract

The interrogation of genomic DNA for the presence of specific sequences is paramount for most biological assays, including clinical diagnostics, functional genomics, food safety and forensic DNA analysis. Here we present a new detection modality, based on hybridization of the target sequence to probes bound to paramagnetic particles. When hybridization occurs, the particles aggregate together in a visual manner, confirming the presence target DNA with a limit of detection of 100 fM for ssDNA. A systematic study into the effect sequence length alterations have on detection sensitivity is demonstrated. The specificity of HIA enables the detection of 1, 2 or 3 single point mutations in the target DNA, working towards applying HIA to future mutation detection. HIA was adapted for the detection of dsDNA, enabling the label-free detection of Salmonella enterica, bacteriophage for the diagnosis of multi-drug resistant tuberculosis and for the detection of thyroid peroxidase (TPOX) for human identification. Furthermore, HIA is interfaced with PCR on a plastic integrated microdevice, where multiplexed IR-PCR is demonstrated for the first time. The microdevice combines low cost and minimal hardware to provide an easy to use system capable of PCR and HIA detection in 30 minutes. In addition, a direct-PCR protocol from whole blood was developed to aid in forensic investigations which was then adapted for use on the integrated device. Therefore, direct-PCR from whole blood and HIA detection can be performed in one hour. Overall, HIA is a new powerful modality in DNA detection technology appropriate for implementation at the point of care.

Table of Contents

1.0 Introduction

1.1 Overview

This chapter aims to introduce and discuss the fundamental concepts and advancements in the scientific fields which pertain to the rest of this dissertation. Particular focus will be given to these areas: sequence-specific DNA detection methods, particles for DNA hybridization detection, current methods for DNA detection in microfluidic devices and finally a review of diagnostic devices used at the point-of-care.

1.2 Techniques for Sequence-specific DNA Detection

Detection of nucleic acids (NA) is a fundamental component of biomedicine, forensic science, homeland security, food safety and clinical diagnosis. Interrogation of DNA sequences can identify individuals, pinpoint the cause of disease or classify the origin of an organism. The human genome has 3.2 billion base pairs[6], however, the DNA sequence of interest is commonly between 100 – 400 bp in size. Therefore, PCR is often used to increase the concentration of the target DNA sequence. The most common way to detect a DNA sequence is to create a hybridization event between the sequence and a probe, producing a signal. There are exceptions including, size-exclusion chromatography[7], gel electrophoresis[8] and dye intercalation with a PCR product[9]. Below outlines the fundamentals of two core methods employed for sequence specific detection of DNA: spectroscopy and optical.

1.2.1 Spectroscopic Methods

1.2.1.1 Fluorescence Spectroscopy

Fluorescence-based detection has many advantages, including sensitivity, diversity and allows for PCR's to be multiplexed for high throughput analysis. The basis of fluorescence is quite simple: a fluorophore (the chemical which can fluoresce) is excited by absorbing a photon to a higher energy state, as it relaxes back to ground state, the photon is emitted as light[10]. The process is clearly depicted in the Jablonski diagram, shown in **Figure 1**. The resulting spectra produced from this process is twofold, first there is an absorption

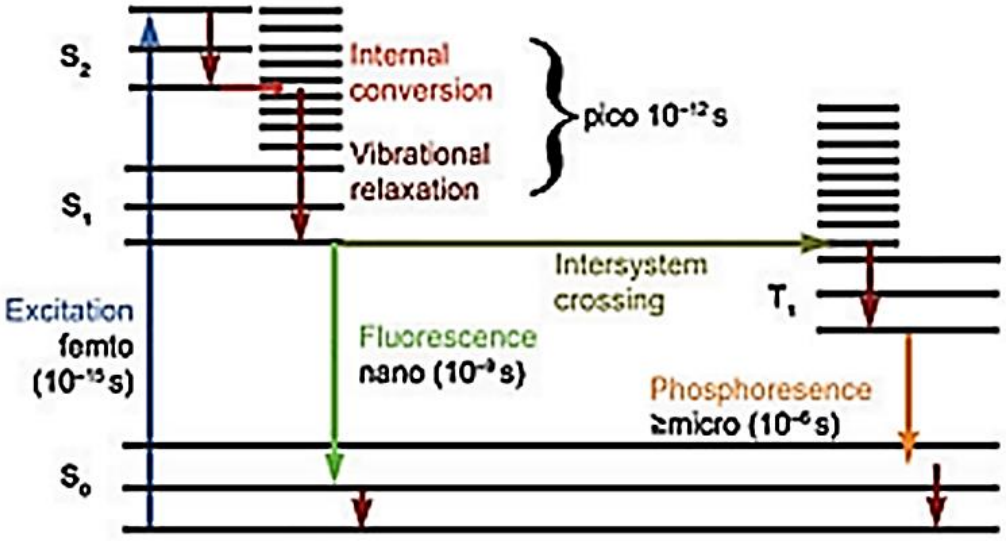

Figure 1: Scheme of the Jablonski diagram, illustrating the process of fluorescence.

spectra, then an emission spectra. The wavelength at which the light emits is governed by the properties of the fluor, at a wavelength higher than absorption. Emission spectra is the most frequently used for DNA detection, and can easily be multiplexed by choosing dyes

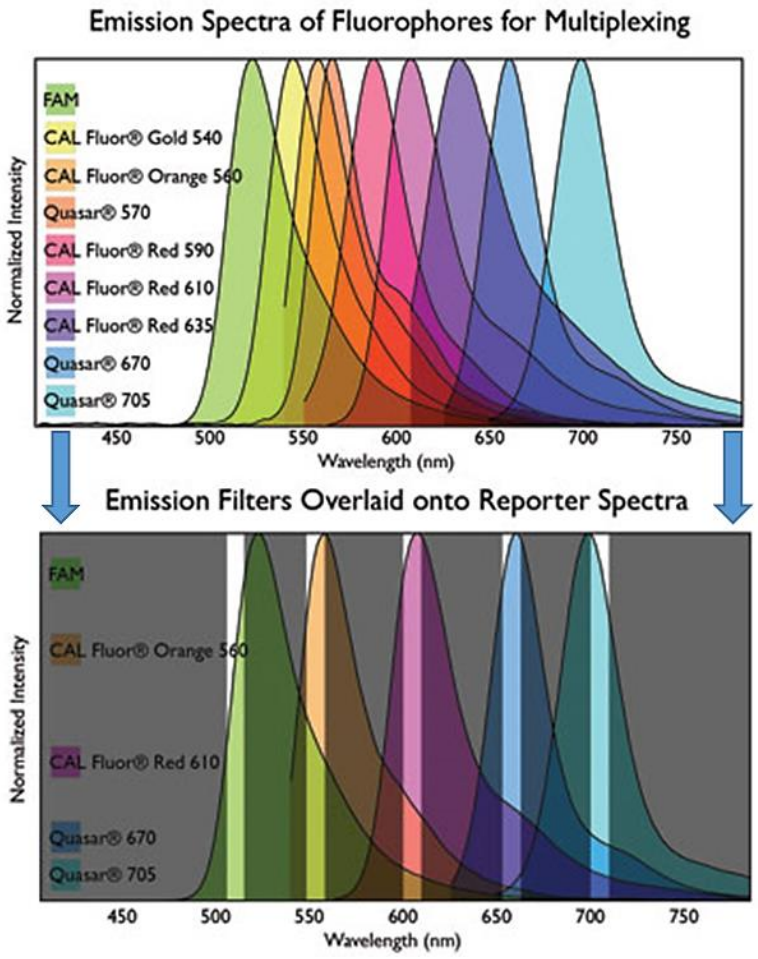

Figure 2: Depiction of how filters are used to isolate the signal from a specific dye at a given wavelength. Courtesy of Biosearch technologies.

which do not emit at the same wavelength (**Fig. 2**). Emission filters are used to selectively detect emission from a given wavelength, producing the most sensitive signal for the given fluor[11, 12]. Filters can be multiplexed to allow for several fluors to be used simultaneously (**Fig. 2**). Often these fluors, known as tags/labels/dyes are conjugated to the DNA of interest Therefore, by detecting the dye you indirectly detect the DNA of interest. Although this process is simple and highly sensitive capable of detecting attomaoles of DNA in bulk solution or a single DNA molecule, the hardware is expensive and sophisticated and not suitable for POC use.

1.2.1.2 Surface-enhanced Raman spectroscopy (SERS)

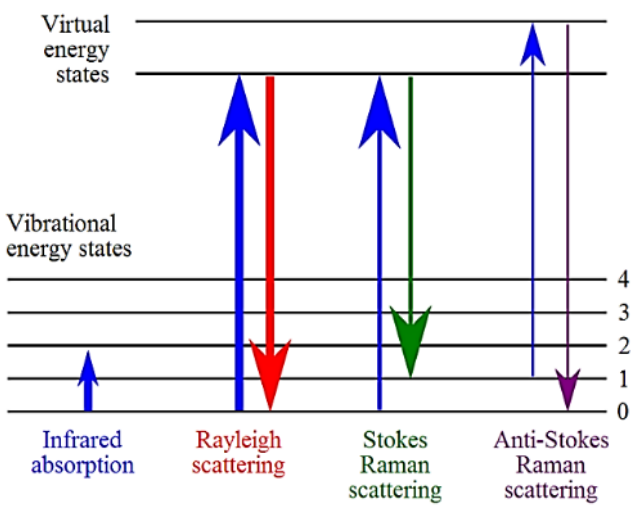

Figure 4: Vibrational and rotational changes associated with Raman spectroscopy. Courtesy of Moxfyre.

Raman spectroscopy is very similar to fluorescence, except Raman detects the lower level energy vibrational and rotational changes through the scattering of photons rather than absorption (**Fig. 3**). A Raman laser provides the incident photon, which bombards the surface with high selectivity, minimizing background interference (**Fig. 4**). The intensity of the Raman signal can be enhanced by up to 14 orders of magnitude through absorbing the analyte of interest onto a metallic surface, such as gold, silver or copper. In particular, when used for DNA detection, it's a powerful label-free method for detecting hybridization. It was observed that adenine has a strong spectral peak at 736 cm^{-1}, therefore, designing a probe

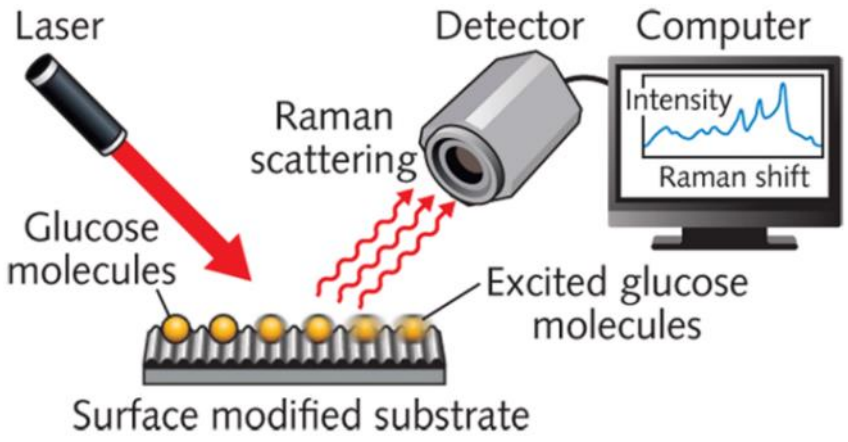

Figure 3: Scheme of workflow in surface enhanced Raman spectroscopy[1]

without adenine bases, but in the target DNA, would only produce a signal following hybridization [14].

1.2.2 Optical-based Detection

1.2.2.1 Colorimetric analysis with nanoparticles

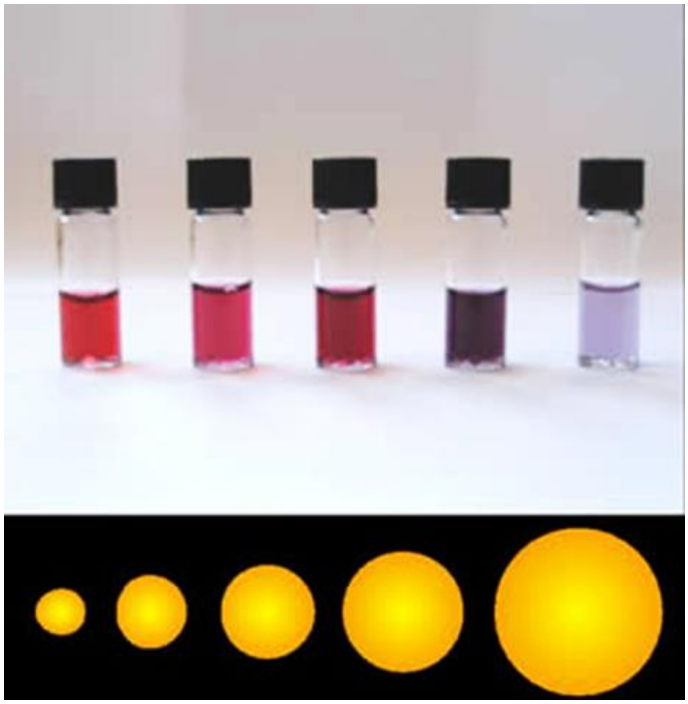

Figure 6: Photograph of vials containing different sized gold nanoparticles (10-100 nm) have different colors when exposed to light. Image courtesy of Aleksandar Kondinski.

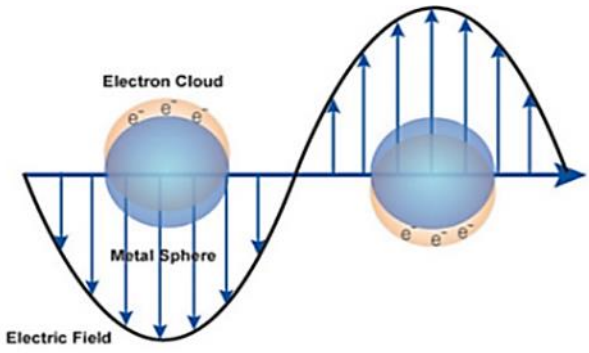

Figure 5: Scheme of surface plasmon resonance. Adapted from Sigma-Aldrich.com®

Colorimetric analysis involves a reaction causing a color change, the intensity of which correlates to the concentration of the target analyte. In DNA analysis this has been applied to the detection of hybridization with gold and silver nanoparticles. Light causes the electrons at the particle surface to collectively oscillate, a process known as surface plasmon resonance (SPR) (**Fig. 6**). The strength of the oscillation is dependent on electron cloud density causing the nanoparticles to absorb light at different wavelengths. Therefore the color the nanoparticles appear correlate with

the size of the nanoparticle. Due to these properties DNA can be detected by a color change signaling that nanoparticles have conjugated, therefore are bigger and absorbs at a longer wavelength giving a blue or purple color. This method is incredibly simple requiring no detection equipment, therefore is ideal for use in POC settings.

1.2.2.2 Transition electron microscopy (TEM)

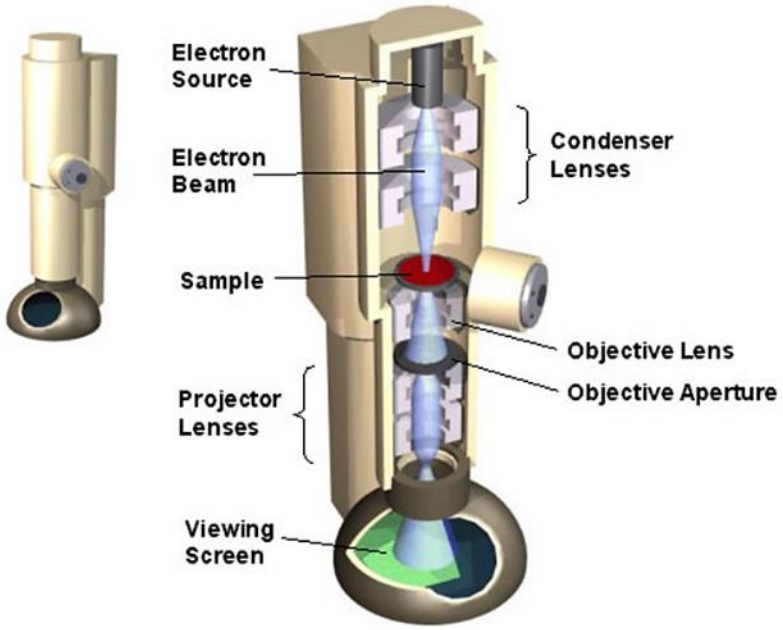

Figure 7: Scheme of the operation of a transition electron microscope. Courtesy of Barrett group, McGill University, CA.

Transition electron microscopy (TEM) uses a high density beam of electrons to pass through a sample that's normally less than 100 nm. The electrons pass through the sample to the detector below to produce an image based on electron negative space i.e. where the electrons were prevented from passing through by the sample. This powerful microscopic technique is capable of discriminating morphology within 1 μm [15]. For DNA detection TEM is coupled either with fluorescene or the conguaation of nanoparticles to indirectly identify the target seequence [16].

1.3 Particles for DNA detection

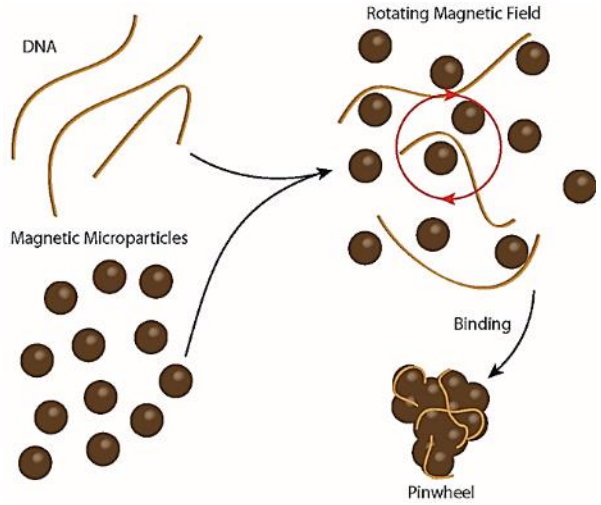

Figure 8: Scheme of pinwheel: paramagnetic particles intertwine with stands of DNA to for visual aggregates[2].

Paramagnetic particles have been synonymous with DNA workflow for over two decades especially in the purification of DNA. With silica-coated particles the DNA will bind to the surface of the particle when the DNA is being dehydrated by a chaotropic salt [2]. Several groups, including our own report that particles will aggregate independent of sequence when these DNA binding events occurred (**Fig. 8**) [2]. With the addition of a rotating magnetic field our group can use the extent of aggregation to quantify DNA (80-4 pg/µL) and enumerate cells [17-19]. More commonly particles are used to detect specific DNA sequences of 20-400 bp's by via hybridization using the particle as a substrate for the complementary probe. The use of nanoparticles as a vehicle for the probe has proliferated since Mirkin, *et al.* developed DNA hybridization with gold nanoparticles (AuNP) in 1996 . The next two decades of particle based detection has mostly focused on refining and improving Mirkin's work. The nanoparticle is functionalized for DNA detection with a thiol , amino r biotin group conjugated to a DNA probe that is complementary to the ssDNA target sequence. Visual detection of this process can be achieved in 5 minutes for femtomolar detection[28] with the lowest reported limit of detection of 50 attomoles reported in a 60 minute assay[29]. It is worth noting that visual-based detection of DNA with nanoparticles is not quantitative, have a small capacity for

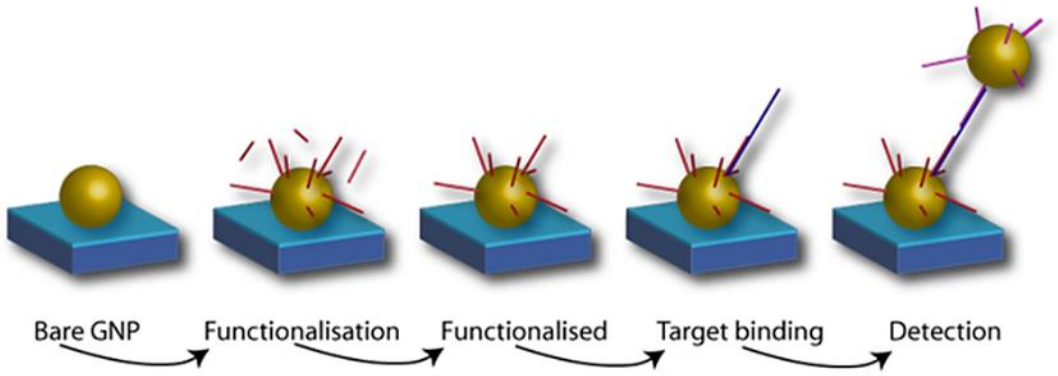

Figure 9: Scheme of preparing gold nanoparticles for the detection of sequence specific DNA. Courtesy of nanobiophysics group, University of Twente, NL.

mass of hybridized DNA[30] and cannot detect a single nucleotide polymorphism in the DNA sequence [20]. Furthermore, longer DNA targets do not produce significant color change as the gold nanoparticles are not being linked close enough increase in their size. Therefore, there is a limit to the length of DNA nanoparticles can detect in a colorimetric/visual manner[31]. However, when coupled with a more sophisticated detection techniques, e.g. fluorescence or TEM, SNPs can be detected at with AuNPs nanomolar concentration [32] and applied to prostate cancer marker detection with femtomolar specificity [33]. Assays can be multiplexed to detect several DNA targets simultaneously, demonstrated by silver nanoparticles which can detect three viruses concurrently when coupled with TEM [28, 34, 35]. The ultrasensitivity afforded by nanoparticle detection is steering the field towards non amplification based detection, i.e. the DNA does not require extraction nor amplification prior to detection This has been demonstrated for the detection of circulating tumor cells [37] and colorectal cancer markers[38] from whole blood when coupled with SERS.

1.4 DNA detection on a microfluidic device

Each method described previously in this chapter for the detection of DNA has been modified to operate on the microfluidic platform. DNA detection methods such as TEM[39] and SERS [40] have been interfaced with a microfluidic device, however, these are impractical and unfeasible techniques to be adapted to the microfluidic format. Methods such as fluorescence and the use of particles for the detection of DNA are more widely used and are the basis for the most microfluidic based detection modalities.

1.4.1 Microchip electrophoresis

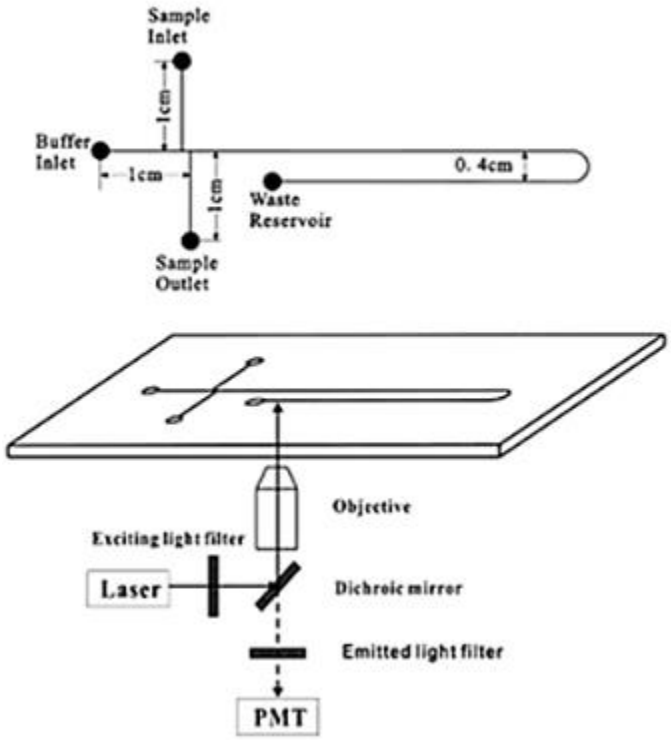

Figure 10: Scheme of a microdevice design for electrophoresis[4]

Microchip electrophoresis uses high voltage to migrate DNA through a long narrow channel to the detector [41, 42]. DNA, regardless of size has the same charge, therefore, simple electroosmotic flow is not suitable for separating DNA, therefore, the channel is filled with a size sieving polymer As the DNA travels through the channel towards the detector, DNA fragments are separated based on size, with the smaller fragments reaching the

detector first [43]. The DNA will have been previously conjugated to a fluorescent dye which absorbs and emits a photon from the laser to give detection[44]. The basic microdevice design has not evolved since the conception of total microfluidic systems in 1990 [45]. Improvements in the technique are due to polymer chemistry[46, 47], microdeive material dyes[49, 50], sample injection qualitynd sample preparation The combined result is that electrophoresis techniques are now capable of detecting a single DNA molecule [54].

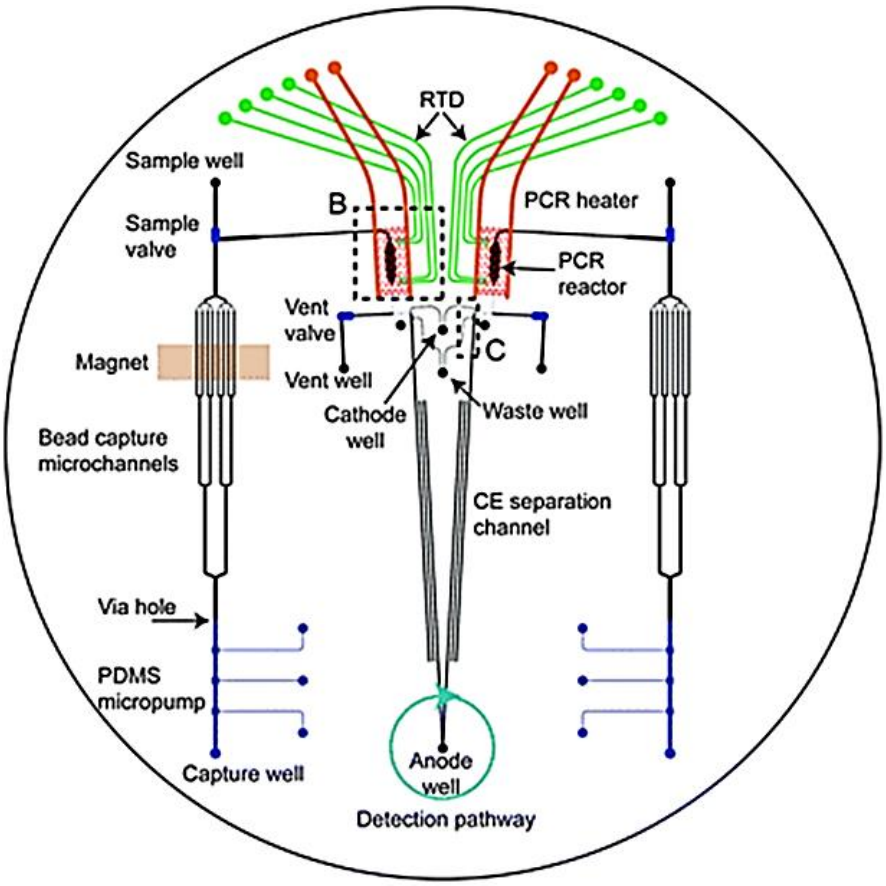

Figure 11: Schematic of fully integrated microdevice for forensic STR analysis. (A) Microchip mask design for performing DNA template purification, PCR, post-PCR cleanup, inline injection and CE separation [3].

Electrophoresis is the leading force in DNA separations for human identification. Individuals can be identified through short tandem repeat (STR) analysis of DNA, which are inherited DNA sequences. The challenge to spearate these DNA fragments is due to the multiplexed nature of the amplification process, which can produce up to 18 DNA fragments, called loci ranging from 100-400 bps[55, 56]. As each loci is generated from a unique set of fluorescently labelled primers, five dyes are used simultaneously to resolve fragemnts of the same size. Separating STRs on a microdevice with one base-pair resolution and minimal broadening is particuarily challenging as the separation channel is between 5-9 cm compared to a capiliary of 47 cm[58]. Despite such challenenges, efforts have been made to separate STRs on micofluidic devices. Initially only four loci were detected in 2004 [59], followed by a full 16-plex loci from a commercial kit in 2008 [3, 60]. Work towards a fully integrated device for sample preparation, PCR and separation began in 2008, which has become a fully integrated for the detection of 9 loci in 2011 **Fig. 11**). The complexity of the separation has caused the development of microchip STR analysis away from acedemia into the commercial sector. Three main compeditors are viing for the rapid human identification market: *IntegenX*®, *Lockheed Martin* and *Network Biosystems*. All these systems use microfluidic devices with multicolor DNA separation.

1.4.2 Microarrays

Microarrays are powerful DNA detection systems combining the benefits of nanoparticle hybridization technology with fluorescence-based detection. Typically probe adducted molecules, e.g. AuNPs are adhered to the microarray surface, which can be glass, silicon or plastic [62]. For DNA detection the probe will be a short oligonucleotide sequence, complementary to the target DNA. The probe will be tagged to this oligonucleotide to enable fluorescence-based detection once hybridization to the target DNA has occurred (**Fig. 12**).

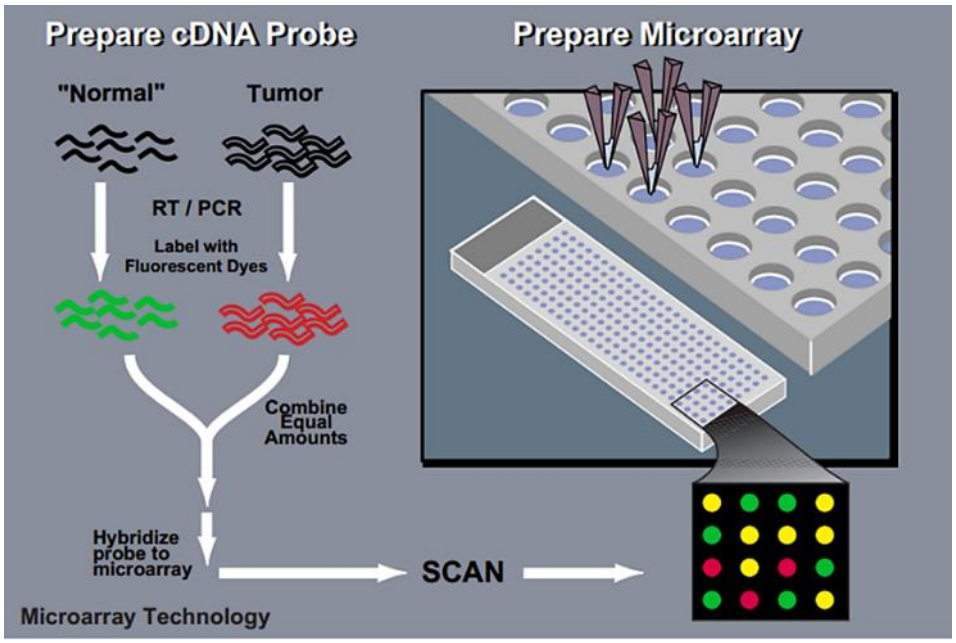

Figure 12: Scheme of a typical microarray format. Image courtesy of Darryl Leja.

The main benefit of microarrays is the vast amount of information that can be obtained in a few hours, often pertaining to gene expression. Expression of a whole genome was first described for yeast in 1997 [63]. Currently *ArrayExpress* is systematically mapping the entire human genome, with over one millon assays in their database [64]. This information has led to specific microarrays for a particular disease including leukemia [65, 66], breast

cancer nd schizophernia [68-70]. With these arrays, disease progress can be predicted, e.g. cancer growth was projected by mointoring the alterations in hybridization events between healthy and diseased DNA samples. In the same manner microarrays can be utilized for the detection of a single nucleotide polymorphisms hich can identify mutations specific to a diagnosis [61]. Microfluidic control of the DNA sample has increased the sensitivity of microarrays while decreasing incubation times from days to hours[74]. These micoarray DNA bases assays can now be completed with only 1 pL of DNA sample[61]. Furthermore, small sample volumes decrease diffusion time for the DNA in the sample to migrate to the probe, increasing efficiency of DNA capture by 10-fold [75].

1.5 Diagnostic devices used at the point-of-care

Pregnancy tests, blood sugar analyzers and HIV testing are among the increasing number of point-of-care tests that are readily used by physicians and patients alike. Widespread implementation of microfluidic technology is hampered by the need for a fully integrated system, requiring interfacing extraction, amplification and detection of the DNA (**Fig. 13**). Such methods are beneficial due to the need for less sample and at least 5-fold reduction in analytical time[76], however, the expense of miniaturizing PCR and fluorescence-based detection has stunted commercialization of microfluidic POC devices.

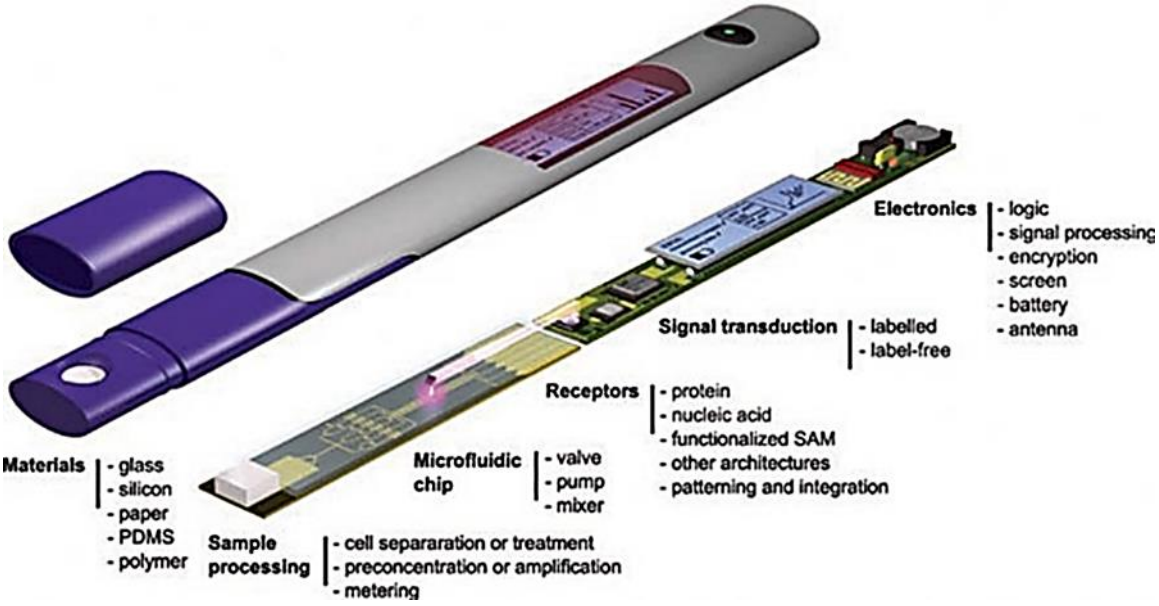

Figure 13: Global overview of the components required for an operation point of care device. Image provided by Advanced Materials, © 2010 IBM Corporation)

1.5.1 Immunoassays

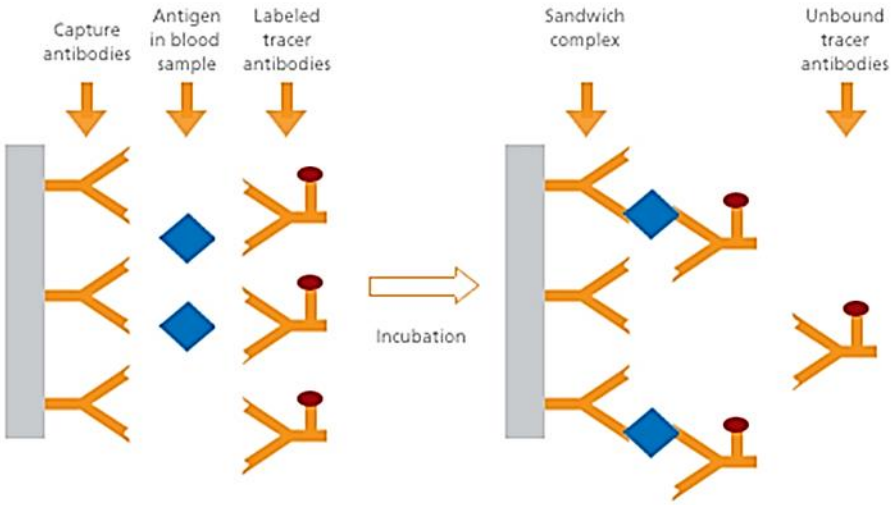

Figure 14: Scheme of an immunoassay. Courtesy of RadioMeter.

Immunoassays are a common format for POC devices due to their chemical simplicity, accuracy and compatibilty with miniturization. The at-home pregnancy test is the most widely used POC immunoassay test and has been commercially available since the 1950's, and although improved in reliability the basic chemistry has not been altered[77]. Immunoassays are based on the interaction between antibodies and their antigens, which are uniquely specific to each other [78]. As shown in **Figure 14**, once antibody/antigen binding has occurred, a labelled set of antibodies are added to provide a signal [79].

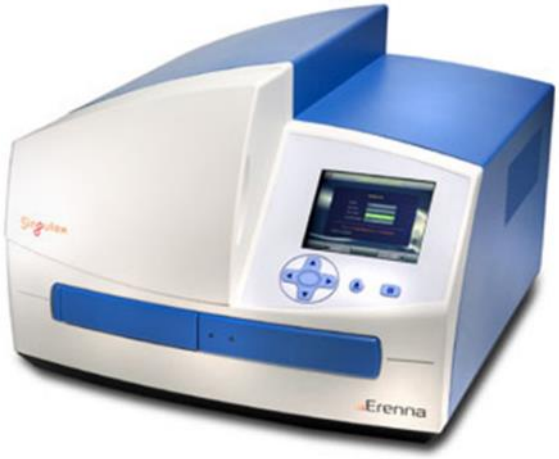

Figure 15: Photograph of the Erenna® Immunoassay system.

The leader in the commercial field of POC immunoassay testing is *Sigulex*®, the manufacturer of the *Erenna*® *Immunoassay System*, capable of

detecting analytes pertinent to inflammation and cytokines, oncology, cardiovascular disease, metabolism and toxicity (**Fig. 15**). The instrument was developed to detect protein biomarkers, with LODs of 10–100 pg/L using 100 μL of sample reported [80]. The system requires a 60 minute incubation phase followed by the removal of a sample aliquot for single molecule counting.

1.5.2 Microfluidic-based point of care devices

Figure 16: Photograph of the GeneXpert™ Infinity 80 Instrument for molecular diagnostics.

Several FDA-approved microfluidic-based POC tests are currently available and being utilized, including the *Piccolo Xpress*® for blood chemistries, and the *PanNAT*® for molecular diagnostics of infectious diseases [81]. Currently, a commercialized microfluidic-based platform, *GeneXpert™*, is available for determining TB resistance [82], and uses a cartridge that accepts sample and interfaces it with the instrument (**Fig. 16**). The *GeneXpert™ Infinity 80* model is capable of 2000 assays per day, with diagnostic cartridge-based assays for the detection of MRSA, *streptococcus* and anthrax. Another cartridge based instrumentation is available including the *Afinion™ Analyzer* which specializes in only a few diagnostic tests, including HbA1c, used to determine blood glucose levels over the previous three month period [1]. A further attempt is being made by *Daktari Diagnostics* to tackle the diagnosis of HIV/AIDS through

Figure 17: Photographs of the Daktari Diagnostics prototype instrument and cartridge

the measurement of CD4+ cells in the patients blood. Their microdevice, shown in **Figure 17**, highlights the complexity of even a simple immunoassay without any hands on interaction, complete with on device reagents for sample processing.

1.6 Concluding remarks

DNA detection is of paramount importance as science strives to improve human identification, understand the mechanism of disease and account for biological differences in the human race. The investigator can chose their method of DNA detection to suit their needs, budget and time-frame. Microfluidic technology is at an exciting crossroad, where finally cost and time effective protocols are used to manufacture desirable point of care products.

Chapter two will introduce a new particle-based detection modality for sequence-specific DNA, modified from the gold nanoparticle hybridization assays mentioned earlier. Data presented pertains to the optimization of the assay, while determining the parameters for target DNA structure to obtain a visual signal through hybridization-induced aggregation

(HIA). **Chapter three** will develop on these concepts further, demonstrating how unlike gold nanoparticles, HIA is not restricted by the length of DNA to maintain a visual qualitative response. Through the introduction of heat HIA is applied to the detection of multi-drug resistant tuberculosis. **Chapter four** discusses the design and fabrication of multiplexed microfluidic device for the integration of IR-PCR and HIA detection of *Salmonella*. This device includes novel fluid control including a geometric valve to prevent flow and torque actuated pressure to initiate fluid flow. **Chapter five** discusses the development of direct amplification of whole blood for the detection of TPOX to determine if the blood came from human. The microdevice described in chapter four is utalized for the integration of whole blood PCR followed by visual HIA detection. Finally **chapter six** addresses potential avenues for this DNA detection technology to persue in the future and the challenges that may be encountered.

1.7 References

1. *SERS advance enables glucose detection, with implication for diabetics*, in *BioOptics World*2011.
2. Leslie, D.C., et al., *Journal of the American Chemical Society,* 2012. **134**(12): p. 5689-5696.
3. Liu, P., et al., *Lab on a Chip,* 2011. **11**(6): p. 1041-1048.
4. Wang, Z., et al., *Journal of Separation Science,* 2011. **34**(2): p. 196-201.
5. Venter, J.C., et al., *Science,* 2001. **291**(5507): p. 1304-1351.
6. Mori, S. and H.G. Barth, *Size exclusion chromatography*1999: Springer.
7. Southern, E.M., *Journal of Molecular Biology,* 1975. **98**(3): p. 503-517.
8. Rye, H.S., et al., *Nucleic acids research,* 1992. **20**(11): p. 2803-2812.
9. Lakowicz, J.R., *Principles of fluorescence spectroscopy*2009: Springer.
10. Chalfie, M., et al., *Science,* 1994. **263**(5148): p. 802-805.
11. Livak, K.J., et al., *Genome Research,* 1995. **4**(6): p. 357-362.
12. Wittwer, C.T., et al., *Biotechniques,* 1997. **22**(1): p. 130-139.
13. Barhoumi, A. and N.J. Halas, *Journal of the American Chemical Society,* 2010. **132**(37): p. 12792-12793.
14. Wang, J., et al., *Analytical Chemistry,* 2001. **73**(22): p. 5576-5581.
15. Chan, W.C. and S. Nie, *Science,* 1998. **281**(5385): p. 2016-2018.
16. Melzak, K.A., et al., *Journal of Colloid and Interface Science,* 1996. **181**(2): p. 635-644.
17. Nam, J.-M., S.I. Stoeva, and C.A. Mirkin, *Journal of the American Chemical Society,* 2004. **126**(19): p. 5932-5933.

18. Stoeva, S.I., et al., *Angewandte Chemie,* 2006. **118**(20): p. 3381-3384.

19. Mirkin, C.A., et al., *Nature,* 1996.

20. Storhoff, J.J., et al., *Langmuir,* 2002. **18**(17): p. 6666-6670.

21. Sandström, P., M. Boncheva, and B. Åkerman, *Langmuir,* 2003. **19**(18): p. 7537-7543.

22. Zanoli, L.M., R. D'Agata, and G. Spoto, *Analytical and bioanalytical chemistry,* 2012. **402**(5): p. 1759-1771.

23. Xu, X., et al., *Small,* 2010. **6**(5): p. 623-626.

24. Niidome, T., et al., *Chemical Communications,* 2004(17): p. 1978-1979.

25. Kerman, K., et al., *Analytica Chimica Acta,* 2004. **510**(2): p. 169-174.

26. Wang, Z., et al., *Journal of the American Chemical Society,* 2006. **128**(7): p. 2214-2215.

27. Li, H. and L. Rothberg, *Proc Natl Acad Sci U S A,* 2004. **101**(39): p. 14036-9.

28. Zhou, X., et al., *J Am Chem Soc,* 2010. **132**(20): p. 6932-4.

29. Hurst, S.J., A.K.R. Lytton-Jean, and C.A. Mirkin, *Analytical Chemistry,* 2006. **78**(24): p. 8313-8318.

30. Li, S., et al., *Theranostics,* 2012. **2**(10): p. 967.

31. Wang, X., et al., *Biosensors and Bioelectronics,* 2012.

32. Alhasan, A.H., et al., *Analytical Chemistry,* 2012. **84**(9): p. 4153-4160.

33. Li, H., et al., *Analytical Chemistry,* 2010. **82**(13): p. 5477-5483.

34. D'Agata, R., et al., *Biosensors and Bioelectronics,* 2010. **25**(9): p. 2095-2100.

35. Rosi, N.L. and C.A. Mirkin, *Chemical reviews,* 2005. **105**(4): p. 1547-1562.

36. Wang, X., et al., *Cancer research,* 2011. **71**(5): p. 1526-1532.

37. Lin, D., et al., *Optics express*, 2011. **19**(14): p. 13565-13577.

38. Chen, L. and J. Choo, *Electrophoresis*, 2008. **29**(9): p. 1815-1828.

39. Strelau, K.K., et al., *Analytical and bioanalytical chemistry*, 2010. **396**(4): p. 1381-1384.

40. Jacobson, S.C., et al., *Analytical Chemistry*, 1994. **66**(7): p. 1107-1113.

41. Barron, A.E., H.W. Blanch, and D.S. Soane, *Electrophoresis*, 1994. **15**(1): p. 597-615.

42. Barron, A.E., D.S. Soane, and H.W. Blanch, *Journal of Chromatography A*, 1993. **652**(1): p. 3-16.

43. Landers, J.P., *Handbook of capillary and microchip electrophoresis and associated microtechniques*2007: CRC press.

44. Manz, A., N. Graber, and H. Widmer, *Sensors and actuators B: Chemical*, 1990. **1**(1): p. 244-248.

45. Kang, Q.S., et al., *Electrophoresis*, 2010. **31**(18): p. 3028-3034.

46. Shadpour, H., et al., *Analytical Chemistry*, 2007. **79**(3): p. 870-878.

47. Székely, L. and A. Guttman, *Electrophoresis*, 2005. **26**(24): p. 4590-4604.

48. Dossi, N., et al., *Electrophoresis*, 2007. **28**(22): p. 4240-4246.

49. Quirino, J.P. and P.R. Haddad, *Analytical Chemistry*, 2008. **80**(17): p. 6824-6829.

50. Yasui, T., et al., *Biomicrofluidics*, 2011. **5**(4): p. 044114.

51. Breadmore, M.C., *Electrophoresis*, 2007. **28**(1-2): p. 254-281.

52. Breadmore, M.C., M. Dawod, and J.P. Quirino, *Electrophoresis*, 2011. **32**(1): p. 127-148.

53. Effenhauser, C.S., et al., *Analytical Chemistry*, 1997. **69**(17): p. 3451-3457.

54. Oostdik, K., et al., *Forensic Science International: Genetics,* 2012.

55. Tachibana, Y., et al., *Journal of Chromatography A,* 2004. **1025**(2): p. 287-296.

56. Das, C. and Z.H. Fan, *Electrophoresis,* 2006. **27**(18): p. 3619-3626.

57. Butler, J.M., et al., *Electrophoresis,* 2004. **25**(10-11): p. 1397-1412.

58. Chen, L. and J. Ren, *Combinatorial Chemistry & High Throughput Screening,* 2004. **7**(1): p. 29-43.

59. Karlinsey, J.M. and J.P. Landers, *Lab on a Chip,* 2008. **8**(8): p. 1285-1291.

60. Liu, P. and R.A. Mathies, *Trends in Biotechnology,* 2009. **27**(10): p. 572-581.

61. Wang, L. and P.C. Li, *Analytica Chimica Acta,* 2011. **687**(1): p. 12-27.

62. Lashkari, D.A., et al., *Proc Natl Acad Sci U S A,* 1997. **94**(24): p. 13057-62.

63. Parkinson, H., et al., *Nucleic acids research,* 2009. **37**(suppl 1): p. D868-D872.

64. Haferlach, T., et al., *Journal of clinical oncology,* 2010. **28**(15): p. 2529-2537.

65. Sotiriou, C. and L. Pusztai, *New England Journal of Medicine,* 2009. **360**(8): p. 790-800.

66. Taube, J.H., et al., *Proceedings of the National Academy of Sciences,* 2010. **107**(35): p. 15449-15454.

67. Pérez-Santiago, J., et al., *Journal of psychiatric research,* 2012.

68. DeRisi, J., et al., *Nature genetics,* 1996. **14**(4): p. 457-460.

69. Campbell, M.J., et al., *Cancer research,* 2006. **66**(17): p. 8707-8714.

70. Bonnet, S., et al., *Cancer cell,* 2007. **11**(1): p. 37-51.

71. Homer, N., et al., *PLoS genetics,* 2008. **4**(8): p. e1000167.

72. Gunderson, K.L., et al., *Nature genetics,* 2005. **37**(5): p. 549-554.

73. Altshuler, D., M.J. Daly, and E.S. Lander, *Science,* 2008. **322**(5903): p. 881-888.

74. Liu, R.H., et al., *Expert Review of Molecular Diagnostics,* 2006. **6**(2): p. 253-261.

75. Easley, C.J., et al., *Proceedings of the National Academy of Sciences,* 2006. **103**(51): p. 19272-19277.

76. Barnhart, K.T., et al., *Obstetrics & Gynecology,* 2004. **104**(1): p. 50-55.

77. Hales, C. and P.J. Randle, *Biochemical Journal,* 1963. **88**(1): p. 137.

78. Hemmilä, I., et al., *Analytical biochemistry,* 1984. **137**(2): p. 335-343.

79. Todd, J., et al., *Clinical chemistry,* 2007. **53**(11): p. 1990-1995.

80. Chin, C.D., V. Linder, and S.K. Sia, *Lab on a Chip,* 2012. **12**(12): p. 2118-2134.

81. Hillemann, D., et al., *Journal of Clinical Microbiology,* 2011. **49**(4): p. 1202-1205.

82. Monnier, L., H. Lapinski, and C. Colette, *Diabetes care,* 2003. **26**(3): p. 881-885.

2 Development of hybridization-induced aggregation (HIA)

2.1 Introduction

The interrogation of genomic DNA for the presence of specific sequences is paramount for most biological assays, including clinical diagnostics, functional genomics, food safety and forensic DNA analysis. The specificity needed for most molecular biological assays relies on hybridization, with sensitivities that have continued to increase since the development of the Southern blot in the mid-1970's [2-4]. Sensitivity, the mass of target required for a signal, is often driven by improvements in detection technology, which is often expensive and complex, with the read-out typically involving fluorescence. Hybridization-based detection generally involves the binding of DNA to a molecular probe attached to either stationary or dynamic a surface. The use of paramagnetic particles (PMPs) as a vehicle for the probe has proliferated since Mirkin, *et al.* developed colorimetric detection of DNA hybridization with gold nanoparticles in 1996 . The properties of nanoparticles have been further exploited with more sophisticated DNA detection modalities. Included in these are Raman spectroscopy[9, 10], electrical stimulation, electrophoresis[12, 13] and optical detection. The latter of these range from colorimetric assays and TEM images[15] which are in general inexpensive, however, there are also more complex microfabrication-dependent systems like cantilever deflection[16].

Optimal DNA hybridization is essential for sensitive detection with many DNA detection modalities, regardless of the platform. This includes the use of the appropriate buffer components, temperature, mechanism of probe mobilization[17], DNA/probe concentration, kinetics[18], assay duration and nucleotide sequence in the target region of the DNA. In addition, successful hybridization is highly dependent on the

complementarity of the target sequence compared to the bead-bound oligonucleotides; the standard is to make the target fully-complementary to the probes, with each base hybridized, maximizing signal, and thus, sensitivity [19]. However, deviations from this convention of target design have been demonstrated with success. Scanometric technology, for example, was capable of 10 pM detection with the hybridization of a 48-base target sequence, where the target had 10 non-complementary bases flanking each end of the probed sequence [20]. In addition, the length of the target is also a significant consideration, as secondary structural effects increase with length, and this can decrease sensitivity [21]. Ultimately, optimization of the sequence design allows for the production of the most selective and sensitive assay. Identification of single point mutations (SPMs) is one of the major driving forces in the development of hybridization assay technology. This is driven by highly selective assays, using fluorescence-based detection, which have been demonstrated successful at detecting a base change in the presence of 50 nM [22] and even 10 nM of target DNA [23]. A number of label-free methods for SPM detection have also been reported, including resonator arrays [24], silicon nanowires [12, 25-28] and colorimetric detection with gold nanoparticles , and these have been associated with limits of detection (LOD's) of 1.95 nM, 1 nM and 50 fM, respectively. However, these assays involve relatively lengthy assay times, cumbersome instrumentation, and/or specialized fabrication techniques.

In the development of any new genetic assay, the aim is to provide a rapid analysis time with good sensitivity at a low cost. The IDEAL assay has the best balance of cost, speed and sensitivity (**Fig.1**). However, playoff between these three parameters almost always

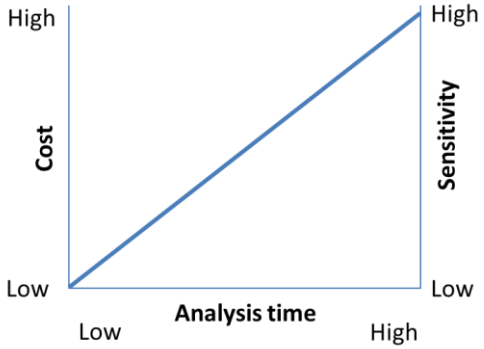

Figure 18: Simple graphical depiction of the relationship between cost, analysis time and sensitivity are inter-related for analytical devices.

translates to compromise in one parameter at the cost of improving another. This applies to detecting SPM in a rapid, cost-effective manner for application to genome-based assays pertinent to diagnostic and pharmacokinetic tests that could be carried out in a point-of-care setting (i.e., using a microdevice). Hybridization assays have been adapted to microdevices in a number of embodiments since their genesis in the early-1990's; attractive features driving this were portability, reduced cost and rapid results. Microarray devices exploiting fluorescence detection can provide so much genetic information (typically fabricated with 2-4 million probes sites[34]) that the bottleneck becomes the bioinformatic component. This technology has been shown applicable in a number of arenas (e.g., monitoring the effect of environment on cancer growth[35]), however, due to complex data processing, high expense and fluorescence microscopy, it is not applicable to rapid point-of-care SPM detection. Simplified label-free detection using PMPs as the probe substrate, provides rapid SPM detection, and is ideal for the end-point analysis within micro-total analysis systems (μTAS).

In this chapter we describe the development of hybridization-induced aggregation (HIA), a PMP based assay for the detection of sequence-specific DNA. The developed method is performed in a homogenous, chaotic system, where particles, probes, and target DNA are in constant motion, due to a rotating magnetic field and chip agitation. Understanding the nuance factors that affect hybridization in this environment is paramount to honing HIA as

part of a microfluidic detection system. A systematic approach to understanding the fundamentals of oligonucleotide-adducted magnetic particle aggregation, and the subtleties of the target and probe sequences for optimal detection is described. This includes evaluating the effect of non-complementary bases flanking the target sequence, the optimal length of the target sequence, and the ability of HIA to detect single point mutation(s) in a DNA target sequence of a particular length. Finally, with a view to the future, HIA is shown to be effective in the presence of several potential chemical interferants that may be encountered in an integrated assay on a single microfluidic device.

2.2 Materials and methods

2.2.1 Reagents

Dynabeads MyOne Streptavidin C1 paramagnetic beads were purchased from Invitrogen (Carlsbad, CA). Biotinylated and unfunctionalized oligonucleotides were purchased from Eurofins MWG Operon (Huntsville, AL). Protenaise K, RNase was purchased from Qiagen (Valencia,CA). PrepGEM™ and saliva buffer were purchased from ZyGEM™ (Hamilton, NZ). Hi-Di formamide was purchased from Life Technologies (Grand Island, NY). Hydrochloric acid, sodium chloride, potassium chloride and ethanol, were purchased from Fisher (Fair Lawn, NJ). 2-Amino-2-(hydroxymethyl)- 1,3-propanediol (Trizma base, 99.9%) was purchased from Sigma (St. Louis, MO). All solutions were prepared in Nanopure water (Barnstead/Thermolyne, Dubuque, IA).

2.2.2 Assay Instrumentation

Images of the microwells were collected by using a T1i DSLR camera with MP-E 65 mm f/2.8 1−5× macro lens purchased from Canon U.S.A., Inc. (Lake Success, NY). A Thermix Stirrer model 120S magnetic stir plate was purchased from Fisher Scientific (Fair Lawn, NJ). Three, 5-mm x 5-mm cylinder neodymium magnets were purchased from Emovendo (Petersburg, WV). A MS3 basic vortexer was purchased from IKA (Wilmington, NC). A Ledu compact desk magnifier lamp was purchased from Guy Brown Products (Brentwood, TN) and used without optics to provide lighting around the entire sample. Magnetic and vortexer rotation speeds were determined using a digital photo laser non-contact tachometer, purchased amazon.com (Seattle, WA).

2.2.3 Microwell Fabrication

A VersaLASER system 3.50 from Universal Laser Systems (Scottsdale, AZ) was used to fabricate microwells, cutting through 1.0 mm-thick PMMA purchased from Astra Products (Baldwin, NY). Each microwell device was prepared as a 4 × 4 matrix of 5-mm-diameter circular wells on a 4-cm square device, designed in AutoCAD. These were then thermally bonded using established methods[36] to a second 4-cm square 1.5-mm-thick PMMA, purchased from McMaster-Carr (Santa Fe Springs, CA). Microwells we sterilized in 2M hydrocholoric acid for 30 min, then rinsed with Nanopure water prior to use.

2.2.4 Biotinylating Oligonucleotide Probes to Particles

Particles were prepared according to the manufacturer's protocol. Final suspension buffer: 500 µL of 200 mM potassium chloride, 10 mM Trizma base, pH 7.5.

2.2.5 Assay Procedure

All assays were performed at room temperature (25°C). Performed in a 5 mm PMMA microwell, with a 20 µL final volume: 17 µL of HIA buffer (10 mM Tris, 200 mM KCl, pH 7.5), 1 µL of each 3'- and 5'- biotinylated particles, 1 µL of non-specific sequence and 1 µL of target DNA sequence. The sample is then exposed to an RMF of 2000 rpm and a vortexing speed of 130 rpm for 12 minutes. A single picture is then taken of the microwell for analysis. Analysis is performed using Mathematica software and a previously described algorithm[37, 38].

2.2.6 Interfernt preparation

The buccal swab lysates were prepared using manufacturers protocol from ZyGEM™. RNase was added following Qiagen protocol. The lysed blood (6.3 $x10^3$ WBC) was prepared by heating the sample for 30 minutes at 56 °C in a water bath.

2.3 Results and Discussion

2.3.1 Probe and target design

For proof of concept experiments, a suitable target would hybridize at room temperature to maintain ease of use. A recently published ssDNA sequence utilized in a proximity ligation assay was chosen for this purpose. The scheme in **Figure 2** illustrates this concept where 46- and 50-base oligonucleotides, complementary to the 5′ and 3′ ends of a 26-base target (connector), are adducted to separate beads. The oligonucleotides were biotinylated and adducted to commercial 1 μm paramagnetic particles derivatized with avidin; estimated probe coverage is 4.3×10^5 probes/particle.

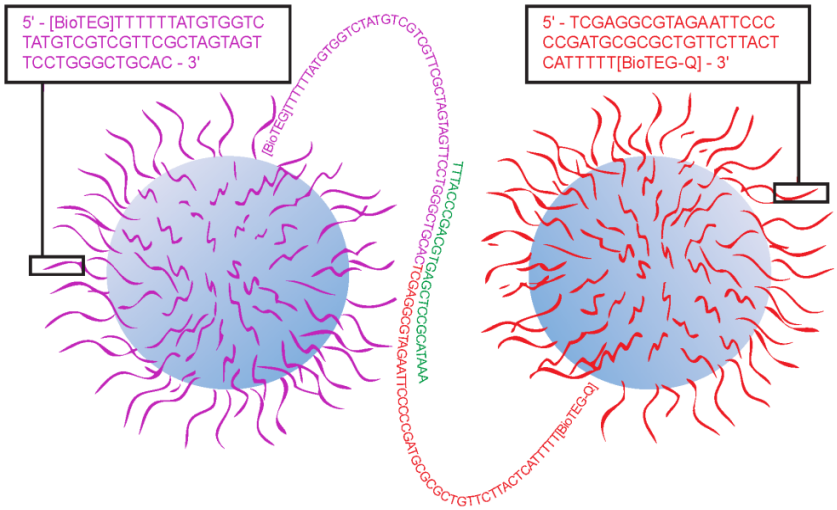

Figure 2: Cartoon of hybridization-induced aggregation (HIA) using a pair of proximity ligation oligonucleotides. Green spheres: 1-μm streptavidin-coated paramagnetic particles. Purple and Red: Biotinylated oligonucleotides. Blue: The target sequence binding the two DNA strands. Only one connection fully illustrated.

2.3.2 Assay Optimization

2.3.2.1 Instrumentation

The pinwheel assay described in **Chapter 1**, utilized an ordinary laboratory stir plate to facilitate the binding of DNA to the particle surface by a rotating magnetic field (RMF)

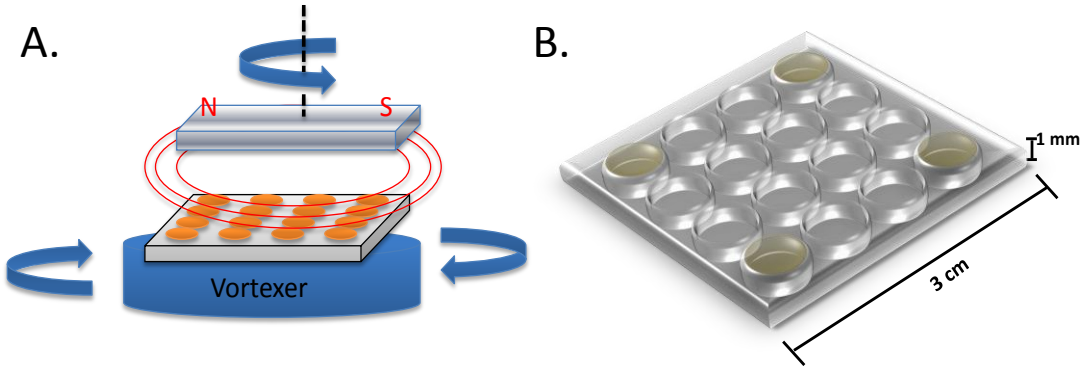

Figure 3: Scheme of HIA and instrument apparatus. ***A)*** *The PMMA microdevice is contained in the vortexer, while the particles are magnetized by the rotating magnetic field from above. The interaction of the particles with the free DNA in the microwell provides favorable kinetics for successful hybridization.* ***B)*** *Microdevice with four corner wells used for the assay.*

[39]. The paramagnetic particles used for the pinwheel assay have an average diameter of 8 µm and are irregular in shape. The streptavidin-coated particles used in HIA are only 1 µm in diameter and spherical. These physical differences results in the magnetic poles of the HIA particles aligning more strongly, causing an increased rate of false aggregates in the HIA assay. To circumvent this an additional agitation force was added to the set-up, in the form of a vortexer (**Fig. 3A**). Combined, the RMF and vortexer work in unison to facilitate the formation of aggregates only when the target DNA is present, while maintaining dispersed particles in a negative sample. This instrumentation set-up is referred to as dual force aggregation (DFA). The microdevice used in the development of the assay was a 4x4 microwell square fabricated in PMMA, creating 5 mm diameter wells which are 1 mm deep (**Fig. 3B**). The four corner wells were used so that the same magnetic field was applied to each sample.

2.3.2.2 Buffer composition

The composition of hybridization buffers is guided by the Wallace equation[40]:

$$\textbf{Eff } T_m = 81.5 + 16.6(\log M\ [Na+]) + 0.41(\%G+C) - 0.72(\%\ \text{formamide})$$

where Tm is the melting temperature, and M is molarity. In the simplest embodiment, the hybridization temperature can be lowered by increasing the salt concentration content of the buffer. However, the addition of salt also has negative effects on the stringency of the assay, i.e. fully non-complementary sequences will hybridize to each other. Guided by previous work by Mirkin *et. al.* [28, 41], two buffers were made, with 0.1 M and 0.2 M KCl, each with the same buffering capacity from 10 mM Tris. Each was used to perform a four minute HIA assay with 10 µM of the target sequence using the DFA system described above (**Fig. 4**). From this sub-optimized assay it was observed that 0.2 M KCl, 10 mM Tris pH 7.5 induced the greatest aggregation. Therefore, this buffer was then adopted and used in all subsequent HIA assays.

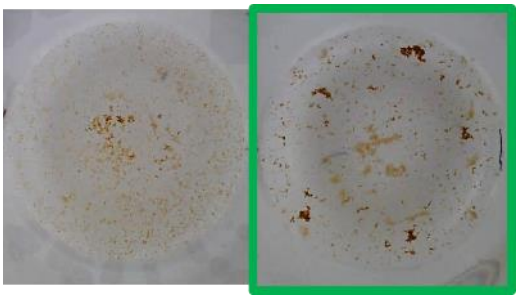

Figure 4: Birdseye photographs of HIA wells following a four minute assay with 10 µM of target DNA with two different buffers. A) 0.1 M KCl, 10 mM Tris, pH 7.5. B) 0.1 M KCl, 10 mM Tris, pH 7.5

2.3.2.3 Assay duration

With the basic chemistry and hardware for a breadboard instrument established, the duration of the assay had to be determined. A series of experiments were conducted from lasting from 3-15 minutes in one minute intervals (13 separate time points). The optimal assay time was determined by comparing the degree of aggregation using 10 µM of target DNA. **Figure 5** shows images captured with T1i DSLR camera with MP-E 65 mm f/2.8 1−5× macro lens, which was backlit by a single white LED. As can be seen in this figure, with 10 µM of target DNA present in the microwell aggregation is seen regardless of time interval. However, these images indicate that a 12 minute assay is optimal and would

provide the greatest sensitivity. Therefore, all of the experiments that follow used 12 minutes as the assay time.

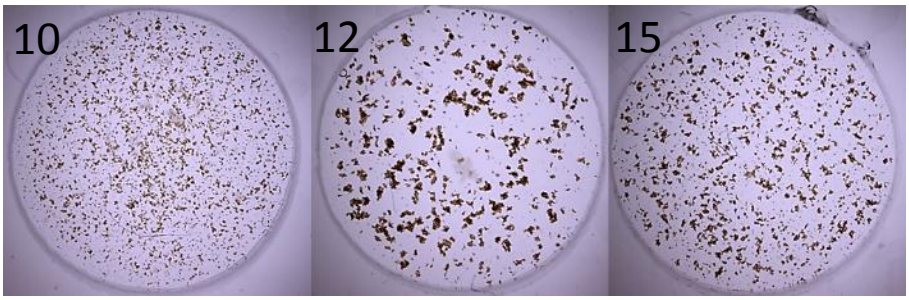

Figure 5: Assay duration time study. Each assay used 10 µM of target DNA and was completed in either 10, 12 or 15 minutes.

2.4 Competitive inhibition

The specificity of the HIA assay had to be defined using non-complementary sequences to ensure aggregation response was induced only by the correct target sequence. A 26-mer ssDNA non-complementary sequence was synthesized and 10 µM was used as the DNA in a HIA assay. To enable direct comparison between the results obtained with 10 µM of non- and fully-complementary sequences, image analysis was performed on each sample. The results are normalized so that 10 µM of the complementary target is set to 100% maximum aggregation, to which all other aggregates are

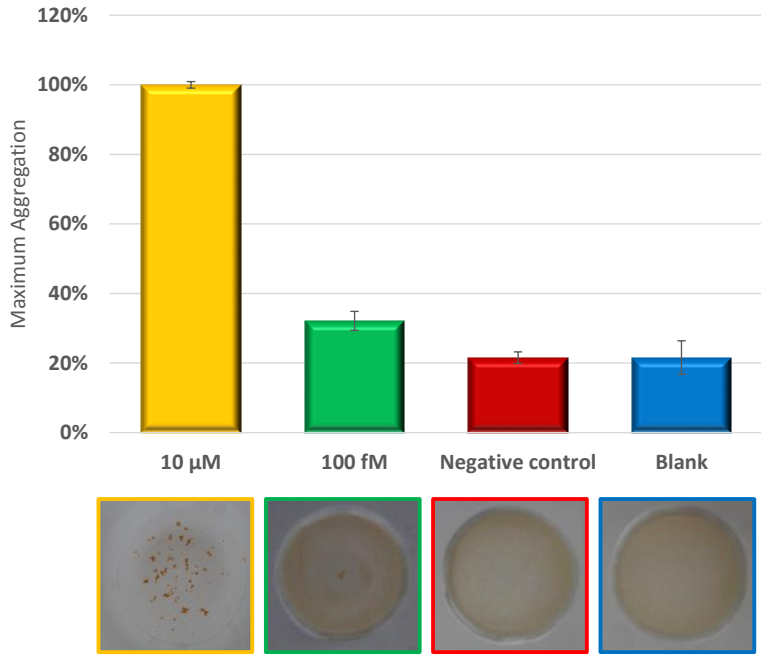

Figure 6: Quantitative response of HIA. Image processing with Mathematica converts bead dispersion into dark area. Aggregates with 10 fM of the target (yellow) are distinguishable 100 fM (green) from a negative control of 10 µM of a non-specific sequence (red) and a DNA-free run (blue) (n=4). Representative photographs are shown below.

compared. As shown in **Figure 6**, the non-specific sequence which was used as the negative control yielded ~20% aggregation, the same degree of aggregation as the sample with no DNA (blank). This confirms that aggregation response is sequence-specific driven, and can be used to detect targets of interest.

With specificity established determining the level of sensitivity associated with the assay was critical to establishing the overall potential of this technology, i.e., is the limit of detection (LOD) comparable to existing sequence-specific methods of detection. A series of 1:10 dilutions of target DNA were made from 10 µM to 100 fM and detected through HIA. Aggregates formed from only 100 fM of the complementary target DNA can be discriminated by image processing from background particles (**Fig. 6**). Therefore, HIA is comparable with established highly sensitive gold nanoparticle hybridization detection (50 fM) for a fraction of the cost and time . Furthermore, these dilution experiments demonstrate HIA is semi-quantitative, in that there is a correlation between degree of aggregation and target concentration. Although non-complementary DNA had been shown to not induce aggregation a more complex matrix including protein may induce a false positive response through interactions with the avidin surface of the particles. To establish whether protein would induce non-specific binding, 1 µL of whole blood was used (**Fig. 7**). The plasma in whole blood

Figure 7: Photographs of effect whole blood has on HIA. Far left, a control aggregation with 10 µM of target DNA. Middle a microwell with 1 µL of whole blood and HIA probes. Right: 10 µM of target DNA and 1 µL of whole blood added simultaneously.

contains the protein, at ~70mg/mL/0.7mg/µL. Whole blood did not cause false aggregation, nor inhibit 10 µM of target DNA from forming aggregate. Therefore, HIA is applicable for specific DNA detection within a complex biological matrix.

Looking towards using HIA in relevant samples, it is important to understand the limitations of the method based on the structure of the DNA target. In the experiments that follow the same probes and 26-mer target DNA sequence described above were used. The target sequence was modified in a systematic manner to demonstrate the effect of alterations made to the 26-mer target sequence. In each experiment, all wells contain 10 µM of the non-complementary sequence described above.

2.5 Hybridization effect from increasing flanking bases to the target

To establish the effect of non-complementary flanking bases on the sensitivity of HIA, 5, 10 or 15 additional bases were added on both sides of the target sequence. These sequences were created to be non-complementary to the probes and maintain near 50% GC content. Each modified target sequence was probed at a starting concentration of 10 µM, and serially diluted in 10X increments, until aggregation values were indistinguishable from ~10%, the value for aggregation with 10 µM of the non-specific sequence. The aggregation response was compared to the response with the unmodified target (**Fig. 8**). The data demonstrate significant loss of sensitivity, with none of these modified sequences

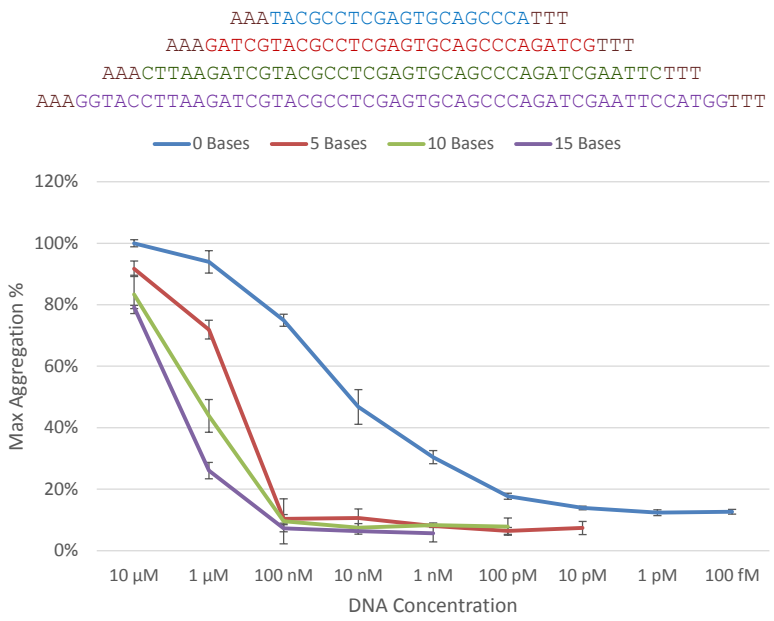

Figure 8: Effect of increasing the number of non-complementary bases flanking the target sequence. 5, 10 and 15 non-complimentary flanking bases are probed. Their aggregation response is compared to the unmodified sequence. The sequences used are shown above the graph for reference.

detectable at sub-micromolar concentrations. For sensitive DNA detection, the HIA target should be designed with as few non-complementary flanking bases as possible.

2.6 Complementary bases

We investigated the length of hybridization duplex required to stabilize aggregation in the DFA system. Five target lengths were synthesized, with 6, 10, 20, 26 and 32 complementary bases (each also retained a further 6 bases for the poly A- and T-tail, therefore total lengths were 12, 16, 26, 32 and 38 bases) (**Fig. 9**). These lengths were chosen to provide a large sample set, without requiring increased hybridization temperatures. Regardless of the variation in target length, the sequence for any target tested contained the same number of bases that were complementary to each probe, i.e., the six-base sequence has three bases complementary to bases on each probe and are positioned at the center of each tested target. With this design selection, several other differences evolved between the sequences (**Table 1**). The most significant of these was a T_m increase

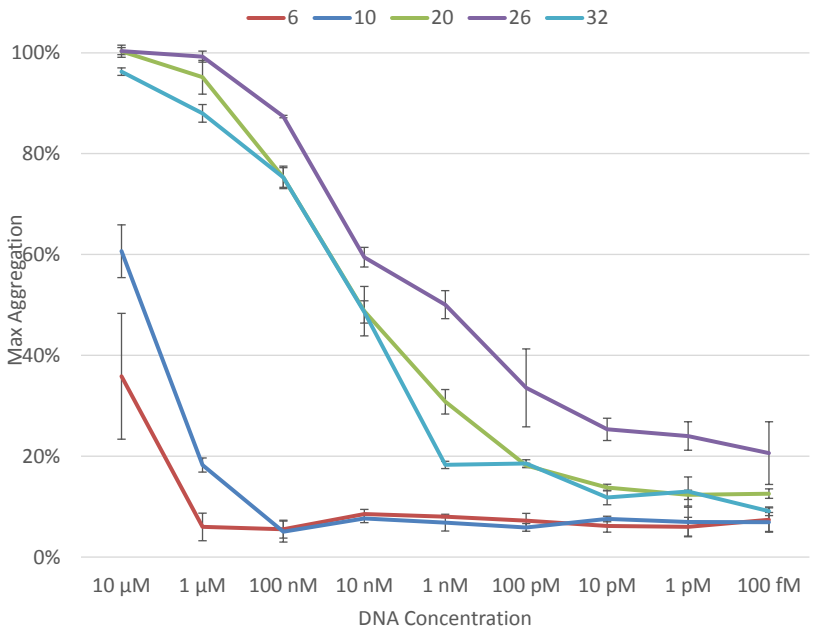

Figure 9: The effect on aggregation when the number of complimentary bases in the target strand is altered. 6, 10, 20, 26 and 32 complementary bases were used.

with increasing length from 33 °C (six bases) to 67 °C (32 bases); this would be expected to detrimentally affect hybridization at room temperature, therefore, this was chosen as the longest target. Unfortunately, Tm differences could not be avoided with sequences so short. Of the complementary bases in each sequence, ~60% were GC; therefore, each sequence (regardless of length) has comparable number of hydrogen bonds per base. This was performed to make number of bases the only significant factor altered. At a concentration of 10 µM, each sequence was readily detected above the ~10% threshold set for the non-complementary target. When the concentration is decreased to 100 nM, aggregation induced by the six- and ten-base sequences was no longer distinguishable from that of the control with no target DNA (**Fig. 9**). The target with 26 complementary bases (six more than the unmodified sequence) induced the most extensive aggregation, with an

Table 1: Differences in the physical parameters associated with each sequence, highlighting the major differences between the shorter and longer targets.

	Sequence	GC %	Melt Temp	Mol Weight	Self-dimer	Hairpin	GC % binding
6	AAACGAGTGTTT	33.3	33.4	3684.5	-5.23	-0.83	66.7
10	AAACTCGAGTGCATTT	37.5	45.5	4880.2	-12.64	0.23	60
20	AAATACGCCTCGAGTGCAGCCCATTT	50	62.8	7915.5	-9.96	-0.61	65
26	AAATTCTACGCCTCGAGTGCAGCCCAGGATTT	50	65.6	9784.4	-9.96	-0.61	61.5
32	AAAGAATTCTACGCCTCGAGTGCAGCCCAGGAACTTTT	47.4	66.7	11646.6	-11.71	-0.61	56.3

aggregation of ~20% observed with target concentrations as low as 100 fM. The degree of aggregation of 32 bases tracked with that of the 20 bases sequence (**Fig. 9**), potentially due to a suboptimal hybridization temperature. Overall, it was clear that 26 complementary bases gave the best sensitivity from the target sequences probed and is therefore the optimal length for a HIA target.

2.7 Single Point Mutation Detection

Despite the longer target sequence providing the greatest sensitivity, the unmodified sequence continued to be used as the benchmark when investigating the effect of point mutations (PMs) on aggregation. Destabilization of a hybridized duplex has been reported to occur when a single point mutation (SPM) is located near the center of the target[43]. However, there is no data for SMP detection in a chaotic dynamic system such as DFA, where particles are in

A.

AAA TAC GCC TCG AGT GCA GCC CAT TT
AAA TAC GCC GCG AGT GCA GCC CAT TT
...ATG CGG AGC TCA CGT CGG GT...
AAA TAC GCC GCG AGT GAA GCC CAT TT
AAA TAC GCC GCG TGT GAA GCC CAT TT

B.

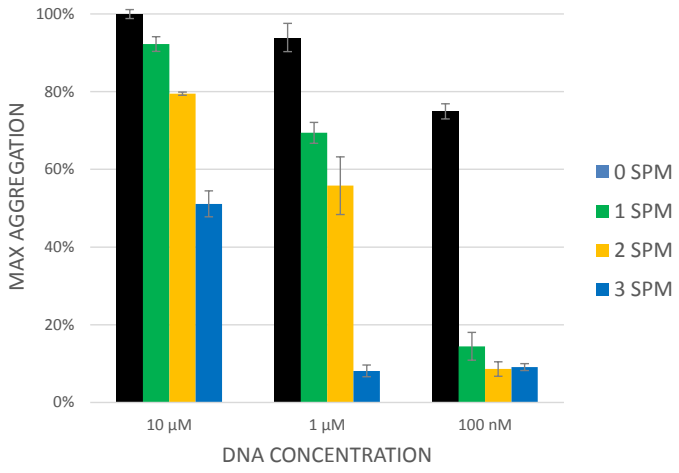

Figure 10: Detection of single point mutations through HIA. A) Sequences used to investigate the effect of aggregation from increasing SPM's. Purple and red bases illustrate the biotinylated probes. B) Results from using 10 µM – 100 nM of the target sequences. Aggregation response is compared to the sequence with no SPMs.

constant motion. Therefore, the placement of the first PM was chosen at random, with a 10T→G mutation (replacing a pyrimidine with a purine) selected to cause maximum disruption of the formed DNA duplex. A second PM, a 17C→A, was inserted at a location that mirrored that of the first, i.e. four bases from the probe junction, to create a double-PM. The third and final PM was located at the probe junction. A 12A→T base change was specifically chosen to maintain the same % GC composition (triple-PM) (**Fig. 10A**). Each of these mutated sequences were probed at three concentrations of 10 µM, 1 µM and 100 nM, at 100 nM aggregation plateaued for each at 9%, therefore, no longer detectable (**Fig. 10B**). The triple-PM sequence was only detectable at high concentrations (10 µM), and even then, yielded an aggregation that was ~50% relative to SMP. The double-PM was detectable at µM concentrations, however, aggregation response dropped from ~55% to 9% between 1 µM and 100 nM target concentrations. The same trend was observed for the SPM, which dropped from ~70% maximum aggregation to ~15% over the same concentration range. These data highlight that the extent of destabilization of the hybridization duplex is proportional to the number of PMs in the sequence, significantly reducing the LOD compared to a fully-complementary sequence. At micromolar concentrations, the extent of aggregation for 0, 1, 2 or 3 SPM are distinguishable from one another, thus, with a known target DNA concentration, the degree of aggregation can be used to determine the number of SPMs present in the target. This is of particular significance with many diagnostic assays that rely on detecting subtle changes in a sequence for genotyping, e.g. detection of the G20 19S mutation associated with Parkinson's disease[44].

2.8 Interferants Analysis

Interfacing HIA as the detection modality within an integrated microdevice is a natural progression, as the method is inexpensive, rapid and requires a small sample size for DNA detection. To ascertain the robustness of HIA, the aggregation induced by the unmodified 26-mer target sequence was evaluated in the presence of 12 different potential interferants. The interferants were chosen for their likelihood to be interfaced with HIA during potential integrated assays. These included PCR reagents (25 mM MgCl and 1.15/11.5/115mg/mL BSA), potential DNA denaturants to make the DNA single-stranded (6M Urea, 6M GuHCl and Hi-Di formamide), and finally reagents or components from DNA preparation that may

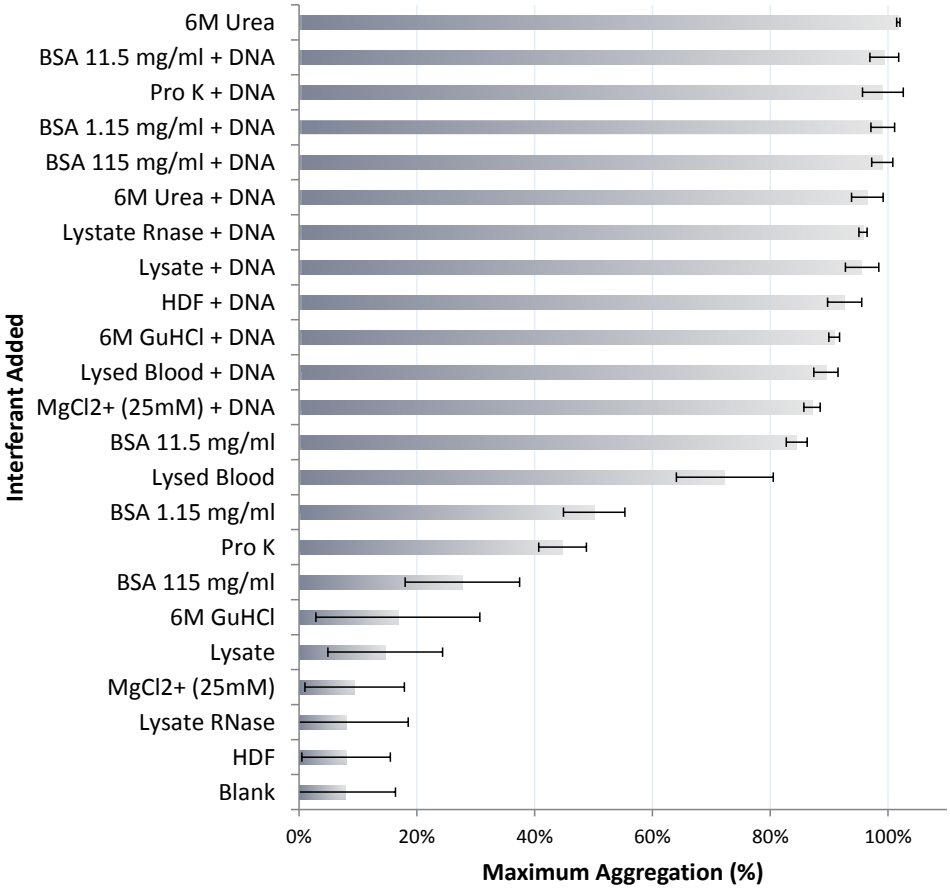

Figure 11: Evaluation of inducing false aggregation, or inhibition of DNA binding, with 12 potential interferants during a theoretical integrated microdevice assay. Aggregation response is compared to the Max aggregation for the DNA alone.

interface with HIA (20 mg/mL Proteinase K, lysed blood, lysate and lysate RNase from a buccal swab). For each of these interferants, an assay was completed with 1 μL of each interferants at the stated concentrations, with and without the unmodified 26-mer target sequence (10 μM), to determine if any would produce an inhibitory effect, preventing aggregation. The assay volume remained as 20 μL, with the interferant volume subtracted from the buffer volume. The reagents required for PCR were of significant interest, as PCR will frequently precede HIA on an integrated device. The aggregation response in the presence of magnesium chloride (25 mM; required to activate the polymerase) was comparable to the minimum aggregation of ~10%, but did not inhibit hybridization when target DNA was added. The addition of bovine serum albumin (BSA), produced a bell-shape response, with extensive aggregation seen with 11.5 mg/mL and 1.5 mg/mL, of ~80% and ~50% respectively. However, 115 mg/mL of BSA only produced minimal aggregation of ~30% (**Fig. 11**). Previous studies have shown that BSA will bind DNA at high concentrations through hydrogen bonding, overcoming protein-protein interactions between the BSA and avidin. Therefore, at elevated concentrations the BSA will bind to the probes more readily, reducing the extent of protein-protein binding causing false aggregation, as demonstrated at 115 mg/mL. However, when BSA is added to PCR master mix reagents for the purpose of either surface passivation or to help stabilize the polymerase; the concentration is typically sub-100 μg/mL, and cause less false aggregation than the concentrations probed here. Lysed blood, an unlikely interferant, also gave an aggregation response of 75%, which was expected due to protein-protein interactions with the avidin surface [45, 46]. False aggregation of ~100% was also induced by 6 M urea therefore should not be interfaced with HIA directly. Although urea is similar in structure

to GuHCl, urea possibly binds to the streptavidin surface and clearly induces aggregation, while GuHCl does not ; this is consistent with our observations. It is possible that the false aggregation could also be due to urea interacting with the silica suface of the particle as a definitive binding study was not performed. When target DNA was added, regardless of interferant, the particles aggregated tightly, therefore, the interferants do not inhibit the hybridization-induced aggregation process. This confirms HIA is a detection method with potential for integration into an integrated microdevice.

2.4 Conclusions

Hybridization-induced aggregation is a powerful new modality in specific DNA detection and this chapter demonstrates the optimization of hardware and chemistry to create a highly specific and sensitive assay, comparable to gold nanoparticle hybridization assays. HIA utilizes biotinylated oligonucleotide probes bound to 1 μm streptavidin-coated paramagnetic beads. The probes are complementary to the target DNA sequence, inducing aggregation of the particles when the probes and target hybridize. The hybridization process is facilitated by a rotating magnetic field and agitation from a vortexer, enabling HIA in minutes. These aggregations are visible to the naked eye for immediate qualitative results, or images of the aggregates can be processed to produce a semi-qualitative value. HIA was shown to be highly specific as 10 μM of a non-complementary sequence has no effect on particle aggregation (they remained dispersed). Using sequences which hybridize at room temperature, HIA can detect a little as 100 fM of a 26-mer target DNA, echoing the LOD of gold nanoparticle hybridization assays.

A systematic investigation into the effect that subtle target composition alterations have on aggregation were compared to the 26-mer sequence, which was used to set a threshold for maximum aggregation. Each assay was performed with 10 μM of a 26 random base sequence, which provided the minimum threshold of 9%: any aggregation which was statistically above 9% was considered detectable. The LOD for HIA is highly dependent on the number of non-complimentary flanking bases, which is reduced to nanomolar concentrations with only five extra flanking bases added. The number of required complimentary bases in the target sequence was also explored, determining that as few as six complimentary bases will induce particle aggregation. However, the greatest aggregation was seen with 26 complimentary bases, outperforming 20 and 32 bases, even at femtomolar concentrations. Additionally the ability of the HIA method to detect a single point mutation was explored, with sequences containing 1, 2 or 3 bases mutations. At micromolar concentrations, each sequence aggregated with a distinct aggregation %, thus, at a known concentration the number of mutations in a sequence can be identified. The specificity of HIA is further demonstrated, as at nanomolar concentrations and below, only the fully complimentary sequence is detectable. Particle driven DNA detection is ideal to interface with other processes within a microfluidic device, and HIA's compatibility with 12 potential interferants was evaluated. Urea, BSA and lysed whole blood all caused aggregations responses greater than 75%, therefore, should not be interfaced with HIA directly. None of the interferants were inhibitors to the hybridization of the target DNA. Through design of the target sequence the sensitivity of the HIA assay is tuneable, with greatest LOD coming from a fully complimentary sequence. This particle driven

hybridization approach is ideal for interfacing as the detection modality in a microfluidic device and is minimally effected by the addition of on-chip assay interferants.

2.5 References

1. Southern, E.M., *Journal of Molecular Biology*, 1975. **98**(3): p. 503-517.
2. Jiang, G., et al., *ACS Nano*, 2009. **3**(12): p. 4127-4131.
3. Zuo, X., et al., *Journal of the American Chemical Society*, 2010. **132**(6): p. 1816-1818.
4. Kumar, M. and P. Zhang, *Langmuir*, 2009. **25**(11): p. 6024-6027.
5. Nam, J.-M., S.I. Stoeva, and C.A. Mirkin, *Journal of the American Chemical Society*, 2004. **126**(19): p. 5932-5933.
6. Stoeva, S.I., et al., *Angewandte Chemie*, 2006. **118**(20): p. 3381-3384.
7. Mirkin, C.A., et al., *Nature*, 1996.
8. Barhoumi, A. and N.J. Halas, *Journal of the American Chemical Society*, 2010. **132**(37): p. 12792-12793.
9. Huang, Y., et al., *Biosensors and Bioelectronics*, (0).
10. Pinijsuwan, S., et al., *Analytical Chemistry*, 2008. **80**(17): p. 6779-6784.
11. Gagnon, Z., S. Senapati, and H.-C. Chang, *Electrophoresis*, 2010. **31**(4): p. 666-671.
12. Sz-Hau, C., et al., *NanoBioscience, IEEE Transactions on*, 2009. **8**(2): p. 120-131.
13. He, Y., et al., *Analytical Chemistry*, 2010. **82**(17): p. 7169-7177.
14. Parab, H.J., et al., *Biosensors and Bioelectronics*, 2010. **26**(2): p. 667-673.
15. Hansen, K.M., et al., *Analytical Chemistry*, 2001. **73**(7): p. 1567-1571.

16. Wong, E.L.S., E. Chow, and J.J. Gooding, *Langmuir*, 2005. **21**(15): p. 6957-6965.

17. Tsourkas, A., et al., *Nucleic Acids Research,* 2003. **31**(4): p. 1319-1330.

18. Wendler, K., et al., *The Journal of Physical Chemistry A,* 2010. **114**(35): p. 9529-9536.

19. Chan, M.-L., et al., *Biosensors and Bioelectronics,* 2011. **26**(5): p. 2060-2066.

20. Gao, Y., L.K. Wolf, and R.M. Georgiadis, *Nucleic Acids Research,* 2006. **34**(11): p. 3370-3377.

21. Zhang, H., et al., *Talanta,* 2011. **84**(3): p. 771-776.

22. Liu, H., et al., *Biosensors and Bioelectronics,* 2010. **26**(4): p. 1442-1448.

23. Qavi, A.J., T.M. Mysz, and R.C. Bailey, *Analytical Chemistry,* 2011. **83**(17): p. 6827-6833.

24. Zhang, G.-J., et al., *Biosensors and Bioelectronics,* 2009. **24**(8): p. 2504-2508.

25. Sorgenfrei, S., et al., *Nat Nano,* 2011. **6**(2): p. 126-132.

26. Thaxton, C.S., D.G. Georganopoulou, and C.A. Mirkin, *Clinica Chimica Acta,* 2006. **363**(1-2): p. 120-126.

27. Wong, J.K.F., S.P. Yip, and T.M.H. Lee, *Small,* 2012. **8**(2): p. 214-219.

28. Xu, X., et al., *Small,* 2010. **6**(5): p. 623-626.

29. Lamture, J.B., et al., *Nucleic Acids Research,* 1994. **22**(11): p. 2121-2125.

30. Lee, T.M.-H., M.C. Carles, and I.M. Hsing, *Lab on a Chip,* 2003. **3**(2): p. 100-105.

31. Fan, Z.H., et al., *Analytical Chemistry,* 1999. **71**(21): p. 4851-4859.

32. Liu, P., et al., *Lab on a Chip,* 2011. **11**(16): p. 2673-2679.

33. Dharia, N.V., et al., *Genome Biology,* 2009. **10**(2).

34. Bech, S., et al., *Parkinsonism & Related Disorders,* 2010. **16**(1): p. 12-15.

35. Yi Sun, Y.C.K., Nam-Trung Nguyen, *Journal of Micromechanics and Microengineering,* 2006. **16**(8).

36. Leslie, D.C., et al., *Journal of the American Chemical Society,* 2012. **134**(12): p. 5689-5696.

37. Gullberg, M., et al., *Proceedings of the National Academy of Sciences of the United States of America,* 2004. **101**(22): p. 8420-8424.

38. Leslie, D.C., et al., *Electrophoresis,* 2010. **31**(10): p. 1615-22.

39. Wallace, R.B., et al., *Nucleic Acids Res,* 1979. **6**(11): p. 3543-57.

40. Lee, J.S., M.S. Han, and C.A. Mirkin, *Angewandte Chemie,* 2007. **119**(22): p. 4171-4174.

41. Cao, Y.C., R. Jin, and C.A. Mirkin, *Science,* 2002. **297**(5586): p. 1536-1540.

42. Lucarelli, F., G. Marrazza, and M. Mascini, *Analytica Chimica Acta,* 2007. **603**(1): p. 82-86.

43. Paisán-Ruíz, C., et al., *Neuron,* 2004. **44**(4): p. 595-600.

44. Phizicky, E.M. and S. Fields, *Microbiological Reviews,* 1995. **59**(1): p. 94-123.

45. González, M.n., C.E. Argaraña, and G.D. Fidelio, *Biomolecular Engineering,* 1999. **16**(1–4): p. 67-72.

46. Kurzban, G.P., et al., *Journal of Biological Chemistry,* 1991. **266**(22): p. 14470-14477.

3 Development of HIA for dsDNA detection applied to the detection of multi-drug resistant tuberculosis

As stated in **chapter two**, HIA was developed as a method for the detection of a ssDNA target that would hybridize to the probes at 25 °C[2]. However, the vast majority of DNA to be hybridized for detection exists in a double-stranded DNA (dsDNA) state. Destabilization of the dsDNA complex is required prior to hybridizing to the oligonucleotide probes in order for aggregation to be effective. Chemical denaturation is not a viable option as denaturants (i.e., DMSO) would adversely affect hybridization. Alternatively, elevated temperature can be used to effectively denature the DNA; however, at temperatures above 90 °C, the avidin-biotin complex (that is used to bind the oligonucleotide probe to the particle surface), will begin to disassociate resulting in loss of probes from the bead surface[3]. This chapter reports the modifications made to the HIA assay to enable sequence-specific dsDNA detection, which was then applied to the detection of multi-drug resistant tuberculosis.

3.1 Introduction

Tuberculosis (TB) is a disease caused by the bacterium *Mycobacterium tuberculosis* (*M. tuberculosis*). This slow-growing bacteria is capable of rapid genetic mutation, leading to patient resistance to antibiotics commonly used to treat the disease[4]. In 2011, there were 310,000 cases of multidrug-resistant *M. tuberculosis* (MDR-TB), with 60% of the cases found in China, India, and the Russian Federation[5]. MDR-TB is classified by strains of TB bacteria that have mutated in a manner that imparts resistance to the first-line drugs, *isoniazid* and *rifampin*; detecting these strains rapidly is essential to initiate the correct therapy. Traditional culture-based methods are accurate, and are based on cell growth in a

single culture dish, with separated regions treated with different drugs. The cell growth in each region is compared against the control; this is termed ‘agar proportion’ detection. Unfortunately, obtaining meaningful diagnostic results can require months, and during this time, patient resistance can increase and/or change[6]. Genotyping assays are available and enable identification of MDR-TB within a few hours. However, despite an excellent correlation between genotype and phenotype for several targets, including *rifampin* (rpoB)[7, 8] and *isoniazid* (inhA, katG), extensive molecular mapping is required before a full panel of drugs can be assessed.

Recently, a method was reported for TB bacteria phenotyping using D29 mycobacterial phage infection and replication . D29 phage, virus-like entities that infect *M. tuberculosis* with high specificity, replicate in a manner that does not result in the immediate lysing of the host cells. They co-opt the replication machinery of the host cell by incorporating their viral genome into the host DNA. The host survives, with phage now part of its genome, therefore, in the presence of viable TB, the amplification factor for D29 phage in TB can be 10^5 [12, 13]. The results from this approach have been shown to be compatible with any drug line and, thus, this emerges as an immediate solution for MDR-TB drug susceptibility testing (DST).

The basis for this approach is simple; the larger the number of viable TB bacteria that exist when exposure to phage is initiated, the more effective phage infection and replication can be. As a result, monitoring the replication of D29 qualitatively determines the effect a drug will have on a specific strain of TB cells. With this method, quantifying the extent of phage replication is simplified by qPCR, with the main advantages being sensitivity, throughput and immediate results once the assay is completed. However, this technology requires

expensive instrumentation, highly degradable reagents, and skilled labor, rendering the method less than ideal for point-of-care (POC) diagnostics. An emerging alternative to traditional fluorescence-based specific DNA detection involves exploiting paramagnetic particles (PMPs). These interact with DNA, and the interaction generates a signal that can be colormetric or electrical [1, 15, 16], or represented by particle aggregation . The latter is preferable for POC diagnostics, because it is visual and doesn't require any extensive hardware/equipment.

The overarching goal for next generation POC diagnostic systems is that they be inexpensive, portable, rapid, and use simple devices that do not require a skilled operator, only user input of a sample; however few devices of this nature exist (See. **Fig. 1, Chapter two**) Several FDA-approved microfluidic-based POC tests are currently available and being utilized, including the *Piccolo Xpress*® for blood chemistries, and the *PanNAT*® for molecular diagnostics of infectious diseases [18]. Currently, a commercialized microfluidic-based platform, *GeneXpert*™ is available for determining TB resistance, [19] which uses a cartridge that accepts sample and interfaces directly with the instrument. Currently, this is an unmatched force in rapid MDR-DST; however, it is based on molecular probing chemistry and currently only assesses rifampin resistance.

In this chapter, we present the interfacing of the D29 bacteriophage assay with HIA, where hybridization of the target DNA specific to the phage genome induces a visual bead aggregation. HIA, while not quantitative, is suitable to replace qPCR in the workflow, reducing analysis time and cost. It is the first step towards creating a fully automated MDR-TB test for use, particularly in developing countries where qPCR is not available.

Furthermore, for the first time, we demonstrate the integration of PCR and HIA on a single microdevice for the detection of MDR-TB.

3.2 Materials and Methods

3.2.1 Reagents

Dynabeads MyOne Streptavidin C1 paramagnetic beads and AmpliTaq Gold® were purchased from Invitrogen (Carlsbad, CA). Biotinylated and unfunctionalized oligonucleotides were purchased from Eurofins MWG Operon (Huntsville, AL). λ-phage genomic DNA (48.5 kb long) from *E. coli* infected with CI8S7Sam7 in storage buffer [10 mM Trix-HCl (pH 7.5, 10 mM NaCl, 1 mM EDTA] was purchased from USB (Cleveland, OH) was purchased from hydrochloric acid, sodium chloride, potassium chloride and ethanol, were purchased from Fisher (Fair Lawn, NJ). 2-Amino-2-(hydroxymethyl)- 1,3-propanediol (Trizma base, 99.9%) was purchased from Sigma (St. Louis, MO). All solutions were prepared in Nanopure water (Barnstead/Thermolyne, Dubuque, IA). SpeedSTAR™ polymerase, magnesium chloride and 10X PCR buffer, is available from Clontech Lab. (Mountain view, CA)

3.2.2 Assay Instrumentation

Images of the microwells were collected by using a T1i DSLR camera with MP-E 65 mm f/2.8 1−5× macro lens purchased from Canon U.S.A., Inc. (Lake Success, NY). A Thermix Stirrer model 120S magnetic stir plate was purchased from Fisher Scientific (Fair Lawn, NJ). Three, 5-mm x 5-mm cylinder neodymium magnets were purchased from Emovendo

(Petersburg, WV). A MS3 basic vortexer was purchased from IKA (Wilmington, NC). TEC1-12710 thermoelectric cooler Peltier and a CyberTech tach-mtr-01 digital photo laser non-contact tachometer were purchased from Amazon.com (Seattle, WA). A Ledu compact desk magnifier lamp was purchased from Guy Brown Products (Brentwood, TN) and used without optics to provide lighting around the entire sample.

3.2.3 Microwell Fabrication

A VersaLASER system 3.50 from Universal Laser Systems (Scottsdale, AZ) was used to fabricate microwells, cutting through 1.0 mm-thick PMMA purchased from Astra Products (Baldwin, NY). Each microwell device was prepared as a 4 × 4 matrix of 5-mm-diameter circular wells on a 4-cm square device, designed in AutoCAD. These were then thermally bonded using established methods[1] to a second 4-cm square 1.5-mm-thick PMMA, purchased from McMaster-Carr (Santa Fe Springs, CA). Microwells we sterilized in 2M hydrocholoric acid for 30 min, then rinsed with Nanopure water prior to use.

3.2.4 Assay Procedure

Four 5 mm PMMA microwells were used simultaneously, with a 20 µL final volume: 18 µL of HIA buffer (10 mM Tris, 200 mM KCl, pH 7.5), 1 µL of each 3'- and 5'- biotinylated particles, and 1 µL of PCR product (target DNA sequence). The sample is then exposed to an RMF of 2000 rpm and a vortexing speed of 130 rpm for 90 seconds. A single picture is then taken of the microwell for analysis. All TB assays were performed at 56°C, using Peltier for temperature control. All λ-phage assays at 70 °C, using a water bath to heat the

buffer and microwell heat maintained using a heated stir plate model 97042-642from VWR (Batavia, IL).

3.2.5 PCR primers and HIA probes

Lambda Fwd GATGAGTTCGTGTTCGTACAACTGG
CCAGTTGTACGAACACGAACTCATCTTTTTT[BioTEG-Q]
Lambda Rev GGTTATCGAAATCAGCCACAGCGCC
[BioTEG]TTTTTTGGTTATCGAAATCAGCCACAGCGCC

D29-Fwd (5'-AGCCGATCAGAAGCACGGGC-3')
5'-[BioTEG]-AGCCGATCAGAAGCACGGGC -3'
D29-Rev (5'-AGCGGCTCTTAGGAGGGGCC-3')
5'-TCGCCGAGAATCCTCCCCGG-[BioTEG-Q]-3'

3.2.6 PCR Protocol

An initial hold at 95 °C for 11 min, (25,30 or 40) cycles of 95 °C for 30 sec, 63 °C for 30 sec, and 72 °C for 30 sec, followed by a final hold at 72 °C for 7 min. The product was separated and detected using an Agilent 2100 Bioanalyzer (Agilent Technologies, Inc., Santa Clara, CA)

For IR-PCR: An initial hold at 95 °C for 2 min, 32 cycles of 95 °C for 5 sec, 63 °C for 15 sec, and 72 °C for 20 sec, followed by a final hold at 72 °C for 2 min. Non-integrated assays were then removed from the microdevice and the product was separated and detected using an Agilent 2100 Bioanalyzer (Agilent Technologies, Inc., Santa Clara, CA). Final concentrations or volumes of reagents were, unless otherwise stated, $MgCl^{2+}$ 3 mM, dNTP's 0.4 µM, 1x PCR buffer, polymerase 2.5 units. Purified D29, replicated in TB bacteria infected cells with antibiotics were supplied by Houpt group, University of Virginia. 5 µL of sample was added to each tube-based amplification. 0.65 µL of sample was available in the 2 µL microdevice PCR chamber. 1ng of λ-phage DNA was used in the tube amplifications.

3.3 Results and Discussion

3.3.1 Detection of Lambda DNA PCR product

As the ssDNA PL sequences used in **chapter one** were specifically selected because hybridization was effective at 25°C; typical oligonucleotide−target hybridization occurs at elevated annealing temperatures (55−70 °C). To demonstrate that hybridization-driven aggregation could be temperature-dependent, effective with longer targets, and applicable to both single- or double- stranded targets, a 500-bp fragment (λ DNA) of the lambda phage genome was used with oligonucleotide-adducted 1 μm beads (λ beads) designed to anneal with the λ target at 70 °C. The probes were designed with only a six base poly-T tail, with each probe hybridizing 20 bases to the same strand of DNA (**Fig. 1**). Elevated temperatures

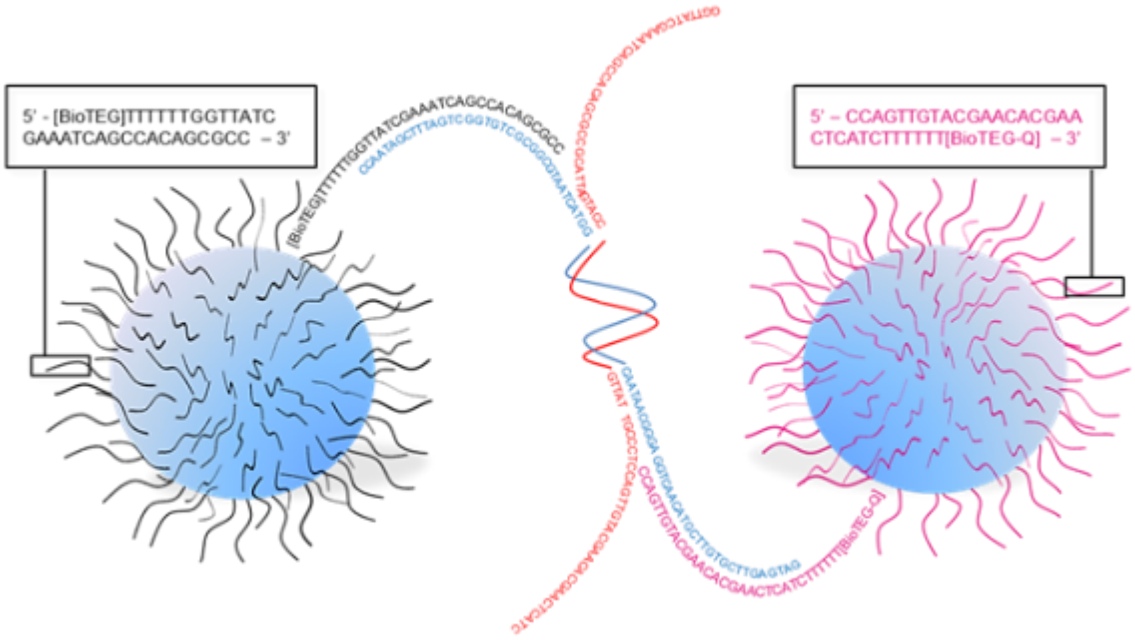

Figure 1: Scheme of hybridization-induced aggregation for the 500 bp amplicon of lambda phage DNA.

were obtained through warming the hybridization buffer in a water bath and maintaining temperature with a heated stir plate set at 75 °C. By setting the maximum aggregation at 100% for 10^{10} copies of the 500 bp product, it is observed that there is little change in

aggregation over two orders of magnitude from 10^{10-8} copies of the λ-phage amplicon (**Fig. 2**). Therefore, by raising the temperature of the assay, hybridization of dsDNA through HIA is not only possible, but effective as a visual DNA detector.

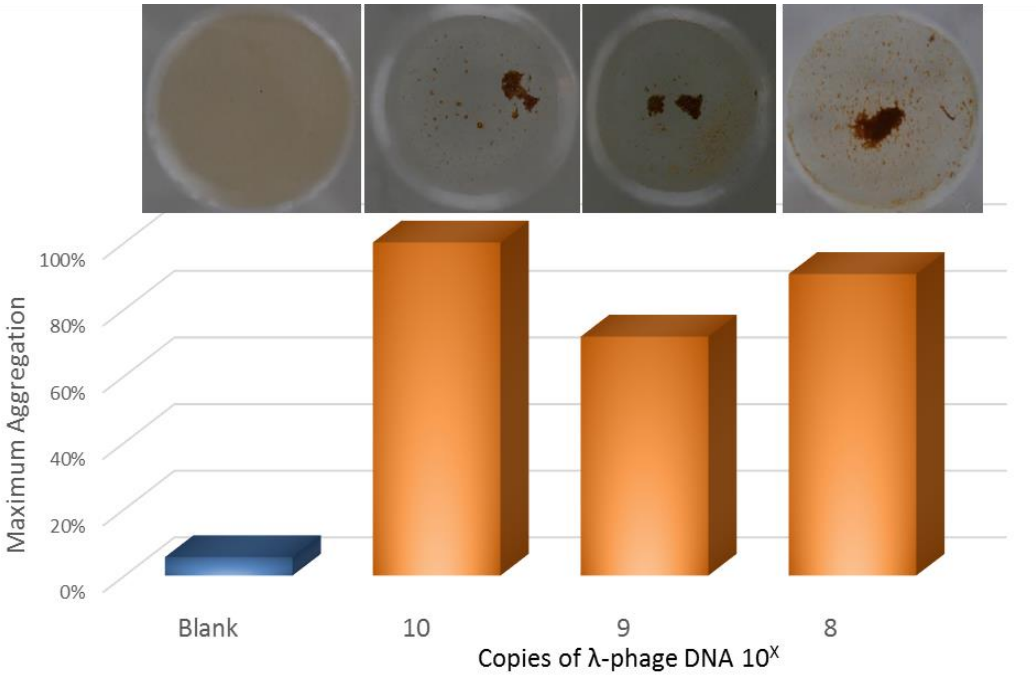

Figure 2: HIA detection of a 500 bp λ-phage amplicon. Quantitative response of HIA with 10^{10} – 10^{8} copies of 500 bp PCR product, compared to a blank (no DNA) (n=3). Representative photographs of aggregation are shown above each concentration.

3.3.2 Multiple Analyte Detection

With two analytes hybridizing at disparate temperatures, it is possible to detect two analytes in the same well, with HIA, by simply transitioning through two buffer temperatures. Using the proximity ligation probes and sequences discussed in **chapter two**, and those for the λ-phage 500 bp amplicon discussed above, the principle of multi-analyte detection was explored. As shown in **Figure 3**, a positive result for λ is indeed observed at the 70 °C annealing temperature, but not at 25 °C. For the PL beads in the

presence of the PL target the reverse is observed: aggregation occurs at 25 °C, but not at 70 °C. When the two assays are combined in a single well, pinwheels form at both 25 and 70 °C. From this result, it seems plausible that a multiplexed pinwheel assay may be defined that can detect multiple targets in a single well by simply ramping through a select temperature range.

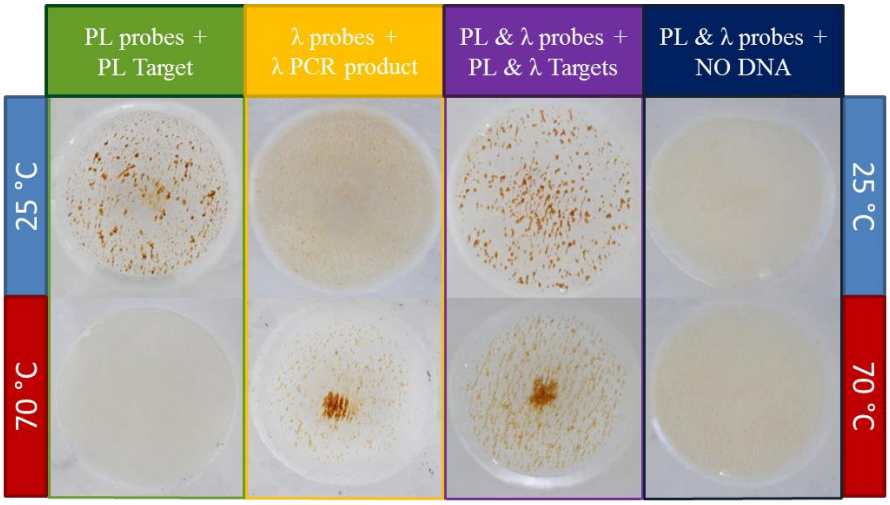

Figure 3: Photographs illustrating temperature sensitive HIA, with and without competitive inhibition, at 25 °C and 70 °C. Green panel – Hybridization of ssDNA PL oligonucleotides occurs only at 25 °C and is denatured at 70 °C. Yellow panel – Hybridization of λ oligonucleotides and target occurs only at 70 °C; at 25 °C, the dsDNA PCR product hasn't denatured, preventing aggregation. Purple panel – demonstration that HIA can work in the presence of competing DNA, producing an aggregation response only at the optimal hybridization temperature for the oligonucleotides. Navy blue panel – No aggregation is seen when no target DNA is present. For each target 10^{10} copies are added (n=5).

3.3.4 Detection of Multi-drug resistant Tuberculosis

The overall approach of applying HIA to MDR-TB detection is simple: add bacteriophage (phage) to viable TB with or without antibiotic(s), allow adequate time for phage replication (hours), then define the number of phage that result via PCR of phage DNA. This is initiated with the addition of 500 PFU (plague forming units) of D29 phage to sputum isolates from TB-positive patients. The amplified product is then used for HIA detection. The basis of this workflow is depicted in **Figure 4**.

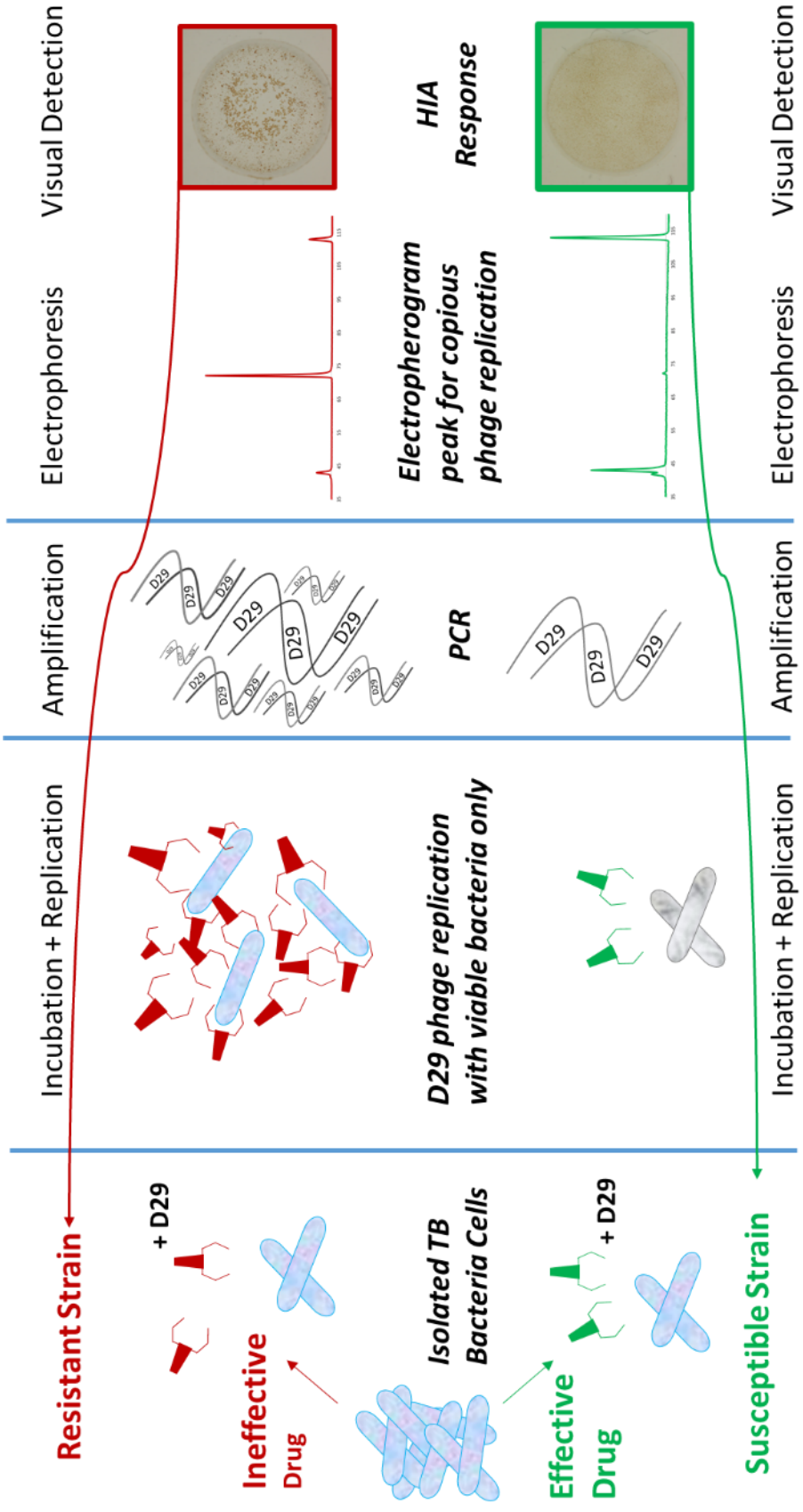

Figure 4: Scheme of workflow for the detection of multi-drug resistant tuberculosis using bacteriophage replication, PCR amplification and HIA detection.

3.3.4.1 Adaptation of DFA system

Although, a simple water bath for heating the temperature of the buffer was effective, this is not a viable approach for technology and is not compatible with high-throughput rapid dsDNA detection. A more effective strategy would be to couple the DFA system with a microwell thermostating capability [20]. A Peltier was built into the stage of the vortexer so that when the microdevice was mounted in the vortexer, it was in intimate contact with the heater, enabling temperature control at elevated assay temperatures (**Fig. 5**). As the

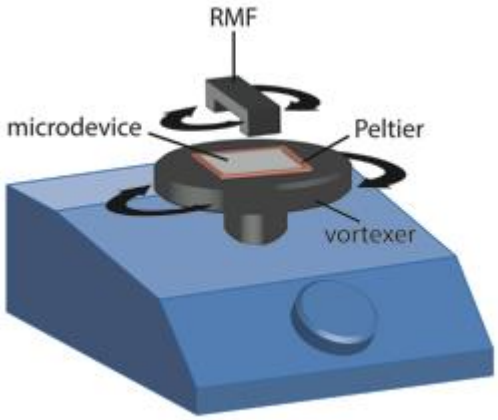

Figure 5: Scheme of dual force aggregation (DFA) instrumentation.

theoretical T_m of the TB probe sequences were 64 °C, this was chosen as the initial buffer temperature, with a range of 52 to 64 °C evaluated to determine conditions that produced the most aggregation with 1 µL of D29 PCR product. The results showed that the greatest difference between maximum particle aggregation and non-aggregates occurred at 56 °C (data not shown). This was achieved without a pre-assay denaturation step at >90 °C to produce ssDNA, which would make the target DNA accessible. Successful hybridization at 56 °C led to the hypothesis that the ends of the DNA strand have denatured, while the central base stacking maintains a double stranded structure (see **Fig. 1**) [1]. The HIA assay previously described [1] required up to five minutes for completion, however, such assay times led to false positive results due to evaporation, which subsequently increased the

concentration of the particles. Creating a closed well was not a viable option, as the buffer and particles tended to adhere to the upper surface, causing 3D aggregates that complicate qualitative analysis of the images. To determine the assay time that would provide maximum hybridization-induced aggregation (and be easily discriminated from minimum aggregation), a series of experiments where dwell time in the RMF was increased in 30 second increments from 0.5-3 minutes. It was found that assay times greater than 150 seconds resulted in significant buffer evaporation, leading to meniscus formation in the microwell, providing sub-optimal conditions for DNA-particle interactions. Assay times substantially less than 90 seconds provide insufficient time for particle aggregation, and were inconclusive for positive phage replication. A dwell time of 90 seconds in the RMF while vortexing was found to be adequate for particle aggregation but not long enough for evaporation problems to ensue. Due to the concentration disparity of D29 PCR product between the two types (resistant vs susceptible TB strains) by limiting the number of PCR cycles (so that no TB growth led to insufficient replication of phage, so that PCR of those starting copies DID NOT yield a peak), and limiting the aggregation time to 90 seconds to ameliorate evaporation as a problem, we could quickly determine whether or not D29 phage was present.

3.3.4.2 PCR cycling limitations

Conventional qPCR amplification of a 254 base pair region from D29 bacteriophage genome, millimoles of target DNA is produced, regardless of starting template mass [17]. The limit of detection for HIA has been reported to be as low as femtomolar [9], indicating detection of target DNA won't be limited by sensitivity. Instead, HIA's sensitivity will

cause any D29 PCR product to hybridize to the probes, aggregating the particles following 40 cycles of PCR. After reviewing the qPCR data from this process [1], we believed that, by reducing the number of PCR cycles, exponential growth of D29 PCR product for non-viable TB cell samples could be avoided. PCR was performed using TB cells known to have prevented D29 replication by the addition of a drug and also on viable unaffected cells, for 25, 30, or 40 cycles and the amplicon peak height measured by electrophoresis. The data demonstrates that, regardless of cycle number, the replicated and amplified phage in a drug-resistant sample (few TB cells destroyed) produces an amplicon peak height greater than 100 RFU (**Fig. 6A)**. However, the effective drug has killed sufficient TB cells, preventing phage replication, and producing a small amplicon peak height after 30 cycles of PCR, with no discernable peak after only 25 cycles (**Fig. 6B**). With this information, it

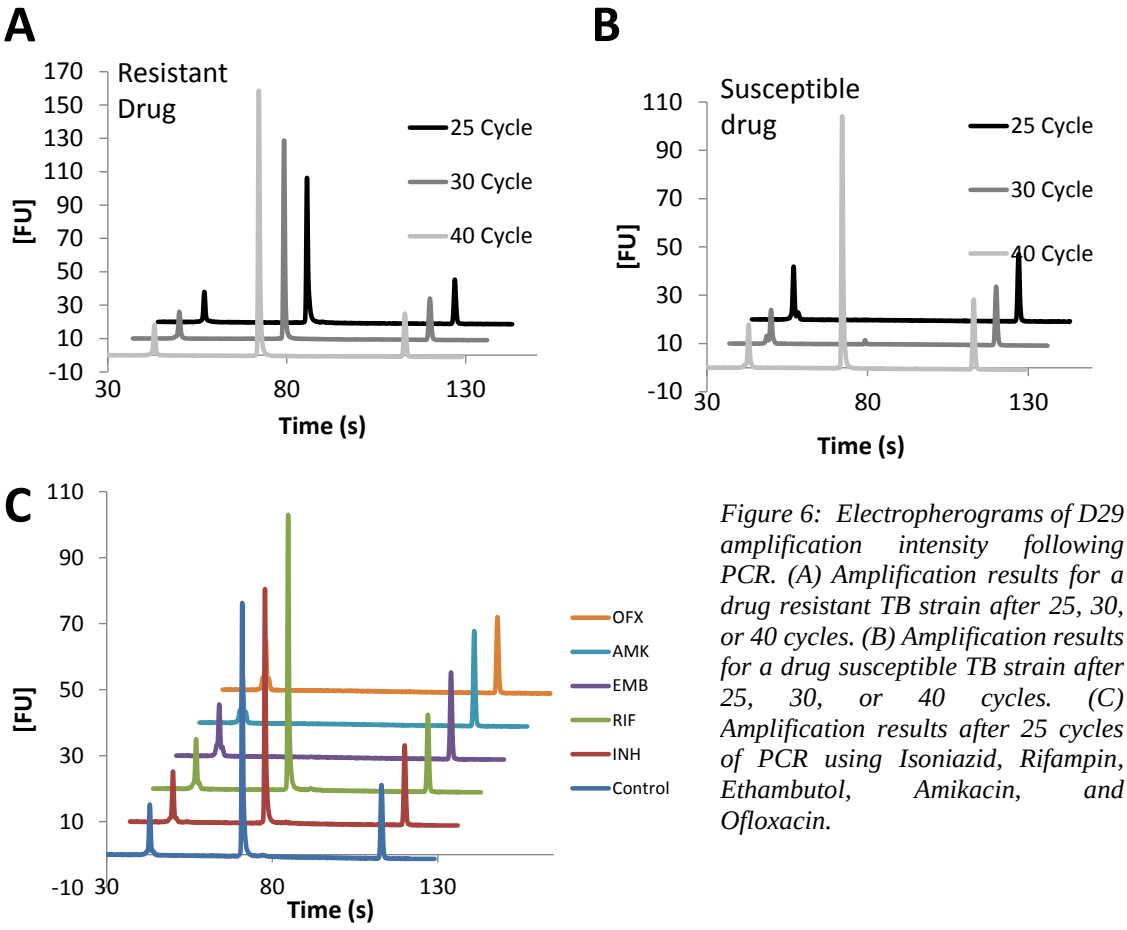

Figure 6: Electropherograms of D29 amplification intensity following PCR. (A) Amplification results for a drug resistant TB strain after 25, 30, or 40 cycles. (B) Amplification results for a drug susceptible TB strain after 25, 30, or 40 cycles. (C) Amplification results after 25 cycles of PCR using Isoniazid, Rifampin, Ethambutol, Amikacin, and Ofloxacin.

was determined that this PCR protocol (25 cycles) could provide a 'digital' response. That is, a resultant PCR peak of the appropriate size indicates the TB strain was resistant to the drug, thus few cells were destroyed, the phage replicated and will be confirmed by HIA with a visible aggregate. The converse applies to a susceptible TB strain; minimal phage replication, no exponential growth of 254 bp product with 25 cycles of PCR and will be confirmed by no visible aggregation by HIA. To verify that this digital response is produced by controlling amplification cycles was not drug dependent, TB cells and D29 incubated samples from a single patient were exposed to five common TB drugs (antibiotics): isoniazid (INH), rifampin (RIF), ethambutol (EMB), amikacin (AMK) and ofloxacin (OFX), and the 254 bp of D29 phage was amplified using the 25 cycle PCR protocol. RIF and INH were both characterized as ineffective, while EMB, AMK and OFX were classed as effective drug therapies (**Fig. 6C**); this was consistent with previous qPCR results. This demonstrated that limiting the number of PCR cycles for amplification of phage-specific product, provided a qualitative readout where PCR product was only observed with samples containing TB cells that were unaffected by the select drug.

3.3.4.3 HIA Aggregation threshold

Using the same patient isolate samples from **Figure 6**, the optimized protocol described above (25 PCR cycles; HIA at 56 °C for 90 seconds) was used to determine the HIA aggregation threshold for classifying the ability of a drug to kill a strain of cells. As stated previously, in theory, the control sample (optimal opportunity for phage replication) should contain the largest number of phage as there is no drug affecting the TB cells. From this control sample, we calculated the 'maximum aggregation' for the sample set through

digital image analysis of the aggregate[21], and this was used as the 'aggregation threshold (AT)' for determining the resistance to each drug. A tighter aggregation can be observed from a sample where greater phage replication occurred. Any aggregation that was greater than or equal to the control AT was classified the TB cells as resistant, while those below the AT were classified the cells as susceptible. The 90 second HIA assay results show that the isolates treated with INH and RIF had an aggregation greater than the AT, indicating drug resistance. Samples treated with EMB, AMK, and OFX produced less aggregation than the control AT, indicating susceptibility (**Fig. 7**). These results mirror those found with electrophoresis (refer to **Fig. 6C**) and qPCR, with the cells classed as resistant to INH and RIF, and susceptible to EMB, AMK and OFX. Although this correlation is a preliminary validation of the HIA detection method, a much larger sample size of cell strains was needed to truly verify the capabilities of the technique.

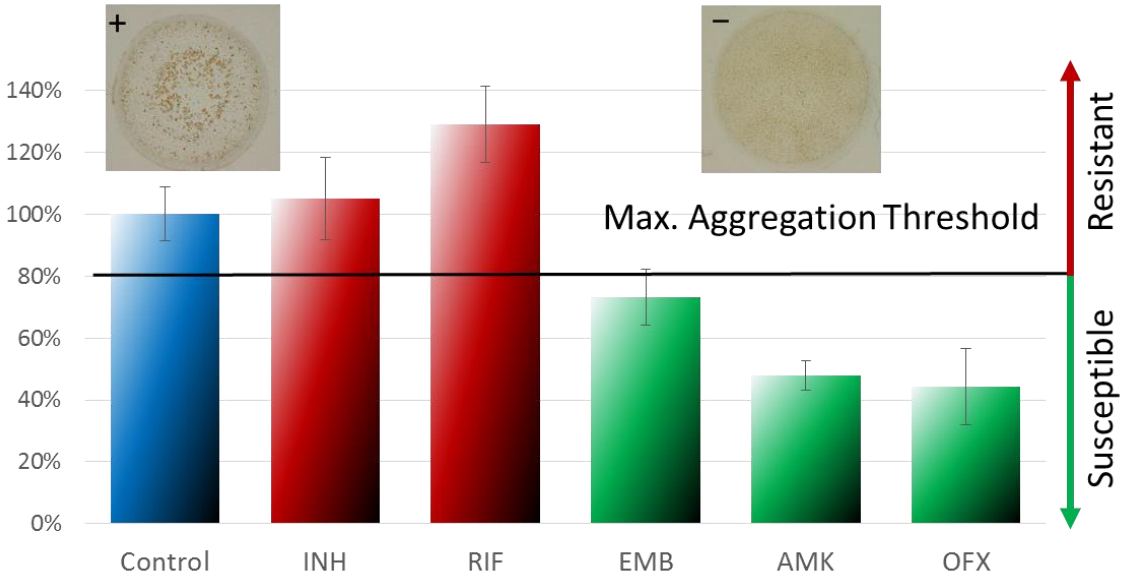

Figure 7: HIA response with 1 μL of product after 25 PCR cycles. HIA assay performed at 56 °C for 90 seconds. Error bars represent n=3. + digital image for a resistant response and − image for a susceptible response.

3.3.4.4 HIA detection compared to qPCR

TB positive isolates were taken from 35 patients, split into six 500 µL aliquots and each treated with either NIH, RIF, EMB, AMK or OFX, with no antibiotic to the sixth aliquot as the control. This provided 175 samples and 35 controls, all of which were amplified for 25 cycles and the 254 bp product was probed by HIA for detection. Based on the HIA response and the maximum aggregation threshold method, the TB strains in the patient isolates were classified as resistant or susceptible to each of the five drugs. The HIA threshold for drug resistant TB cells was determined by observing any aggregation exceeding 80 % of Max Aggregation relative to the control. Results from independent qPCR analysis of the same samples were compared with the HIA results and scored as '–/–', '–/+', '+/–', or '+/+', where e.g., '+/–' represents sample cells classified as 'resistant' by qPCR but 'susceptible' by HIA (**Fig. 8**). Overall, this novel method was able

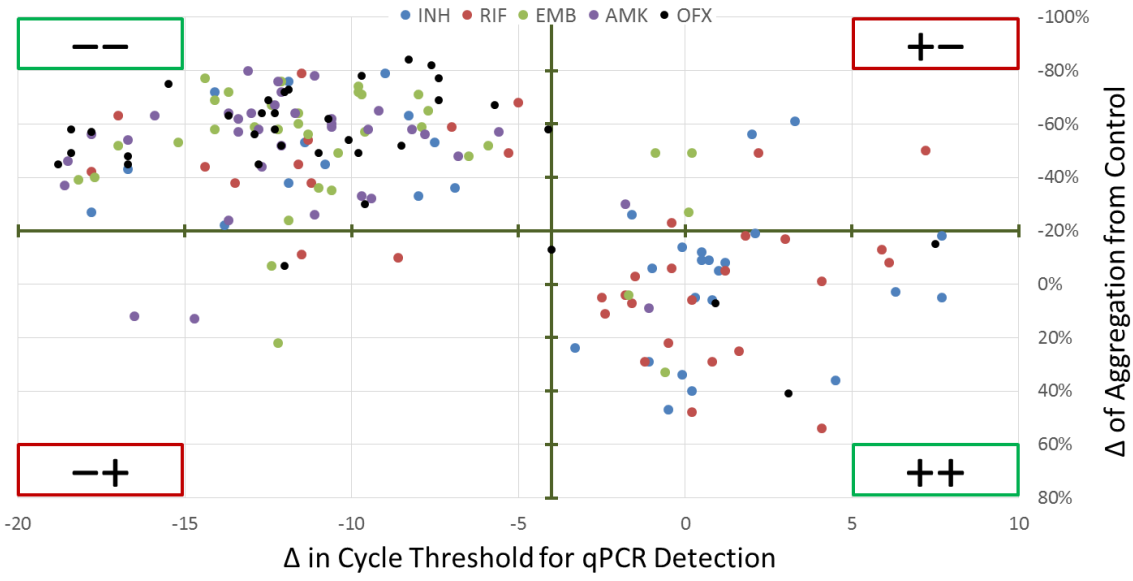

Figure 8: Graphical analysis comparing two detection methods for the D29 phage assay; qPCR and HIA. Position of the axes corresponds to the set threshold for each method to distinguish resistance or susceptibility. Results from the qPCR and HIA assays were scored as "-/-", "-/+", "+/-", or "+/+", representing the classifications given by the two methods (e.g., "-/-" means the strain was classified as "susceptible" by both methods; "-/+" means the sample was classified as "susceptible" by qPCR and "resistant" by HIA to a given drug)

to correctly classify 155 of 175 drug treated patient isolate aliquots for an accuracy of 89 % using the optimized conditions (25 PCR cycles; 90 second HIA detection), compared to 95 % (164 of 175 correct) for qPCR. There were discrepancies. Seven samples of the 35 (4%) were classified as resistant by HIA but susceptible by qPCR, while 10 strains (5.7%) were classified by HIA as susceptible but resistant by qPCR. The obvious types of 'classification' errors – 'false positive resistant' and 'false positive susceptible' – have different clinical consequences. Falsely classifying a susceptible strain as resistant is less problematic, since the patient will still be treated with a drug cocktail. Falsely classifying a resistant strain as susceptible is obviously more problematic, since the patient could potentilly be treated with the incorrect drug cocktail. Although the HIA method is slightly less accurate than qPCR, this offers discrete advantages as an alternative method from the perspective of time, cost and labor.

It is valuable to compare the qPCR and HIA results to the gold-standard traditional 'culture-based agar proportion' test results for these isolates in order to gauge the overall accuracy of the two methods. Assuming the agar results were accurate, qPCR and HIA called 9 and 20 of 175 strains incorrectly, respectively (**Table 1**). Of those, qPCR classed

Method	# Correct	# False	% Accuracy	Misclassified	
				Res	Sus
Agar	175	0	100	0	0
Phage qPCR	164	9	95	2	7
Phage HIA	155	20	89	13	7

Table 1: Comparison of accuracy of 3 methods with data collected from 35 patient samples. This data assumes the Agar results to be 100% accurate. A false result occurred when classification of resistant/susceptible does not agree with the agar result.

8 samples (4.7%) incorrectly as susceptible (thus leading to superfluous drug treatment), while HIA identified 13 samples (7.4%) as susceptible, again, adversely influencing patient care. While HIA had a lower accuracy (higher error rate), with TB, drug therapies are

given in parallel as a cocktail, from both qPCR and HIA results, no patient would have been given a drug combination that did not contain an effective antibiotic. Therefore, patient care is not adversely affected, but testing does limit the number of drugs a patient takes, minimizing side effects and cost.

3.3.4.5 Development of assay for IR-PCR

While HIA is in its infancy as a detection modality, these results provide encouragement that HIA might function as an end point detection in a POC diagnostic testing platform for MDR-TB. With a view towards this goal, we sought to miniaturize PCR and integrate it with HIA on a single microdevice. From the perspective of 'chemistry', the main challenge is adapting the tube-based PCR protocol for successful microdevice-based amplification. Our group has had success at such adaptations, creating microdevices that allow for sub-microliter volume PCR (substantially reduced from the standard 25 µL reaction volume). Using this knowledge base, the additional polymerase (3X) and primers (2X) were added to the master mix. To further decrease cycling times, commercially-available polymerase, *SpeedSTAR*™, with kinetics a higher extension rate and better processivity was chosen as a replacement for *AmpliTaq Gold*® (used to optimize the tube-based amplification of D29 DNA). This, in combination with infrared-mediated (IR) cycling[1, 2], enabled miniaturization of the PCR (from 25 µL to 2 µL) and allowed the thermocycling to be completed in under 30 minutes; this represents an ~5-fold reduction in time relative to the conventional method. Recall how the number of PCR cycles (25; **Fig. 6**) was critical for distinguishing the number of viable TB cells in resistant versus susceptible samples. For

the microfluidic PCR method, it was established that 27 cycles was optimal for producing that result, as determined by electrophoretic separation (**Fig. 9**).

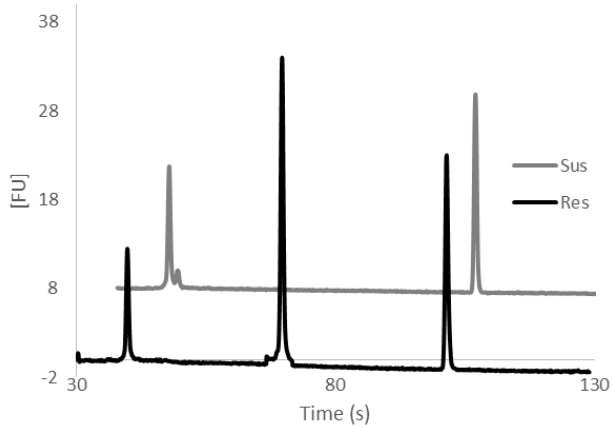

Figure 9: Electropherogram showing amplification intensity following 27 cycles of on-chip PCR, with a resistant sample (black) and a susceptible sample (grey).

3.3.4.6 Integration of IR-PCR and HIA detection on a single microdevice

An approach for interfacing PCR and HIA on a single plastic microdevice is described in full in **chapter 4**. In that work, three 2 µL PCR chambers are symmetrically located in the focal spot of an infrared heating source used to induce low volume thermocycling (**Fig. 10**). Once PCR is completed, the PCR product is migrated through a passive geometric valve, via torque-actuated pressure into the HIA chambers for detection. Each HIA chamber is filled with buffer and particles and interfaced with an individual magnetic field to enable rapid aggregation. Each aspect of the device is designed to require minimal hardware and ease of use. The device is multiplexed, allowing for three integrations to be run simultaneously, allowing for a negative and positive control for visual comparison of the HIA aggregates to the sample (**Fig. 10**). With the same patient isolates as used in **Figures 6 and 7**, each drug sample was analyzed in duplicate, with negative and positive controls, for a total n=10 (10 devices for 5 drugs). Using the same data analysis process as described above and setting the control as 100% max aggregation, the integrated PCR-

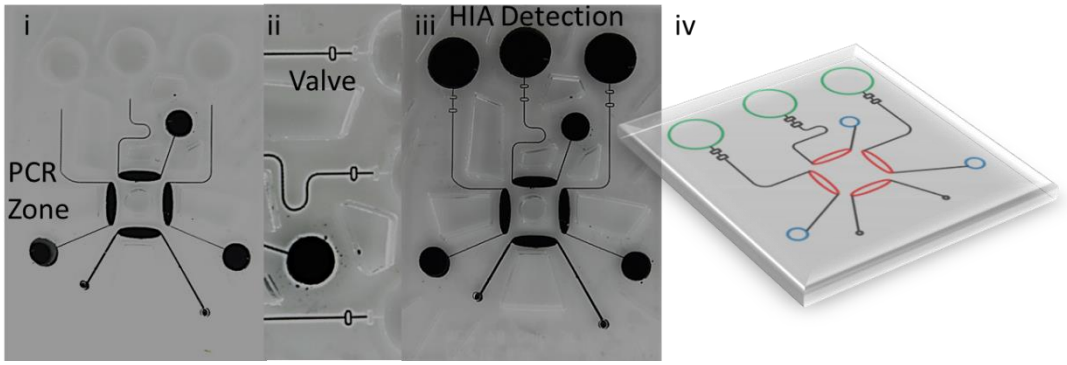

Figure 10: (i-iii) Birdseye photographs of the integrated microdevice used for the microfluidic based assays. iv) Scheme of an integrated microdevice with a PCR region (red) and a HIA detection region (green).

HIA device yielded qualitative results, correctly classifying the TB strains as resistant or susceptible for a given drug (**Fig. 11**). This shows encouraging progress over the conventional qPCR method as it is cost-effective and the total analysis was completed in under 32 minutes (30 min PCR + 1.5 min HIA), representing a ~5-fold reduction in analysis time. Combining D29 phage replication with a microdevice-based PCR and HIA detection is a first step towards generating a universal POC diagnostic device for MDR-TB.

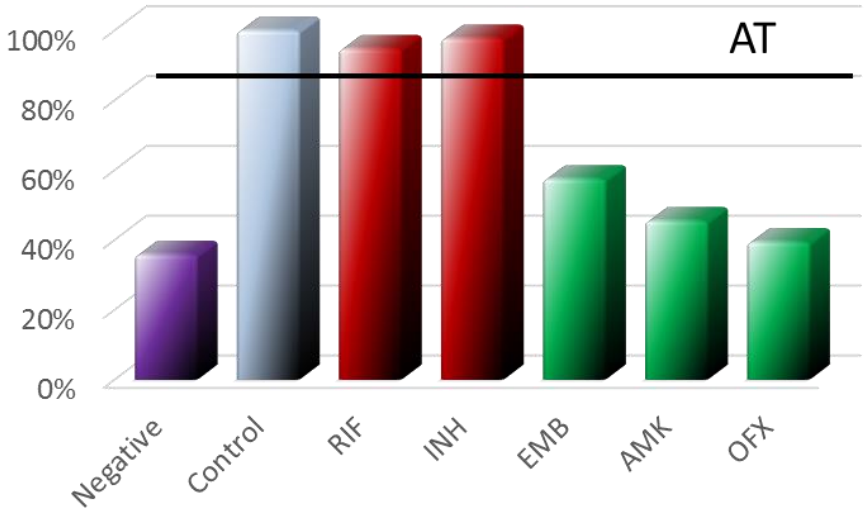

Figure 11: Results from 10 integrated runs, each with a positive and negative control, and two integrated runs for each device

3.4 Conclusions

This work demonstrated key progress towards delivering a universal, rapid, accurate POC diagnostic test for determining the drug susceptibility of MDR-TB strains. Initially, we established a 25-cycle PCR protocol for limiting the amplification of a 254 bp section of D29 phage so that only strains resistant to TB drugs were detectable through electrophoresis. To enable particle driven detection through hybridization, previous hardware was adapted to incorporate a heating modality, allowing for the detection of D29 PCR product using HIA in just 90 seconds, without the need for fluorescence tags. Using the degree of aggregation from a control sample, a threshold was set where any sample aggregate that was $\leq$ 80 % of the control was deemed to have responded to a given drug therapy. Analysis of 175 patient isolates showed an 89 % correlation between the classifications made using the D29-PCR-HIA method and conventional agar proportion. The PCR protocol was adapted to a multiplexed plastic microdevice, interfacing PCR and HIA, creating the first step towards a portable rapid POC diagnostic device. For each of the five drug treated D29 phage samples, the integrated device correctly classified the TB strains as resistant or susceptible to a given drug in only 32 minutes, a ~5-fold reduction in analysis time compared to qPCR. Although a fully integrated MDR-DST TB device may be far in the distance, this work marks the first steps towards this goal a as proof-of-principle microdevice.

3.5 References

1. Leslie, D.C., et al., *Journal of the American Chemical Society,* 2012. **134**(12): p. 5689-5696.
2. Donovan, J.W. and K.D. Ross, *Biochemistry,* 1973. **12**(3): p. 512-517.
3. Sandgren, A., et al., *PLoS Med,* 2009. **6**(2): p. e1000002.
4. WHO, *Tuberculosis*, W.H. Organization, Editor 2013.
5. Ramaswamy, S. and J.M. Musser, *Tubercle and Lung Disease,* 1998. **79**(1): p. 3-29.
6. Jin, D.J. and C.A. Gross, *Journal of Molecular Biology,* 1988. **202**(1): p. 45-58.
7. Banerjee, A., et al., *Science,* 1994. **263**(5144): p. 227-230.
8. Musser, J.M., et al., *Journal of Infectious Diseases,* 1996. **173**(1): p. 196-202.
9. Pholwat, S., et al., *Journal of Clinical Microbiology,* 2012. **50**(3): p. 754-761.
10. Hemvani, N., V. Patidar, and D.S. Chitnis, *International Journal of Infectious Diseases,* 2012. **16**(5): p. e332-e336.
11. McNerney, R., et al., *Journal of Clinical Microbiology,* 2004. **42**(5): p. 2115-2120.
12. Sz-Hau, C., et al., *NanoBioscience, IEEE Transactions on,* 2009. **8**(2): p. 120-131.
13. He, Y., et al., *Analytical Chemistry,* 2010. **82**(17): p. 7169-7177.
14. Parab, H.J., et al., *Biosensors and Bioelectronics,* 2010. **26**(2): p. 667-673.
15. Park, S.-J., T.A. Taton, and C.A. Mirkin, *Science,* 2002. **295**(5559): p. 1503-1506.
16. Sato, K., K. Hosokawa, and M. Maeda, *Journal of the American Chemical Society,* 2003. **125**(27): p. 8102-8103.
17. Chin, C.D., V. Linder, and S.K. Sia, *Lab on a Chip,* 2012. **12**(12): p. 2118-2134.
18. Hillemann, D., et al., *Journal of Clinical Microbiology,* 2011. **49**(4): p. 1202-1205.

19. Yi Sun, Y.C.K., Nam-Trung Nguyen, *Journal of Micromechanics and Microengineering*, 2006. **16**(8).

20. SantaLucia, J. and D. Hicks, *Annual Review of Biophysics and Biomolecular Structure*, 2004. **33**(1): p. 415-440.

21. Roper, M.G., et al., *Analytical Chemistry*, 2007. **79**(4): p. 1294-1300.

4 Development of an integrated microfluidic device for IR-PCR and HIA detection

4.1 Introduction

The sensitive and specific identification of nucleic acid (NA) targets, commonly referred to as nucleic acid testing (NAT), is central to the fields of clinical diagnostics, food safety, forensics and environmental microbiology. NAT incorporates powerful amplification and detection technologies, which often require complex operational steps and expensive, complex instrumentation . Such resource-intensive processing limits the use of NAT assays to skilled personnel in centralized laboratories, and presents challenges for its use at the point-of-care (POC). However, important applications, such as pathogen detection in remote environments and time-critical diagnostics, require assays that can be performed in POC settings . The profound impact promised by a truly portable POC NAT device has attracted extensive efforts toward the development of POC-compatible NAT technologies .

Substantial advances toward a POC NAT device involve the transition of amplification and detection strategies onto a microfluidic platform [8]. Microfluidic assays offer the advantages of rapid analysis, low power consumption, and functional integration of multiple analytical processes [9]. By exploiting the strengths of microfluidics, microdevice-based NAT is capable of being low cost, portable, and easy to use, which are qualities that are critical for implementation at POC.

As the amount of NA recovered from either sample preparation or from the raw sample is usually too low for immediate identification, therefore, a method of amplification is required. Among the various nucleic acid amplification techniques, polymerase chain

reaction (PCR) has been the most popular due to its simplicity and amplification power[10, 11]. Various micodevices capable of PCR have been demonstrated, where thermal management is achieved using either contact or non-contact type heaters . Many contact type heaters such as thin films, metal heating blocks, and Peltier units are commercially available at low cost and are thus widely adopted[9, 11]. However, non-contact methods are more favorable for simple chip designs as they provide more flexibility for system integration, do not require fabrication of heaters or temperature sensors, and provide precise heating control . Our group has successfully integrated noncontact infrared (IR)-mediated PCR (IR-PCR) with CE as well as SPE and CE [16] on a single glass device. Recently, we have further exploited IR-PCR on a plastic, polymer-based device, integrating DNA extraction with amplification [1, 9]. The advantages of IR-PCR – a simple, rapid, and inexpensive approach to microdevice-based amplification - provide a solid platform for a functional POC NAT device. An additional factor to consider when choosing a PCR method is the ability to multiplex the processing of samples. Multiplex PCR affords reliable detection, as controls can be included to eliminate false negatives due to failed amplification or failed sample preparation.

Amplified DNA can be examined at the end of the amplification reaction (end-point detection) or while the reaction is progressing (real-time detection). A plethora of well-established and novel strategies have been demonstrated on a microdevice, most commonly employing fluorescence-based technology . Despite the fact that these detection methods have been adapted for a microfluidic platform, most are unsuitable for implementation at POC as a result of the relatively expensive and complex instrumentation required. An appropriate detection method would require minimal peripheral instrumentation and

provide a simple output for interpretation. As such, visual detection methods, such as lateral flow techniques, are a welcome tool for POC applications [17]. **Chapters 2 and 3** reported a novel particle-driven hybridization-based visual detection technique on a microfluidic platform, called hybridization-induced aggregation (HIA) [1]. HIA utilizes a pair of oligonucleotide probes that are complementary in sequence to the target DNA. The probes are individually-immobilized on the surface of paramagnetic particles (via biotin-streptavidin conjugation), and their interaction with target DNA is facilitated by a rotating magnetic field (RMF). The hybridization of the target sequence to the probes induces aggregation of the particles, which provides a visual confirmation that the target DNA is present in the sample, in minutes post-PCR. A significant advantage of the HIA method is that it is able to differentiate target-specific amplicons from non-specific amplification products, which adds an additional level of specificity to the NAT assay. The inherent simplicity and specificity of the HIA technique makes it an ideal approach for end-point detection on a NAT device.

Although numerous techniques for microdevice-based amplification and detection have been demonstrated, the integration of both analytical procedures onto a single device in a cost-effective, robust, and user-friendly format remains challenging. Most of the practical devices that have been reported are single-function, owing to the technical obstacles involved in combining these functionalities while maintaining low cost and simplicity [5]. Notable challenges facing the integration of amplification and detection processes are related to microfluidic control and device operation [18]. Necessary fluid handling and actuation nearly always requires the use of complex and bulky peripherals, such as large gas tanks and syringe pumps, which are not amenable to POC devices. A true POC

platform should have compact actuating controlling modules for easy operation and high portability.

In this chapter, we integrate multiplex IR-PCR and HIA-based detection onto a single microdevice without the need of external macro apparatus. Fluid control is achieved using a passive approach, which leverages differences in fluid behavior from varying microchannel geometries in capillary systems [19]. This control mechanism is especially suitable for use at POC, as it does not require external power and moving off-device parts. Fluid actuation is achieved with torque-actuated pressure (TAP), using small, easily-manipulated machine screws to provide elastomeric deflection [20].

We demonstrate the utility of our integrated NAT device with the rapid detection of the zoonotic pathogen *Salmonella enterica* from a pre-purified sample. The substantial public health and economic burden associated with *Salmonella enterica* emphasizes the need for a POC NAT device to enhance timely recognition and intervention [21]. Our integrated NAT device facilitates the sensitive and specific identification of *Salmonella enterica*, in a simple, rapid, and low-cost format. This work represents exciting strides toward the development truly portable POC NAT device.

4.2 Materials and Methods

4.2.1 Microdevice design

Four ellipsoid PCR chambers (dimensions, 0.5 mm deep) are symmetrically oriented within the 1 cm^2 focal spot of the halogen lamp for IR-PCR to allow even heating across all chambers. Three of the PCR chambers are each connected to a separate TAP inlet (1.33 cm radius, 1 mm deep) and HIA detection chamber (5mm radius, 1 mm deep). Along each of the channels connecting the PCR and HIA chambers (14 mm long, 150 µm wide, 170 µm deep), there are two adjacent oval-shaped capillary burst valves (170 um deep) Though only one valve is functionally necessary, and additional valve is added to account for any fabrication failure that may cause the first valve to fail. The channels are designed such that the HIA chambers are vertically aligned.

4.2.2 Chip and discrete magnetic field Fabrication

A VersaLASER system 3.50 from Universal Laser Systems (Scottsdale, AZ) was used to fabricate the microdevices, ablating 0.5 mm thick PMMA purchased from Astra Products (Baldwin, NY). AutoCAD was used to design unique microdevice architecture in each of the three layers. These were then thermally bonded using established methods creating a microdevice of 1.5 mm thick[13, 15, 16]. The discrete magnetic field was fabricated in the same manner from 1.0 mm PMMA from Astra Products. Three MAGNETS were enclosed in the PMMA using a layer of adhesive film. Each was placed directly under each of the HIA detection wells. Channel depths were calculated using Zeiss Axio A1 microscope fitted with a 5X objective.

4.2.3 Reagents

Dynabeads MyOne Streptavidin C1 paramagnetic beads were purchased from Invitrogen (Carlsbad, CA). Biotinylated oligonucleotides were purchased from Eurofins MWG Operon (Huntsville, AL). Potassium chloride and ethanol were purchased from Fisher (Fair Lawn, NJ). 2-Amino-2-(hydroxymethyl)- 1,3-propanediol (Trizma base, 99.9%) was purchased from Sigma (St. Louis, MO). All solutions were prepared in Nanopure water (Barnstead/Thermolyne, Dubuque, IA). SpeedSTAR™ polymerase, magnesium chloride and 10X PCR buffer, is available from Clontech Lab. (Mountain view, CA)

4.2.4 Biotinylating Oligonucleotide Probes to Particles

Particles were prepared according to the manufacturer's protocol. Final suspension buffer: 500 µL of 200 mM potassium chloride, 10 mM Trizma base, pH 7.5.

4.2.5 PCR protocol

An initial hold at 95 °C for 2 min, 32 cycles of 95 °C for 5 sec, 60 °C for 15 sec, and 72 °C for 20 sec, followed by a final hold at 72 °C for 2 min. Non-integrated assays were then removed from the microdevice and the product was separated and detected using an Agilent 2100 Bioanalyzer (Agilent Technologies, Inc., Santa Clara, CA)

4.3 Results and Discussion

4.3.1 Multiplex IR-PCR

Our previous reports on IR-PCR-based devices are limited in sample throughput demonstrating only single-sample amplification . Here, we extend our previous work to allow for the simultaneous amplification of multiple samples on a single plastic microdevice. A multiplexed PCR capability allows for the inclusion of on-chip controls, obviously allowing us to flush out false negatives due to failed amplification or failed sample preparation; this enhances reliable detection. Multiplex analysis also facilitates easy interpretation of the results by unskilled personnel, where side-by-side visual HIA comparison with a positive and negative control allows for the immediate classification of the sample.

To achieve this, four ellipsoid PCR chambers were symmetrically orientated within the 1 cm^2 focal spot of the halogen bulb (defined by the height of chip above the bulb), where the fourth chamber was used for temperature control (**Fig 1A**). Each chamber is 50 mm in

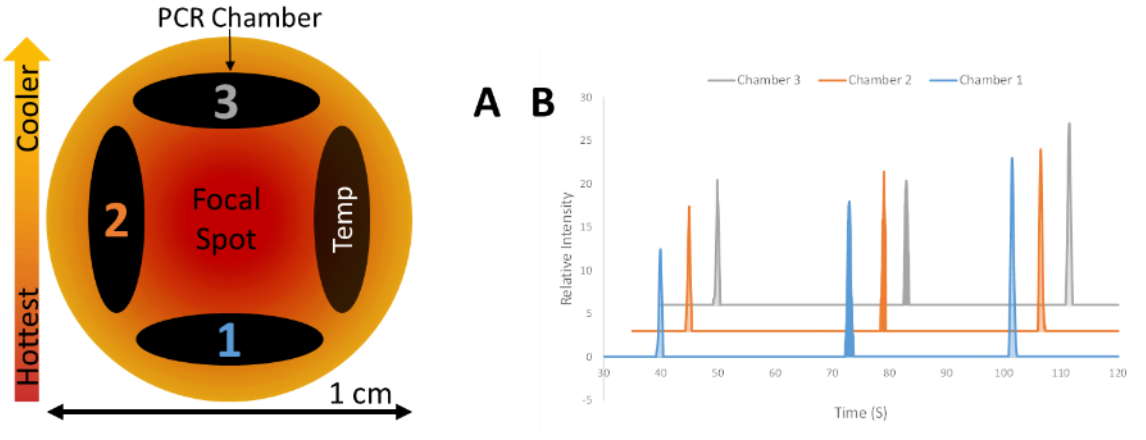

Figure 1: Design and results of multiplex PCR with a halogen bulb. A) Scheme of PCR chamber symmetrical arrangement around the focal spot of the halogen bulb. The 1 cm diameter represents the hottest section, providing fast heating rates. Each PCR chamber is sized to scale. B) Electropherograms of multiplex IR-PCR amplification of a 278 bp region of salmonella enterica. Lightly shaded peaks are the 15 and 1500 bp markers respectively. Each chamber position corresponds to those in A.

length and 12.5 mm wide. The 0.5 mm depth of the PCR chambers was determined by the thickness of the commercial poly(methylmethacrylate) (PMMA) used to create three layers in the microdevice. This depth was chosen so that the top two layers could create a HIA detection chamber with a 1 mm depth, matching the chamber dimensions in previous work where this was shown optimal for ssDNA (see **Chapter 2**)[22]. With these defined parameters, each PCR chamber was calculated to have a volume of 2 µL. To verify that the focal spot would heat the PCR amplification mixture equally, each chamber temperature was measured simultaneously with independent thermocouples and characterized to have the same temperature within ± 2 °C (data not shown). The efficiency of the amplification was assessed by measuring the relative intensity of the 278 bp amplicon from pre-purified *Salmonella enterica* in each of the three sample chambers, using electrophoresis (**Fig. 1B**). Consistent peak height results across all chambers of ~15 fluorescence units, confirmed that the efficiency of PCR in each chamber was comparable and unaffected by the subtle inter-chamber temperatures (**Fig. 1B**). Note, these values are not quantitiative, but by measuring the area under the peak an approximate DNA concentration can be obtained. These microchip PCR's produced 3 ng of amplified DNA, compared to 5 ng in a conventional 25 µL tube-based amplification. Therefore, we felt confident that the efficiency of the PCR was consistent from chamber to chamber, provided that the amount of starting DNA template is equivalent and, thus, the PCR chamber location is irrelevant to the final detection signal observed by HIA.

4.3.2 Sealing and pressurizing the microdevice

Previously, we have shown that the ablated surface PMMA is coarse, thus, prone to bubble formation [20]. Sealing and pressurization of the device was required to prevent bubble expansion, which would otherwise drive the PCR reagents out of the chamber during thermal cycling, causing PCR to fail. In previous work, sealing and pressurization was achieved using biocompatible film for qPCR and a PMMA manifold; however, this was applied to seal inlets with a radius of 0.5 cmand proved insufficient for our TAP inlets with nearly 3X the surface area (1.33 cm radius) (**Fig. 2A**) [16]. Therefore, an additional sealing component was required to prevent bubble expansion. Additional pressure was applied through placement of a septa (used to seal sample vials in CE) above the inlets; the septa silicon coating prevented any sample loss through the bio-film pores, and was easily deformedwith the application of the mechanical screw for fluid actuation (see section, 4.3.4). The combination of bio-film, septa and a PMMA manifold successfully minimalized bubble expansion in the PCR chambers at 95 °C, allowing PCR to be performed successfully (**Fig. 2B**).

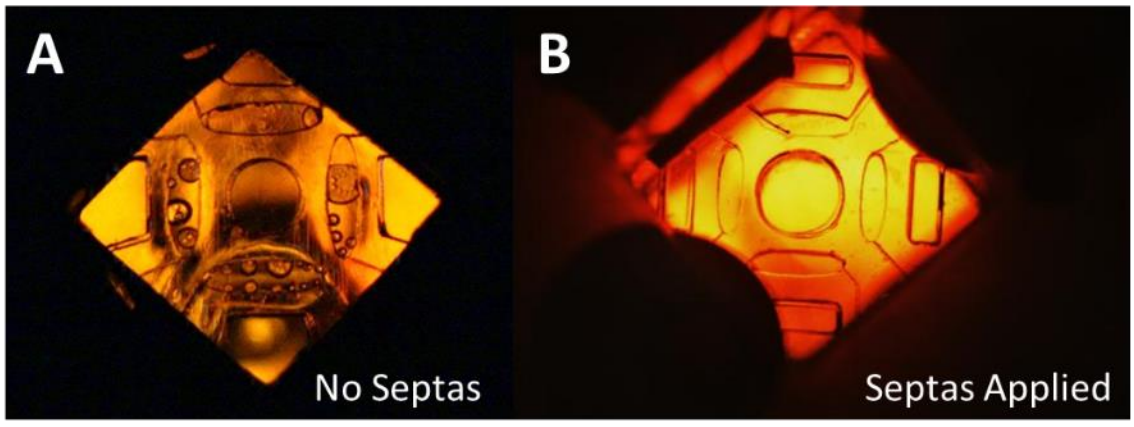

Figure 2: Birds-eye photographs of the PCR chambers at 95 °C. A) Bubbles are seem in the PCR chambers when no septa is applied. B) No bubbles are visible to the naked eye with the addition of a septa for additional pressurization. To seal microdevice: fill with reagents, cover with biofilm and apply septa's with manifold. Screw to tighten and pressurize.

4.3.3 HIA particle stability at elevated temperature

As stated in **chapter three**, the avidin-biotin complex tethers the probe to the bead, and this is susceptible to dissociation at temperatures above 90 °C. Therefore, we considered a design change to keep the particles isolated from direct irradiation (heating) from the halogen bulb (IR source). To measure the maximum possible HIA buffer temperature during denaturing at 95 °C, a simple device was fabricated with a two linear microchannels; each contained a thermocouple for temperature sensing. The first was placed in the center of the 1 cm^2 focal spot and feedback-controlled to maintain 95 °C, the maximum temperature used in PCR for the denaturing of DNA. The second thermocouple measured the buffer temperature 0.2 cm from the edge of the focal spot, the distance representing the closest possible positioning of the HIA chamber relative to the PCR chambers (**Fig. 3A**). The temperature from thermocouple T2 measured ~68 °C, therefore, HIA particles (with biotinylated probes) were held in a thermocycler at 70 °C for 60 minutes (time for IR-PCR) to determine stability at elevated temperatures. The probes chosen for this study were those discussed in **chapter two**, with a 26-mer ssDNA target sequence which readily hybridizes to complementary probes at room temperature.

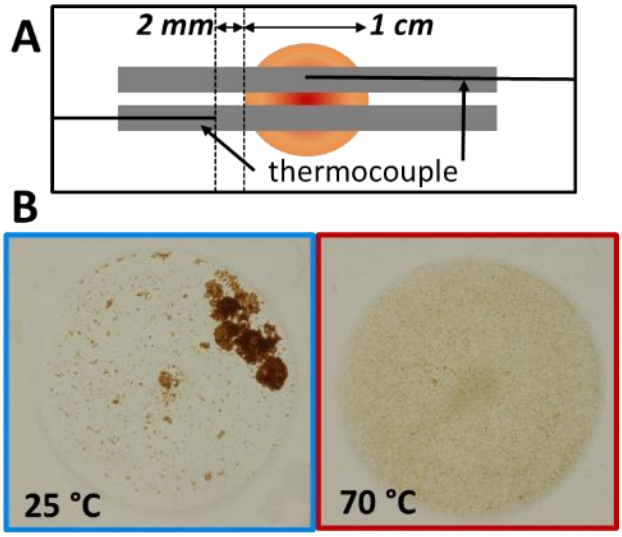

Figure 3: Hybridization results following particle-probe heating. A) Scheme of microdevice used to measure maximum temperature the HIA chambers could reach. Focal spot of the halogen bulb is highlighted in red/orange. B) Results following a one hour incubation at 25 °C and 70 °C with 10 µM of a 26-mer target, which hybridizes at room temperature.

This enabled a non-heated control to be run concurrently. Once the incubation was complete and the heated particles passively cooled to room temperature, 10 µM of the ssDNA 26-mer target DNA was added to two microwells, one with the heated particles and the other with those held at room temperature. As with previous experiments, the particles and DNA were exposed to a rotating magnetic field for 3 minutes, while the microdevice was held in, and agitated by the vortexer. Images of the resulting HIA aggregations from these assays are shown in **Figure 3B**. We observed that the particles heated to 70 °C did not aggregate, while those held at room temperature hybridized readily. Therefore, it was clear that the particles could not be held at elevated temperatures (> 70 °C) for a period of time more than 60 mins without dissociation of the avidin-biotin complex. This required that a device design was required to position the chambers as far from the IR source as possible to maintain the avidin-biotin bonds.

4.3.4 Torque actuated pressure

Following the completion of PCR, the amplified product must be transferred, as a reproducible volume, to the HIA chamber for specific DNA detection. With the aim of avoiding the use of syringe pumps for flow control or any form of external hardware (especially if we wanted this to be low cost, portable and easy to use), we created a torque actuated pressure (TAP) system for fluid actuation. With the use of a 6-32 mechanical screw to provide deflection into the sample inlet, the PCR product is driven through the channel into the HIA detection chamber (**Fig. 4**). The screw placement is kept constant as part of the manifold design to aid in reproducible volume delivery from TAP. The volume dispensed is defined the dimensions of the inlet cavity. We created a cavity with a 1.33

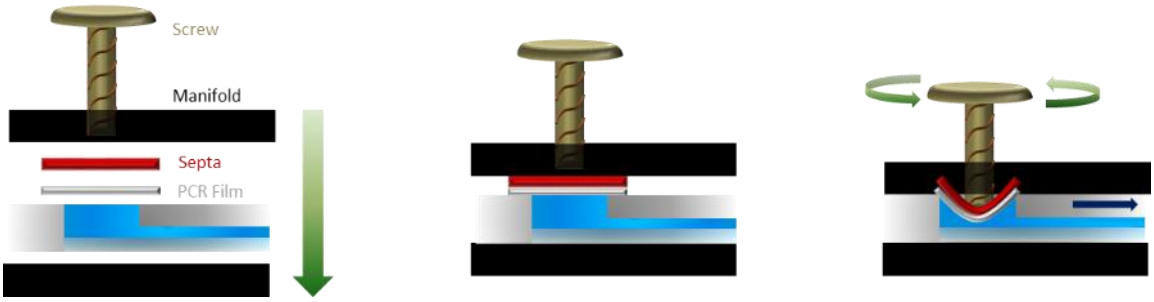

Figure 4: Scheme of TAP configuration and actuation by the depression of the screw, displacing the fluid below in the cavity through the microchannels.

cm radius, 1 mm deep, yielding a total volume of 5.6 µL, to provide a sufficient void for deformation of the bio-film and septa. To verify the intra and inter device reproducibility of the TAP delivery system to mobilize the same volume of fluid , dye studies were performed to measure volume of fluid dispensed (**Fig. 5A**). Blue food dye, representing PCR reagents, was used to fill the inlet, PCR chamber and the channel to the valve, while yellow food dye was used to fill the HIA detection chambers. As blue dye is added to the yellow following TAP, the resulting color difference is measured by a change in hue, which increased proportionally with the volume of blue dye added (**Fig. 5B**). A calibration curve was created by adding 3 µL of blue dye into yellow in increments of 0.25 µL, with a digital image taken, then processed using Mathematica software to determine hue is the sample [17]. Hue will increase as blue is added to yellow, determined by the software processing of the digital image. Three separate trials showed that our TAP system was capable of reproducibly moving 2 µL of fluid into the HIA chamber with a reproducibility of 3% (**Fig. 5B**). Accounting for dead volume in the channel and both capillary valves, 1 µL of PCR product was transferred into the HIA domain. This volume of PCR product was determined to be optimal for HIA[23].

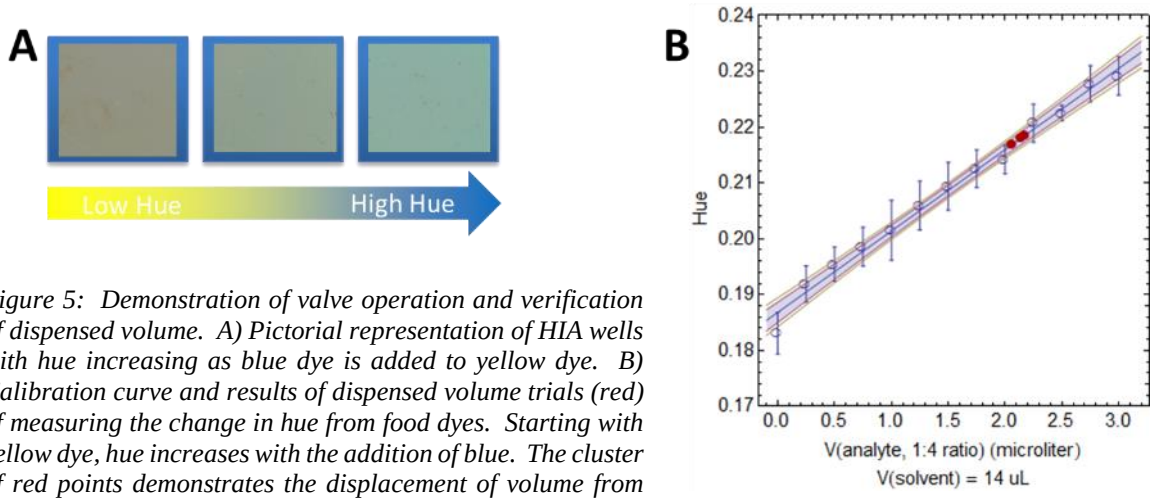

Figure 5: Demonstration of valve operation and verification of dispensed volume. A) Pictorial representation of HIA wells with hue increasing as blue dye is added to yellow dye. B) Calibration curve and results of dispensed volume trials (red) of measuring the change in hue from food dyes. Starting with yellow dye, hue increases with the addition of blue. The cluster of red points demonstrates the displacement of volume from three separate channels.

4.3.5 Integrating PCR and HIA on a single device

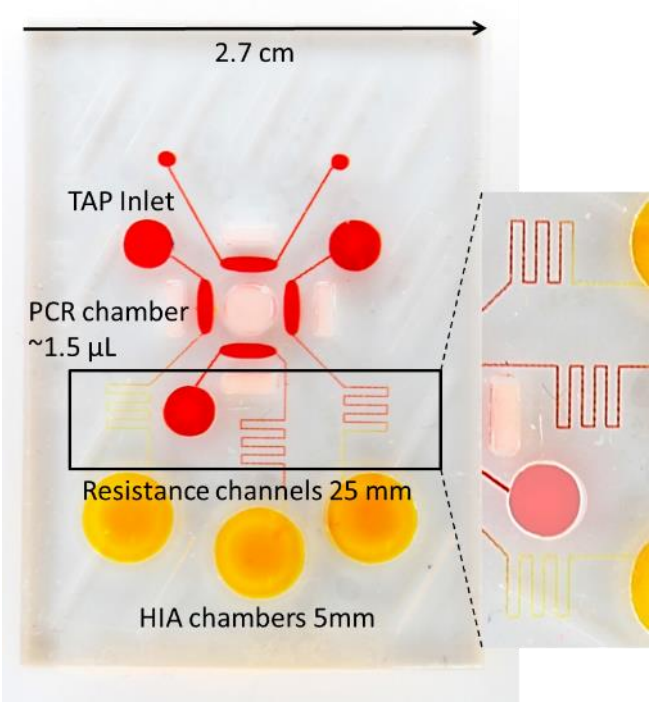

Figure 6: Photograph of an early design on the integrated device to study the diffusion of dyes in a long microchannel. Red dye represents the PCR reagent and the yellow dye, the HIA buffer.

Maintaining the separation the PCR reagents and HIA buffer is paramount to PCR being successful, as dilution of reagents will result in a sub-optimal PCR, possibly increasing the number of false negatives. We believed that since diffusion time is defined by $Length^2/Depth$, the channels would be long enough to prevent significant diffusion and subsequent dilution of PCR reagents. An early version of the device design can be seen in

Figure 6. The PCR and HIA chambers were separated by a 25 mm channel, designed and fabricated without concern for channel volume. The serpentine structure was used to increase the resistance of the channel, to aid in reducing bubble expansion during thermocycling. The PCR chambers, TAP inlets and channels were filled with red dye first, followed by yellow dye to fill the HIA chambers. The device was left uncovered on the bench top for 60 seconds before the photograph was taken (**Fig. 6**). It was clear that significant diffusion had occurred, illustrated by the interconnecting channel being filled with yellow dye. Furthermore, with TAP design affording only 1 µL of dead volume, the connecting channel could only be half the length used here, therefore, diffusion would always lead to a mixing of fluids during an integration. This was confirmed by sealing the microdevice with biofilm and pressurizing with septas and PMMA manifold, with and without IR cycling. In each case, the dyes mixed as a result of diffusion, confirming that a more intricate design was necessary.

4.3.5.1 Capillary burst valve

As you pressurize one area of a microdevice the fluid will move through the path of least resistance. In this microdevice, sealing the TAP inlets causes the undesired movement of fluid through the PCR chamber and down the microchannel into the HIA detection region. This can be avoided by applying even pressure across the device at all times. As required above, concurrently pressurizing the HIA detection and PCR chambers would have proven

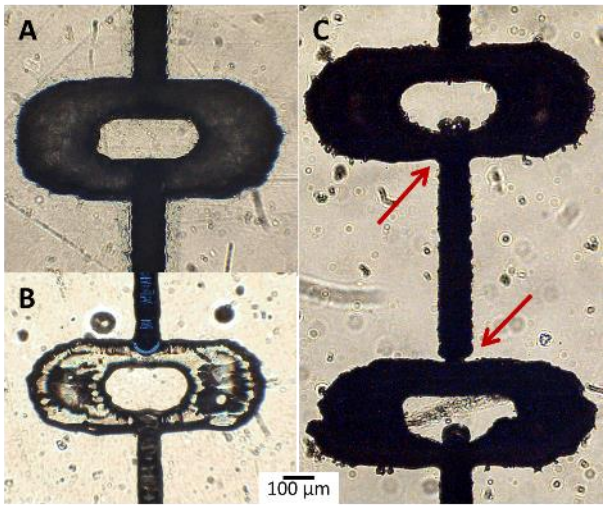

Figure 7: Microscope images of capillary burst valves made by rastering the PMMA surface. A,B) Images of a well aligned valve, preventing fluid flow by surface tension. C) Mis-aligned valve design, red arrows highlight were channel breaks occur.

cumbersome, requiring individual manifolds to be sealed simultaneously over the TAP inlets and HIA chambers. An alternative to a pressurization scheme is to contain the PCR reagents in the channel prior to TAP by introducing a valve into the channel architecture. To maintain simplicity, a geometric capillary burst valve was chosen avoid the addition of a further substrate to create hydrophobic/hydrophilic regions, or complicated fabrication techniques. The basis of our design, stems from the "fishbone valve" which widen a microchannel at a 90° angle to create the necessary surface tension to prevent fluid flow, however, these valves were fabricated with photolithography techniques [17]. Based on this "fishbone" model, and given the constraints of the CO_2 laser ablation for channel features, we fabricated a novel capillary burst valve design (**Fig. 7**). Fabrication of the capillary valve using laser "rastering" was preferred, where the laser sweeps over the PMMA surface rapidly with little power. This creates wide, shallow, smooth channels, with the aim to create increased surface tension by reducing the coarseness associated with vector cuts. Large areas of shallow rastering causes channels to collapse during bonding, therefore, rastering was used sparingly for only the circles and not the connecting channels. However, as shown in **Figure 7C**, fabrication of these valves was problematic as the laser was not designed for precise designs and often misaligned the channels, frequently channels and valves were not

connected. To circumvent this, a single continuous vector cut was chosen, easily reproduced by the laser (**Fig. 8**). Two burst valves were designed into the channel to account for any error in fabrication, ensuring if the first failed, there was a second back-up valve.

To minimize the dead volume, the valve is created with an oval shape and a depth of 170 µm – these were the shallowest channels that could be reproducibly fabricated without the channels collapsing during bonding (**Fig. 8C**). The functionality of the valve in preventing fluid movement with both food dye and PCR reagents was validated by observing the halting of fluid flow once the fluid reached to 90° widening channel (**Fig. 8A,B**). Both fluid types were seen to wick to the valve junction and remain immobile due to surface tension (**Fig. 8B**). The valve was determined to be burst at 0.4 PSI / 2758 pa, ensuring the bursting of the valve occurs only when TAP is initiated (turning the mechanical screw) for fluid movement following PCR (data not shown). With the given volume constrains for channel dimensions (1 µL

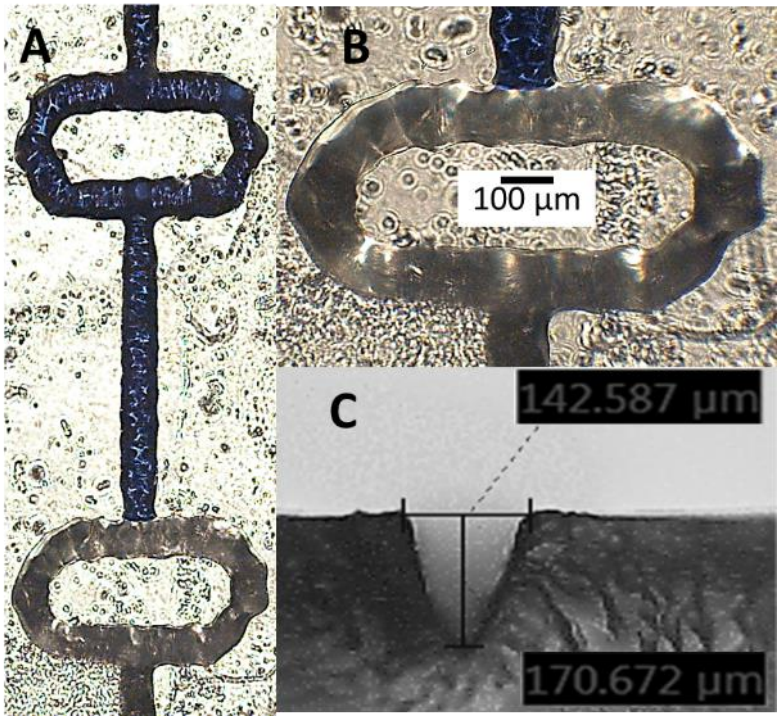

Figure 8: Microscope images of the capillary valve and channel shape and depth. A) Image demonstrating that once valve one is broken, valve two will hold. B) Close-up of the valve preventing fluid flow through surface tension. C) Cross-sectional view of the channel architecture used in the device. All channels are ~150 µm wide and ~170 µm deep.

capacity with channels of 170 µm depth), the HIA chambers were located 10 mm from the edge of the IR focal spot. This distance was sufficient to isolate the HIA detection region of the device from the effects of heating by the IR heat source, with measured buffer temperature rising to of 38 °C during the course of 32 cycles of PCR. Furthermore, sub 40 °C temperatures will not cause bubble expansion in the channels, thus, fluid movement to burst the valve. By combining multiplexed IR-PCR, the TAP and a capillary burst valves in a serial, integrated manner, the microdevice shown in **Figure 9** resulted.

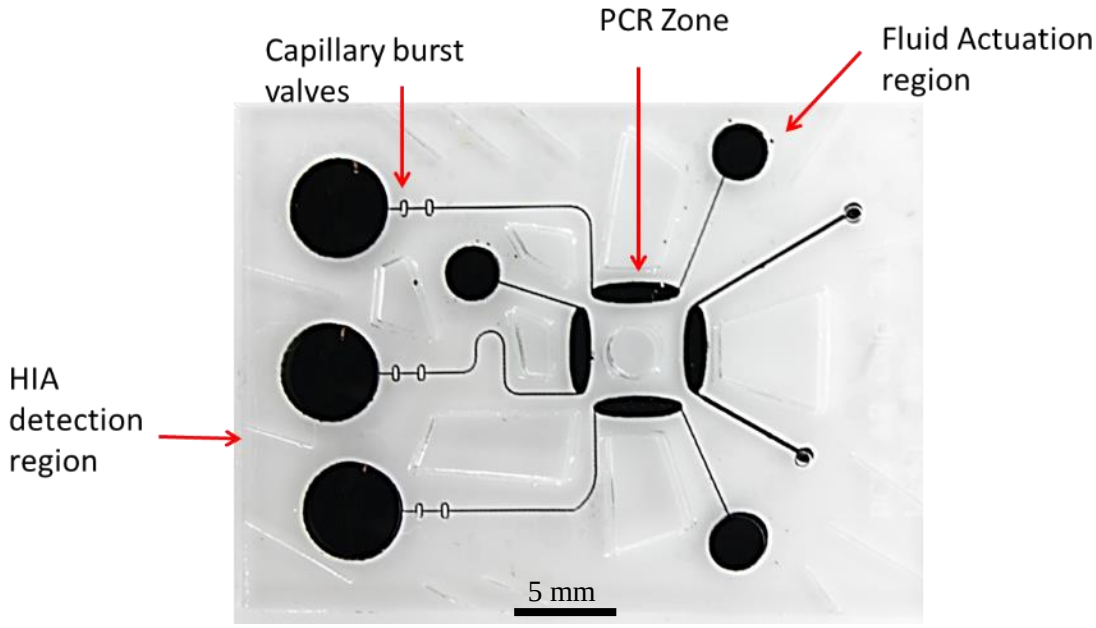

Figure 9: Birdseye photograph of the fabricated plastic multiplex integrated microdevice. Highlighted are the four main components of the device: PCR, capillary burst valve, fluid actuation and HIA detection region.

4.3.5 Discrete rotating magnetic field for HIA

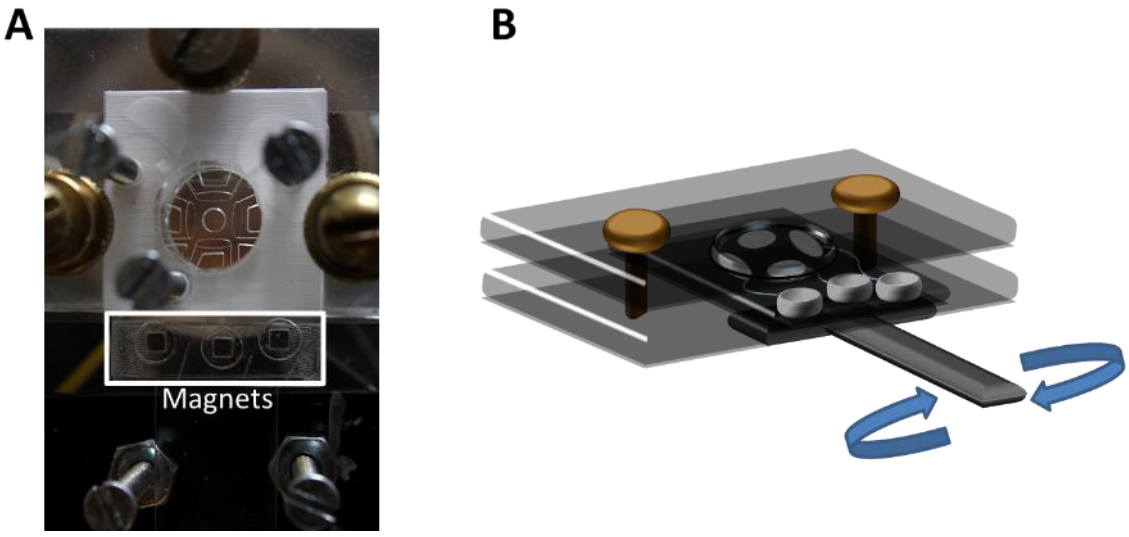

Figure 10: Placement of discrete individual magnetic field for HIA detection. A) Birdseye photograph of the HIA chambers with individual magnets below. B) Scheme of microdevice held in manifold following pressurization with placement of the magnets held in a PMMA cross-T.

Once PCR is completed and 1 µL of PCR product has been moved to the HIA detection chamber using TAP, the oligonucleotide-adducted particles needed to interact efficiently with the DNA to facilitate rapid hybridization. Previously, this was achieved by the application of a rotating magnetic field using a single large magnet to move the particles as a means of enhancing aggregation (described in **chapter two**, DFA) [17]. That system is not possible with this device once the ¼" manifold is affixed, as the magnet cannot be positioned to provide the required magnetic field. Therefore, individual 2 mm^3 neodymium magnets were position under each detection chamber as a separate source of magnetic fields (**Fig. 10A**). The resulting magnetic field has a "Goldilocks" quality, in that it is strong enough to get the particles to move, but not too strong that the magnetic fields are compounding. Furthermore, for the effective aggregation and dispersion of particles in positive and negative controls, respectively, the magnetic field must be rotated [16, 24]. To avoid magnetic cross-talk (magnet from one chamber affecting another chamber), the

radius of rotation for each magnet required confinement to 3.5 mm underneath the 2.5 mm HIA well. This was achieved by embedding the magnets in PMMA, which is connected to a motor for a controlled rotation of 150 rpm (**Fig. 10B**). Applying an RMF in this manner, the particles aggregated within 30 seconds, or remain dispersed in the absence of target sequence, presumably allowing for rapid, specific DNA detection in seconds.

4.3.6 Integrated amplification and HIA detection of salmonella on a single microfluidic device

Following optimization and characterization of the design, the overall functionality of the microdevice as a POC NAT system was demonstrated with the detection of *Salmonella enterica*. Following the same PCR protocol used in **Figure 1B (**and described in *materials and methods*) 32 cycles of IR-PCR was performed in only 35 minutes . In both the positive and "sample" chambers (chambers three and two respectively from **Fig. 1A**), 1 ng of pre-purified bacterial DNA template, while the remaining chamber had no DNA added as the 'no template' control (Chamber 1). Following PCR, the HIA detection chambers were filled with HIA buffer and the oligonucleotide detection particles. TAP was initiated moving the product through the burst valves into the HIA chamber. Immediately following this, the motorized magnets held in PMMA were rotated at 150 rpm for 30 seconds. In addition to visual conformation, the results were further verified by taking birds-eye photographs of the aggregates and analyzed using Mathematica software, to correlate the degree of aggregation with a qualitative 'yes or no' result (see **chapters two** and **three** for more detail). The greater the extent of aggregation of the particles, the greater the concentration of amplified DNA in the sample (**Fig. 11A**). The software filters out the background, so only the aggregated particles are considered and counted as 'pixels' (**Fig**

11B). Following analysis, it was determined that the sample containing *Salmonella* DNA was as aggregated to the same extent as the control sample, confirming the presence of *Salmonella enterica* in the sample (**Fig. 11C**). These experiments represent the first instance of integrating PCR with HIA detection on a single microdevice for a bacterial target relevant to environmental safety.

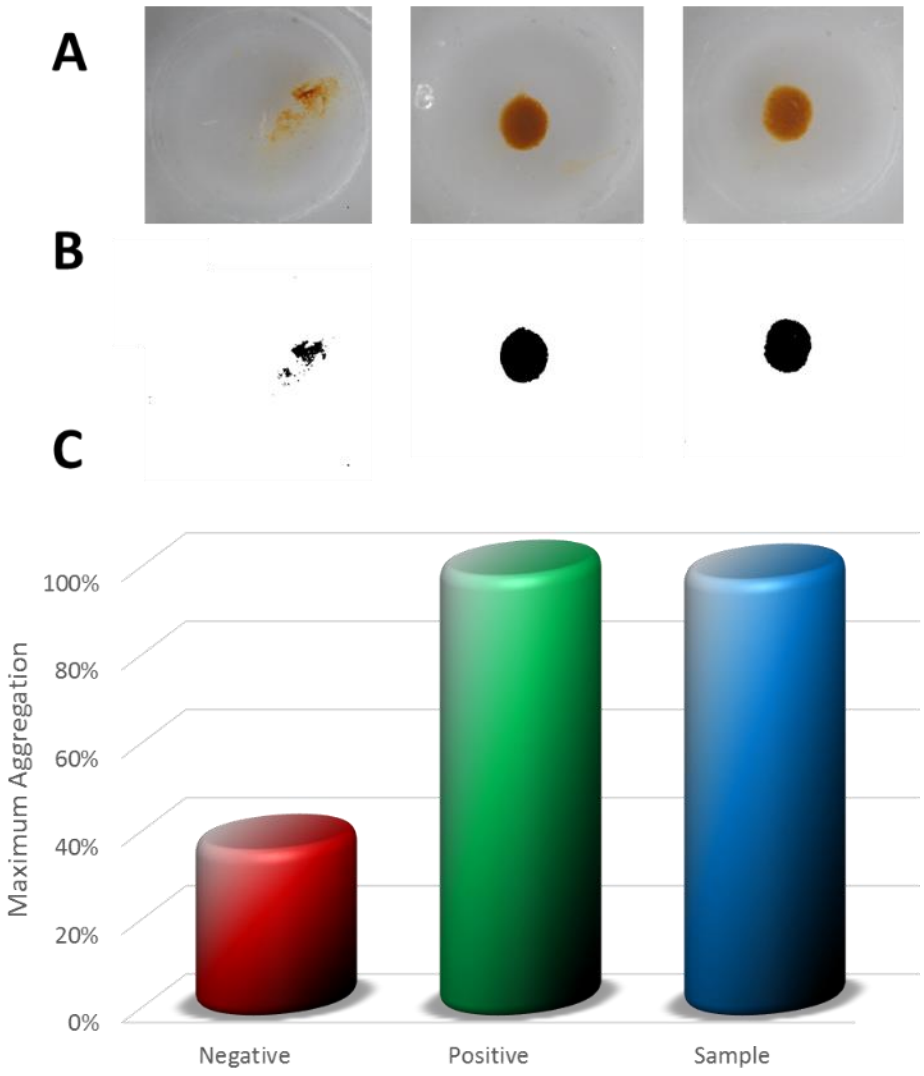

Figure 11: Results from integrated runs for the detection of salmonella enterica. A) Photographs of HIA aggregation following 30 seconds of applied RMF. B) Images of the aggregations being converted into pixels for a semi-quantitative aggregation response. C) Bar graph generated from software analysis of the aggregation photographs. For n=3 % CV for negative, positive and sample are 5, 9 and 8% respectively.

4.4 Conclusions

This work described key advances for the future integration of chemical processes on a single microdevice suitable for POC NAT. Initially, we have successfully demonstrated IR-PCR with a halogen bulb to be multiplexed for the first time, enhancing the throughput of this technology by 66%. Bubble expansion during 95 °C PCR denaturation, caused by coarse nature of laser ablated PMMA microdevices, was eliminated through additional pressurization of the device by septas, normally used in capillary electrophoresis. Highly functional simplistic fluidic control was established, for preventing and initiating fluid flow. First, TAP was created and shown to reproducibly transport 2 µL upon the turning of a mechanical screw. Secondly, a burst valve was fabricated into the PMMA, minimizing dead volume and providing adequate surface tension to prevent fluid flow. Novel isolated rotating magnetic fields were created for specific DNA detection in 30 seconds, a 10-fold reduction in detection time. These advances conjugate to facilitate the interfacing of PCR and HIA for the first time, delivering assay results for the successful detection of *Salmonella enterica* in under 35 minutes. These results are a significant step to creating a functional, portable, easy to use POC microdevice for bacterial organisms. The versatility of this device will be utilized further, exploring targets of forensic and clinical value.

4.5 References

1. Niemz, A., T.M. Ferguson, and D.S. Boyle, *Trends in Biotechnology,* 2011. **29**(5): p. 240-250.
2. Holland, C.A. and F.L. Kiechle, *Current Opinion in Microbiology,* 2005. **8**(5): p. 504-509.
3. Duarte, C., et al., *Biomedical Microdevices,* 2013: p. 1-10.
4. Yager, P., G.J. Domingo, and J. Gerdes, *Annual Review of Biomedical Engineering,* 2008. **10**(1): p. 107-144.
5. Lee, T.M.-H. and I.M. Hsing, *Analytica Chimica Acta,* 2006. **556**(1): p. 26-37.
6. Craw, P. and W. Balachandran, *Lab on a Chip,* 2012. **12**(14): p. 2469-2486.
7. Chen, L., A. Manz, and P.J.R. Day, *Lab on a Chip,* 2007. **7**(11): p. 1413-1423.
8. Sia, S.K. and L.J. Kricka, *Lab on a Chip,* 2008. **8**(12): p. 1982-1983.
9. Zhang, C. and D. Xing, *Nucleic acids research,* 2007. **35**(13): p. 4223-4237.
10. Zhang, Y. and P. Ozdemir, *Analytica Chimica Acta,* 2009. **638**(2): p. 115-125.
11. Park, S., et al., *Biotechnology Advances,* 2011. **29**(6): p. 830-839.
12. Lagally, E.T., C.A. Emrich, and R.A. Mathies, *Lab on a Chip,* 2001. **1**(2): p. 102-107.
13. Easley, C.J., J.M. Karlinsey, and J.P. Landers, *Lab on a Chip,* 2006. **6**(5): p. 601-610.
14. Roper, M.G., et al., *Analytical Chemistry,* 2007. **79**(4): p. 1294-1300.
15. Easley, C.J., et al., *Proceedings of the National Academy of Sciences,* 2006. **103**(51): p. 19272-19277.
16. Lounsbury, J.A., et al., *Lab on a Chip,* 2013. **13**(7): p. 1384-1393.

17. Leslie, D.C., et al., *Journal of the American Chemical Society*, 2012. **134**(12): p. 5689-5696.

18. Chin, C., et al., *Low-Cost Microdevices for Point-of-Care Testing*, in *Point-of-Care Diagnostics on a Chip*, D. Issadore and R.M. Westervelt, Editors. 2013, Springer Berlin Heidelberg. p. 3-21.

19. Weibel, D.B., et al., *Analytical Chemistry*, 2005. **77**(15): p. 4726-4733.

20. Patterson, A.S., et al., *Appl Environ Microbiol*, 2013. **79**(7): p. 2302-11.

21. Yi Sun, Y.C.K., Nam-Trung Nguyen, *Journal of Micromechanics and Microengineering*, 2006. **16**(8).

22. Lounsbury, J.A., et al., *Journal of Micromechanics and Microengineering*, 2012. **22**(8): p. 085006.

23. Lu, C., et al., *Analytical Chemistry*, 2006. **79**(3): p. 994-1001.

24. Lounsbury, J.A., et al., *Forensic Science International: Genetics*, 2012. **6**(5): p. 607-615.

5 Development and application of a direct PCR assay for TPOX detection by HIA on whole blood using a microfluidic device

5.1 Introduction

In forensic science, it is necessary to confirm that a red-brown stain is blood, specifically human blood, prior to further analysis of the sample. Of all the tests available to investigators, none combine the accuracy and specificity required for a cost-effective, user-friendly preliminary test. The polymerase chain reaction (PCR) is a universal method used to provide specific DNA sequences and has numerous applications, including human identification. Direct PCR from whole blood is viewed as highly desirable by the forensic market, as it eliminates the requirement for a separate DNA extraction step in sample processing. Extraction techniques frequently result in 10% sample loss, which can often be the difference between obtaining the suspect's STR profile or not [2]. In addition, DNA extraction is a lengthy process that can take up to two hours and with many physical handling steps, leading to possible contamination [3]. This chapter demonstrates a direct-PCR assay for a 63 bp section of human-specific TPOX locus as a novel modality for scene-of-crime testing for human sample identification. Through interfacing this PCR protocol with the integrated microdevice detailed in **Chapter 4**, whole-blood direct-PCR and HIA identification of the 63 bp TPOX amplicon was completed in 60 minutes.

5.1.1 Preliminary Forensic Blood Tests

Prior to more complex processing of a red-brown stain suspected as blood, a simple test is performed to determine if the sample is serological fluid is of human origin. This is done to ensure that only viable, human DNA-containing samples are carried through the costly

process of STR profiling for human identification. Such tests can be parsed into two categories; presumptive or confirmatory. Presumptive tests are an inexpensive but inaccurate approach to define sample origin, whereas confirmatory tests are expensive, but highly accurate. As shown in **Table 1**, several techniques and chemistries are utilized in

Detecting	Method Class	Available Assays/Methods	Analysis Time	Cost
Whole Fluid	ALS	Polilight®	Seconds	$1-15K
Hemoglobin	Chemiluminescent	Luminal, Fluorscien, BlueStar®	~2 min	$35
	Chemical	Benzidine, Kastle-Mayer, *O*-toluidine, TMB/Hemastix®, LMG	Seconds	$1
	Crystal Test	Teichman, Takayama	1 min	$3
	Spectroscopic	UV-Vis, Fluorescence (hematororphyrin)	~5 min	$5K+
	Chromatographic	PC, TLC	~5 min	$4
Elements	Spectroscopic	SEM-EDX	20 min	$150K +
Isozymes	Immunological	LDH	~5 min	$6
Antibodies	Immunological	HemeSelect™, ABAcard®, HemaTrace®, Hexagon OBTI, Elisa	~2 min	$4-10

***Table 1**: Overview of methods used in the preliminary identification of human blood. Table adapted from Virkler et. al. [5]*

preliminary blood identification. Presumptive methods that rely on the peroxidase-like activity of hemoglobin are popular due to rapid analysis time[4]. However, these assays are prone to false positives by cross-reaction with peroxidases from vegetation and are unable to distinguish between human and animal samples[1]. Furthermore, following application of benzidine to blood, no additional DNA testing can be completed due to cross-linking, while luminol and *Bluestar*® increase the rate of DNA degradation, preventing long-term storage of a sample[5]. Typically, immunological tests are used as confirmatory tests for human blood, utilizing Human Hb-antibodies for detection [6-8]. The most common of these is *ABAcard HemaTrace*, which was commercialized over 15 years ago. The main criticism of these assays is that they are expensive (~$10 a test) and lack of universality (i.e., a different test is required for blood, semen or saliva).

An ideal system would combine the pros from each category: accuracy, inexpensive, rapid. And minimize the cons to produce a preliminary test that can be applied to any serological sample, is rapid, inexpensive, accurate, simple, portable, and robust. .

5.1.2 Blood Resistant Polymerases

The polymerase derived from thermophilic bacterium *Thermus aquaticus*, known as *Taq*, is the most common polymerase used for PCR and genotyping analysis. *Taq*, however, is inhibited by common components from blood (heme), bone (minerals) and soil (humic acid). Through library cloning, modifications to *Taq* have increased the tolerance of the polymerase in blood [9, 10]. This includes the enzyme *Klentaq1*, a *Taq* truncated by a N-terminal deletion of 278 amino acids. This alteration produced an enzyme with a 100-fold improvement in blood volume tolerated to 10% vol/vol. [11]. Other polymerases have a natural resistance to blood inhibition, including *Tfl*, *rTth*, *HotTub* and *Pwo*[12]. However, it has been shown that of these, only *rTh* is capable of amplification in the presence of purified immunoglobin G, indicating other components of blood work cooperatively for successful amplification[13]. Despite research into the structural differences in polymerases and their interactions with inhibitors, the mechanism for successful PCR in the presence of whole blood is not understood[14].

5.1.3 Commercially-available Whole Blood Direct-PCR Kits

Attempts to develop a whole blood direct-PCR kit started in the early 1990's [15, 16], however, it has been only in the last 5 years that commercial kits have become available (**Table 2**).

Manufacturer	Blood Volume	Total Volume uL	Multiplex PCR	Cost $	Single tube
Sigma Extract-N-Amp	10 uL	20	N/A	1.90	no
Kapa Blood PCR Kit	0.5-20%	25/50	yes PP16	1	yes
GenScript BloodReady	1 uL	25	yes 12	1.1	no
Phusion Blood Direct PCR Kit	1-20%	20	N/A	1.2	yes

***Table 2**: Overview of commercial whole blood direct PCR kits currently available.*

Of the four kits commercially-available, only *Kapa* and *Phusion*® offer true direct PCR, i.e., adding the blood sample and initiating PCR without any pretreatment. The *Sigma Extract-N-Amp*™ and *GenScript BloodReady*™ protocols both require a purification of the DNA prior to PCR in a separate tube. Minimal independent research has been carried out with the *Kapa Blood PCR* kit[17, 18], which is the most significant to forensic science as it has been developed with multiplex STR amplification capabilities. To the author's knowledge, it has never been used on a microfluidic device. *Phusion® Blood* direct PCR has been utilized in multiple assays[19, 20] and has been shown to be compatible with microdevice amplification [21].

5.1.4 TPOX as the Target DNA Sequence

There are a plethora of options for genetic targets which are specifically human[22]. Our group has previously developed an assay for the amplication of a 63 bp region of thyroid peroxidase (TPOX) which is well-established in forensic science as human-specific used in identification[23]. The primers used in this work yield a short 63 bp product from the TPOX gene, which is an ideal HIA target as it minimized problems with denaturing often seen with longer targets (discussed in **Chapter 3** as the 238 bp D29 sequence for TB identification).

5.2 Materials and Methods

5.2.1 PCR Protocol and Electrophoretic Detection

All PCR master mixes, including EA1 and buffer concentrations followed manufacturers' protocols. Cycling conditions were as follows: for tube-based amplifications with AmpliTaq Gold - an initial hold at 95 °C for 11 min, 32 cycles of 95 °C for 30 sec, 60 °C for 30 sec, and 72 °C for 30 sec, followed by a final hold at 72 °C for 11 min; for tube-based and microdevice amplifications with *Pwo* polymerase - an initial hold at 95 °C for 2 min, 32 cycles of 95 °C for 30 sec, 60 °C for 30 sec, and 72 °C for 45 sec, followed by a final hold at 72 °C for 2 min; for buccal swab microdevice amplification with SpeedSTAR™ - an initial hold at 95 °C for 2 min, 32 cycles of 95 °C for 5 sec, 60 °C for 15 sec, and 72 °C for 20 sec, followed by a final hold at 72 °C for 2 min. Non-integrated assays were removed from the microdevice and the product was separated and detected using an Agilent 2100 Bioanalyzer (Agilent Technologies, Inc., Santa Clara, CA). Final concentrations or volumes of reagents were, unless otherwise stated,

$MgCl^{2+}$ 3 mM, dNTP's 0.4 μM , 1x PCR buffer, PrepGEM™ CaCl 0.5 uL1x PrepGEM™ blood buffer, EA1 0.25 uL, polymerase 2.5 units.

5.2.2 Microdevice Fabrication and Operation

A VersaLASER system 3.50 from Universal Laser Systems (Scottsdale, AZ) was used to fabricate the microdevices, ablating 0.5 mm thick PMMA purchased from Astra Products (Baldwin, NY). AutoCAD was used to design unique microdevice architecture in each of the three layers. These layers were thermally bonded using established methods, creating a microdevice 1.5 mm thick[24]. The discrete magnet bracket holder was fabricated in the same manner from 1.0 mm PMMA from Astra Products. Three 2 mm^3 neodymium magnets, purchased from Emovendo (Petersburg, WV), were enclosed in the PMMA using a layer of adhesive film. Each was placed directly under one of the HIA detection wells. Following PCR, TAP was initiated to move the fluid to the HIA chambers for detection. The magnetic field was rotated for 30 seconds. A single photograph was taken of each chamber and analyzed through Mathematica software[25].

5.2.3 Reagents

Dynabeads MyOne Streptavidin C1 paramagnetic beads were purchased from Invitrogen (Carlsbad, CA). Biotinylated oligonucleotides and dNTP's were purchased from Eurofins MWG Operon (Huntsville, AL). Potassium chloride, ethanol, magnesium chloride and PCR buffer were purchased from Fisher (Fair Lawn, NJ). 2-Amino-2-(hydroxymethyl)-1,3-propanediol (Trizma base, 99.9%) was purchased from Sigma (St. Louis, MO). All

solutions were prepared in Nanopure water (Barnstead/Thermolyne, Dubuque, IA). EA1 enzyme is available from ZyGEM (Hamilton, NZ). AmpliTaq Gold® was purchased from Life Technologies (Grand Island, NY). SpeedSTAR™ polymerase, magnesium chloride and 10X PCR buffer were purchased from Clontech Lab (Mountain view, CA). Phusion® Blood Direct PCR kit was purchased from New England Biolabs (Ipswich, MA). *Pwo* polymerase was purchased from Roche (Indianapolis, IN). De-identified, discarded human blood samples were provided by Dr. Haverstick and animal blood stains by Dr. Feldman, both of UVa medical center in accordance with current IRB standards.

5.2.4 HIA Probe Sequences

HIA Probes: Forward: 5’ CTTACTCCTGTTCCCTTCCCGTTTTTT - [BioTEG-Q] - 3’

Reverse: 5’ [BioTEG] - TTTTTTCCAATCCCAGGTCTTCTGAACA - 3’

5.3 Results and Discussion

5.3.1 Commercially-available whole blood direct PCR

Initially, chemistry that had been developed previously was utilized and optimized for simultaneous DNA extraction and amplification from whole blood for microfluidic-based amplification. Since the *Phusion*® Direct-PCR kit had been successfully demonstrated on a microfluidic format previously[21], this was chosen instead of the direct kit from *Kapa biosystems*. In accordance with the manufacturer's protocol, the effectiveness of *Phusion*® tube-based PCR for amplification of TPOX was evaluated. Through electrophoresis of the PCR product, it was determined that non-specific peaks in addition to the desired 63 bp TPOX peak were present (**Fig. 1**).

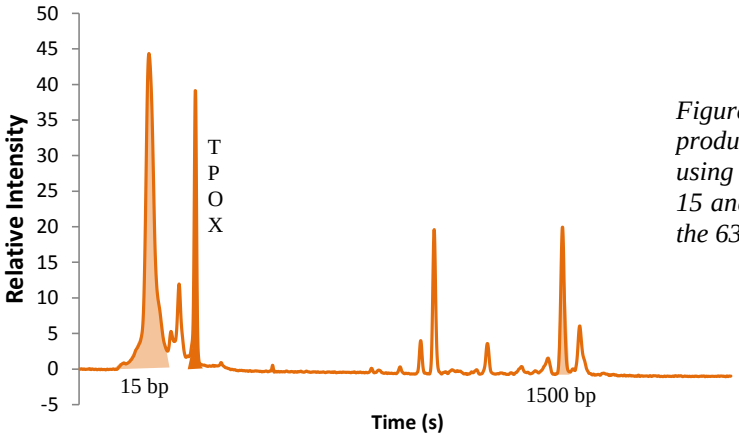

Figure 19: Electropherogram of PCR product from whole blood amplification using Phusion® and TPOX primers. The 15 and 1500 bp markers are shaded and the 63 bp TPOX amplicon is coloured.

These extra peaks could lead to problems when this PCR product is detected through HIA. Although HIA is nonresponsive to non-complementary bases, it is possible that these additional non-specific PCR products contain a base sequence with enough complementarity to generate a false positive aggregation. As a result, an alternative protocol had to be developed in order to minimize non-specific amplification products.

5.3.2 Polymerase performance with EA1

Although proprietary, all of the direct blood PCR kits almost certainly contain a proteinase to breakdown cellular material, enabling DNA to be accessible to the polymerase, dNTP's, etc. Our laboratory has worked extensively with the EA1 enzyme (ZyGEM™) to validate and optimize the performance its ability to liberate DNA from a sample. EA1 is a neutral proteinase, isolated from *Bacillus sp*. EA1, and has been shown to rapidly liberate DNA with high yield [26]. To minimize non-specific amplification, a new direct-PCR master mix was devised using EA1 in addition to traditional PCR reagents.

Taq polymerase is universally utilized in forensic science, specifically *AmpliTaq Gold®*, therefore, trials for compatibility of EA1 with this polymerase were conducted. (**Fig. 2**).

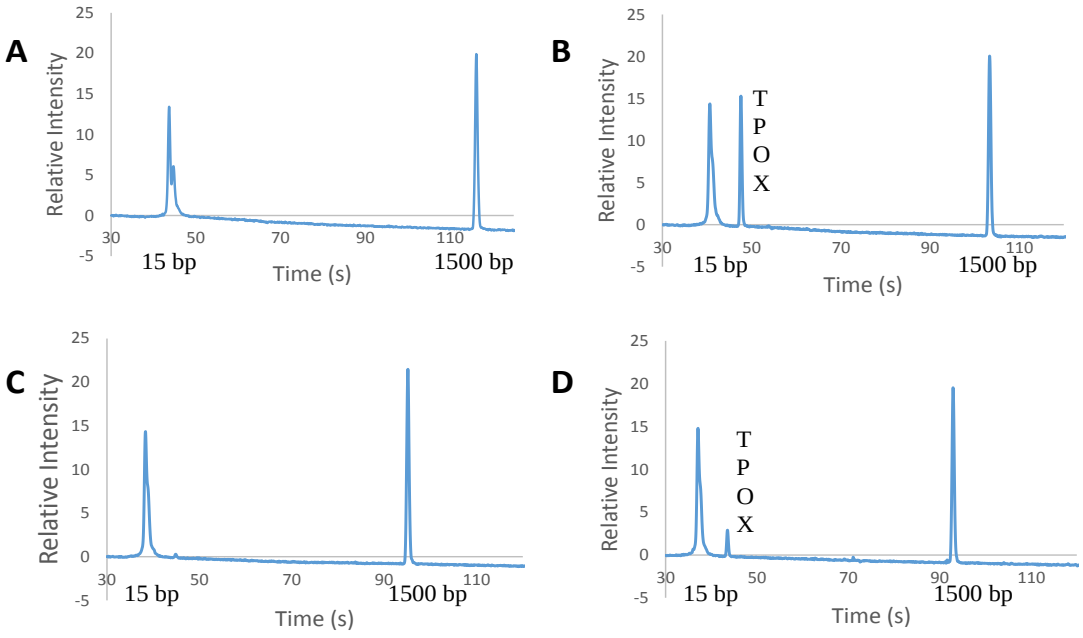

Figure 20: Electropherograms of EA1 and AmpliTaq Gold® combined in a direct-PCR reaction. A) Control with no DNA added. B) Control with 1ng of pre-purified hgDNA. C) 1 µL of whole blood was added as the DNA template. D) 0.5 µL of whole blood added as the DNA template. In each case the electrophoresis 15 and 1500 bp markers are indicated.

It was found that the performance of *AmpliTaq Gold*® was unaffected by the presence of EA1, as shown in **Figure 2B**, where a TPOX amplicon of 15 RFU is seen with 1 ng of purified hgDNA template. When 1 µL of whole blood is added, no TPOX peak is observed (**Fig. 2C**). With 0.5 µL of whole blood, a small amplicon of 2 RFU is seen (**Fig. 2D**). This demonstrates that EA1 enzyme has minimal effect on the efficiency of *Taq* polymerase and that inhibition is due to the components of whole blood. Therefore, an alternative polymerase, one with a defined resistance to inhibitors found in whole blood, had to be used. Previous studies have determined the relative effectiveness of several polymerases in the presence of whole blood[12]. From this study, *Pwo* polymerase was chosen as the enzyme for the in-house direct PCR assay. Using the master mix described in *Materials and Methods*, 1 µL of whole blood was amplified in a single PCR containing EA1 and *Pwo*

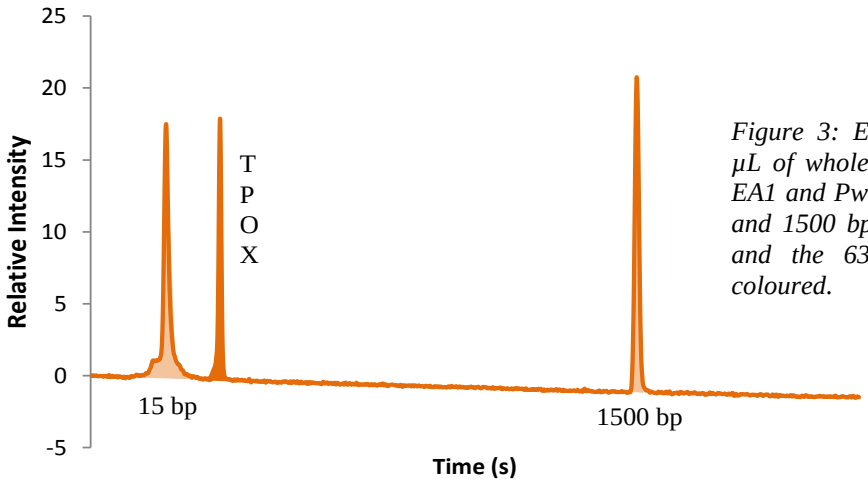

Figure 3: Electropherogram of 1 µL of whole blood amplified with EA1 and Pwo polymerase. The 15 and 1500 bp markers are shaded, and the 63 bp TPOX peak is coloured.

polymerase. Analysis of the resulting PCR product via electrophoresis showed that our modified assay resulted in a single amplicon, with no non-specific amplification (**Fig. 3**). This successful amplification of TPOX confirmed EA1 does not have a negative effect on PCR, and *Pwo* polymerase is resistant to inhibitors in whole blood. To verify that the non-specific amplification peaks from the *Phusion*® chemistry were not sample-related, and to

determine whether peak height was related to template DNA, both *Phusion*® and EA1 *Pwo* master mixes were used to amplify blood samples with varying white blood cell (WBC) counts. In each case, 1 µL of whole blood, with WBC of 4.7, 7.6 or 9.9 x10^3 cells/mL, was added to the mix, amplified and separated through electrophoresis. The *Phusion*® direct-PCR blood kit yielded non-specific peaks in addition to the TPOX amplicon with each amplification (**Fig. 4A-C**). EA1 with *Pwo* did not exhibit any non-specific amplification, and only TPOX amplicon was observed (**Fig. 4D,E**). The data are inconclusive as to whether the WBCs has an effect on peak height of the product.

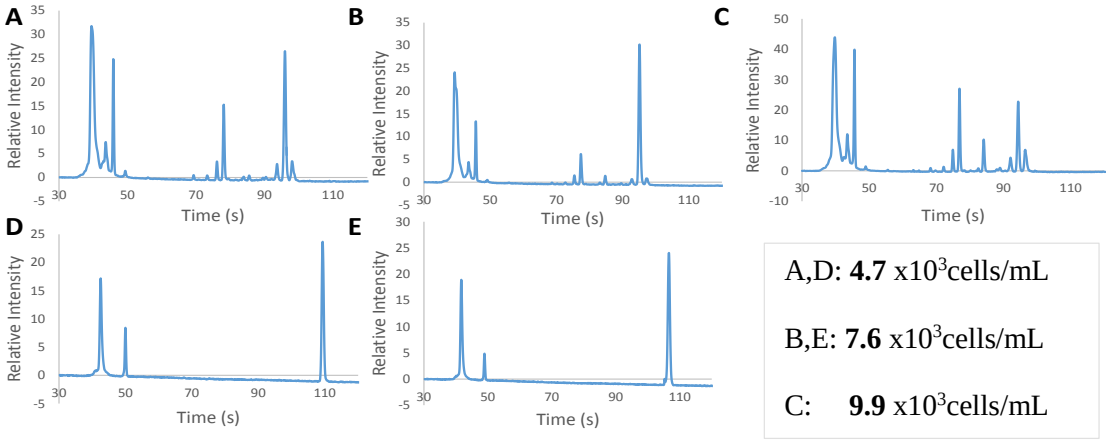

Figure 21: Electropherograms of PCR amplifications of 1 µL of whole blood with varying WBCs. A) 4.7 x10^{3}cells/mL amplified with Phusion Blood Direct-PCR kit. B) 7.6 x10^{3}cells/mL amplified with Phusion Blood Direct-PCR kit. C) 9.9 x10^{3}cells/mL amplified with Phusion Blood Direct-PCR kit. D) 4.7 x10^{3}cells/mL amplified with EA1 and Pwo polymerase. E) 7.6 x10^{3}cells/mL amplified with EA1 and Pwo polymerase.

5.3.3 Whole blood direct PCR from a stained substrate

Once we had established that the EA1:*Pwo* direct-PCR was effective for the amplification of liquid whole blood, it was necessary to evaluate a mock real-life sample. Very few forensic samples analyzed for human identification occur as liquid blood, but rather are generally found dried on a substrate. Four common substrates were used to examine inhibitory effects that the substrate may cause on the developed EA1 and *Pwo* PCR

chemistry. Sections of Whatman™ 3 filter paper, denim, cotton, and cotton-polyester blend were irradiated with short-wave UV light for 30 minutes to degrade any trace DNA. A 10 µL whole blood sample was pipetted onto the substrate and air-dried at room temperature. A 1 cm^2 section was removed and added directly into the PCR tube (**Fig. 5**).

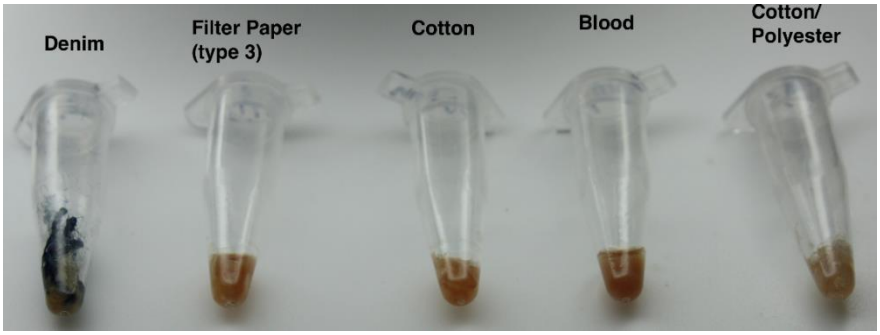

Figure 22: Photograph of substrates added directly to the PCR tube for Direct whole blood amplification with EA1 and Pwo polymerase. Photograph is taken following PCR.

For each substrate, the effectiveness of the amplification was by electrophoresis; these were compared to the liquid blood control (**Fig 6**). It is noted that the migration for the 1500 bp marker for the cotton-polyester sample is not equal to that of the other samples. Further investigation into the cause of the anomoly should be undertaken.

In each case, the substrate did not appear to inhibit the amplification of the DNA as confirmed by the amplification of the 63 bp TPOX PCR product. When compared to the liquid blood control (1 µL), each substrate-based amplification resulted in a lower TPOX 63 bp amplicon peak height. This is due to less DNA template being liberated from the substrate for amplification, and/or loss of active reagents to the substrate through adsorption. The ability to directly amplify DNA from a blood stain is a powerful time-saving tool for rapid analysis, circumventing the need for extraction, streamlining forensic DNA processing.

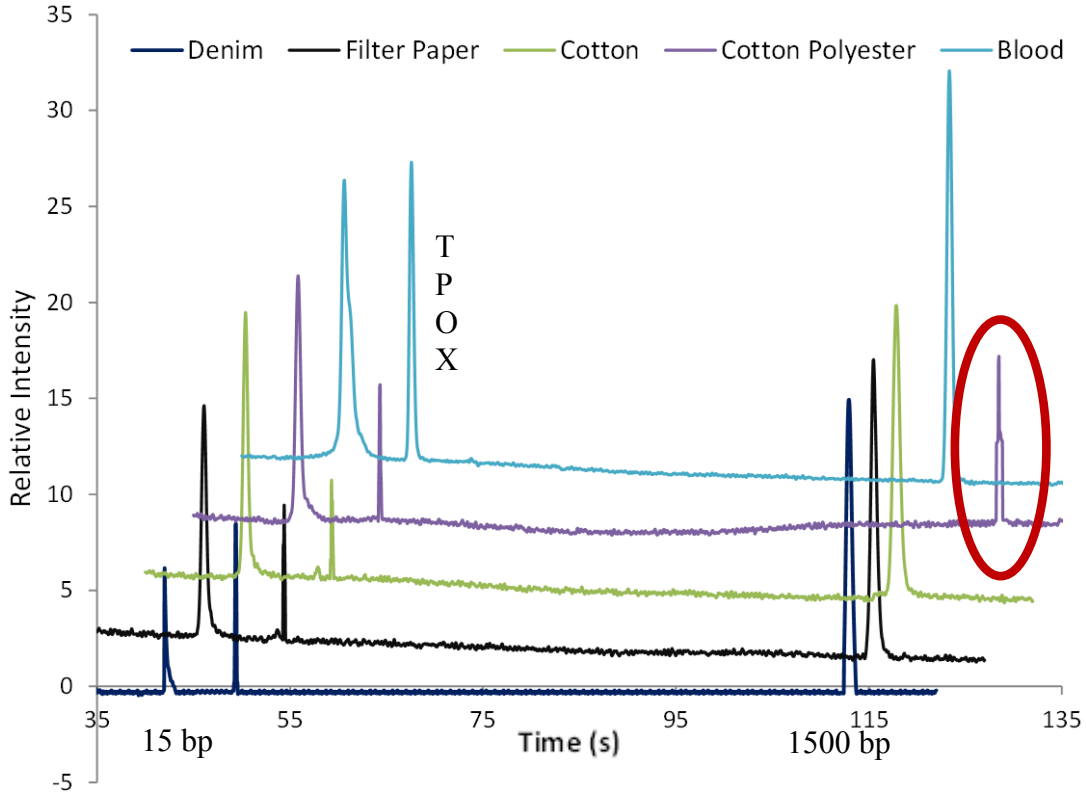

Figure 23: Electropherograms of Direct-PCR of whole blood with EA1 and Pwo polymerase chemistry from dried blood on four substrates: denim, filter paper, cotton and cotton polyester. A 1 cm^2 section of substrate wqas used in each instance. A liquid blood sample was amplified as a control. The same blood sample was used for all experiments. The electrophoresis markers at 15 and 1500 bp are indicated. The red circle around the 1500 bp marker for cotton polyester is highlighted.

5.3.4 Human Specificity

A key purpose in developing this assay was to have the ability to determine whether blood was of human origin. To verify the specificity of the assay, blood samples from six different mammals were amplified using the devised protocol and the PCR product was separated by electrophoresis, with the corresponding elctropherograms compared to the those from a human sample. Blood from pig, rabbit, feline, canine, mouse, and monkey were provided as 100 µL blood stains dried on *Whatman*™ 3 filter paper. The human sample was prepared as before: 10 µL of blood created a stain on *Whatman*™ 3 filter paper

and left to dry. A 1 cm^2 section was removed and added to each PCR tube for Direct-PCR with the EA1 and *Pwo* master mix. As before, the success and specificity of amplification was determined by electrophoretic analysis, which defined the presence of a 63 bp TPOX amplicon. The electropherograms displayed no amplicon from the PCR product with any of the mammal samples other than human, strong evidence that the assay was human specific (**Fig. 7**).

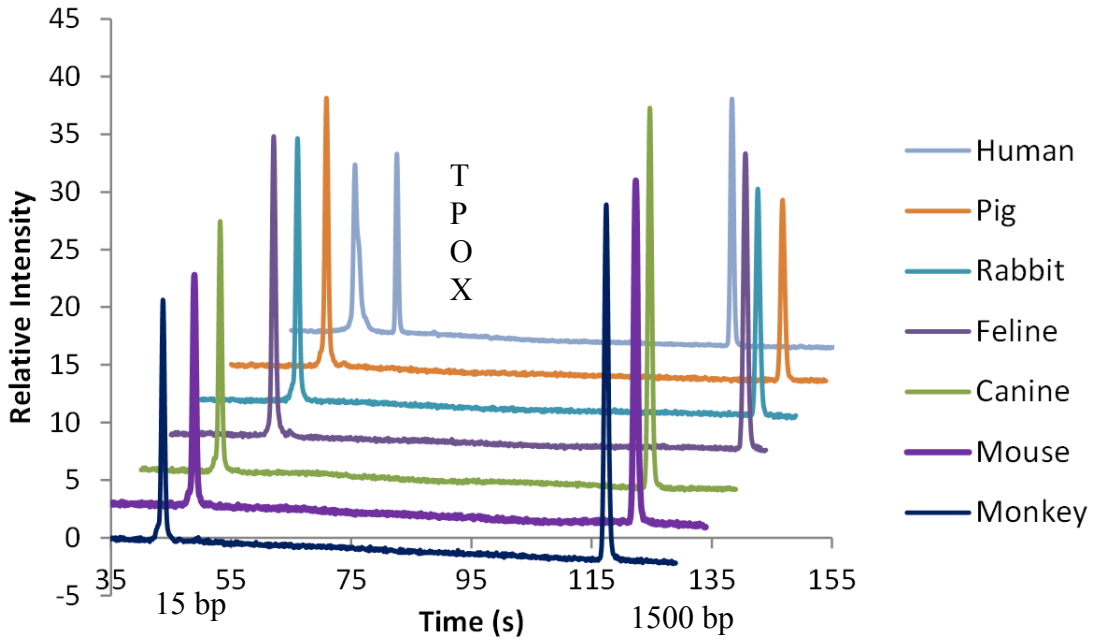

Figure 24: Electropherograms of Direct-PCR Blood amplification from six mammals, compared to a human blood sample. Each sample was provided as a 100 µL dried blood sample on Whatman™ 3 filter paper. The electrophoresis markers at 15 and 1500 bp and TPOX amplicon at 63 bp are indicated.

5.3.5 Microdevice-based Amplification

With an assay capable of human-specific substrate-based amplification established, adapting the protocol to a microdevice became a focus towards the goal of having a rapid test for human-specific DNA. The conventional block thermocycler used for all tube-based

assays, involved an amplification time of 160 minutes, by following the manufactures protocol (see *materials and methods*). An effective method for reducing thermocycling times is to use smaller reagent volumes, and increase the rate of heating and cooling the PCR master mix. Our laboratory has pioneered infrared-mediated PCR (IR-PCR) [27], with the IR radiation provide by a 50 watt halogen bulb. As discussed in **Chapters 3 and 4**, this method of heating is highly efficient, as only the PCR reagents are heated, induced by the vibration of hydrogen bonds in water when exposed to IR. To reduce overall reagent volume a single domain PCR microdevice was fabricated with a 5 µL PCR chamber. The polymerase concentration in the PCR master was doubled to compensate for the increased surface area-to-volume ratio, which enhances the opportunity for polymerase to adhere to the surface. All other concentrations remained constant, including that of template DNA and the EA1. When the EA1 protease degrades blood, a fine precipitate is formed (see **Fig. 5**), and this was expected to cause a reduction in efficiency in such a small PCR chamber, due to preventing reagent mixing. Despite the cycling hold times remaining constant, total cycling time was reduced to 68 minutes from the three hour tube-based protocol, due to the improved heating and cooling ramp rates. The amplified product was removed from the device and analyzed by electrophoresis. The resulting electropherogram showed a TPOX amplicon at 63 bp, although smaller in peak height than the tube based assay, it was detectable above 15 RFU, representing approximately 2 ng of DNA. (data not shown). In an effort to further reduce reagent volume, and with a view to use the integrated device previously described (see **Chapter 4**), this experiment was repeated in a 2 µL chamber (**Fig. 8**). This resulted in the same peak intensity of 15 RFU for the TPOX amplicon that

observed in the 5 µL chamber, demonstrating that this chemistry was adaptable to the microfluidic format.

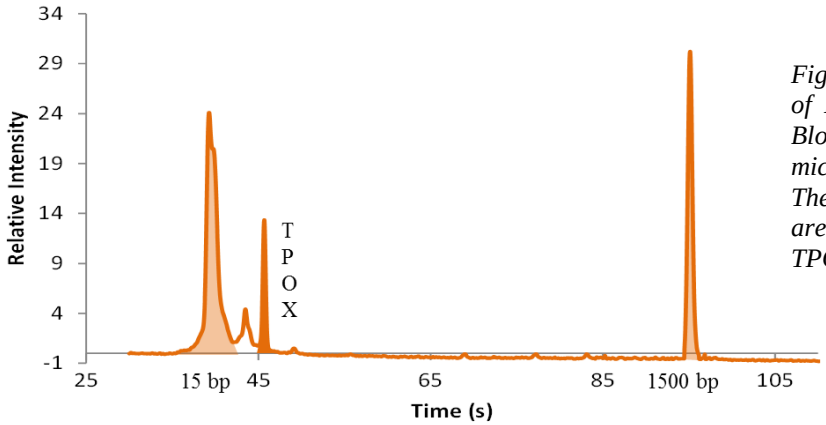

Figure 25: Electropherogram of PCR product from Direct Blood PCR, in 2 µL PMMA microdevice PCR chamber. The 15 and 1500 bp markers are shaded and the 63 bp TPOX amplicon is coloured.

5.3.6 Integrated microdevice amplification of whole blood and HIA detection

With the ultimate goal being creation of a rapid confirmatory test, the amplification had to be interfaced with a simple, inexpensive, rapid and accurate detection modality. Hybridization-induced aggregation, as discussed in **Chapters 2-4**, is a recently developed method that allows for the visual detection of specific target sequences, and is indicated by the aggregation of magnetic particles facilitated by a RMF. As described in **Chapter 3**, the HIA probes were designed to be complementary to one strand of DNA. Initial experiments were carried out using tube-based 63 bp TPOX PCR product from pre-purified hgDNA, to ensure the individual rotating magnetic fields described in **Chapter 4**, would enable HIA to differentiate between PCR product, with or without the target DNA. The same experiments was then repeated using PCR product following the direct PCR of whole blood. For both experimental data sets, images were taken of the microwells and the images were processed using Mathematica software to pixilate the images to determine the degree of aggregation. It was determined that the images were sufficiently different in

degree of aggregation that it was determined the small individual magnetic fields were a suitable driving force for particle aggregation (**Fig. 9**).

The integrated microdevice described at length in **Chapter 4**, was used for direct PCR from whole blood interfaced with HIA detection for the identification of human blood. Briefly, the device has three sample chambers enabling a simultaneous positive and negative control to be processed for comparison. The PCR chambers are 2 µL in volume and are connected to the HIA detection chamber by a 12.5 mm channel which has two burst valves to prevent unwanted fluid flow. Once PCR was completed a mechanical screw would be used to drive the PCR product into the HIA chamber for detection of the product in less than one minute.

It was seen that, by reducing the PCR chamber volume to 2 µL (an 80% volume reduction from tube based amplification) the PCR reaction time was further reduced to only 56 minutes, a 3-fold reduction compared to a block thermocycler. This was due to only to faster heating and cooling of the PCR reagents, afforded by the IR-PCR technology. For comparative purposes, liquid animal blood would have been the ideal template. However, such a sample could not be procured from collaborators, so UV-irradiated human blood was used as the negative control. With computer software, the aggregates were analyzed as described in **Chapters 2-4**. Aggregation in the negative control was at a level that was 50% that of the positive control, and this was then normalized to be '100% of the maximum aggregation'. The fully-integrated PCR-HIA method was able to distinguish between a

human blood sample and a blood sample containing no amplifiable DNA in less than an hour (**Fig. 9**).

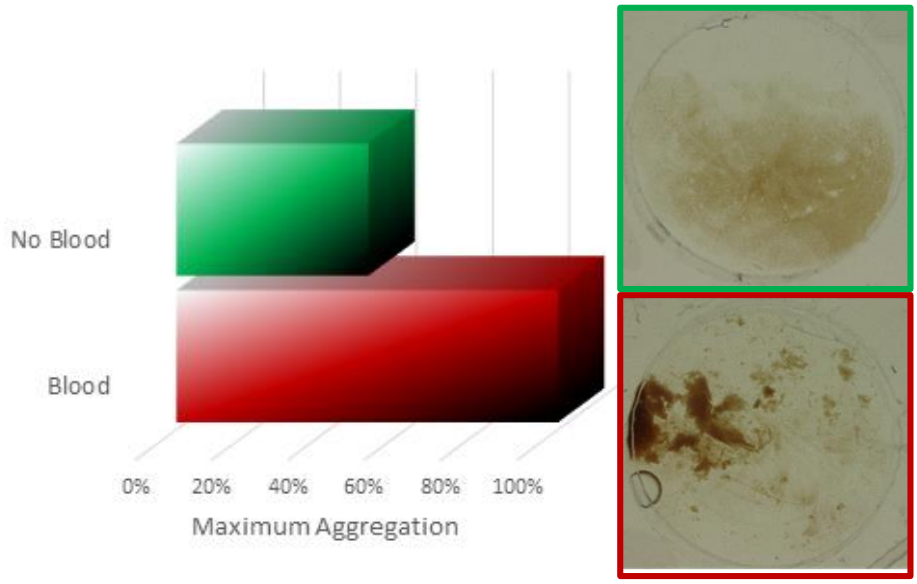

Figure 26: HIA results for the detection of a 63 bp TPOX PCR product on an integrated microfluidic device. Green: The HIA result when fully degraded human blood is added to the PCR reagents. Red: The result from amplification of human blood for the 63 bp TPOX product.

5.3.7 Integrated microdevice amplification of buccal swab sample with HIA detection

Forensic science uses three main biological fluids for investigative purposes; blood, semen and saliva. The latter is a common sample type, found on trace evidence such as cigarette butts and beverage containers. Furthermore, an oral swab is the preferred method for gathering baseline genetic information. It was, therefore, a ideal biological fluid to use in the direct PCR-HIA integrated device. An individual provided a saliva sample via the collection of cheek cells for 30 seconds with a foam swab. The buccal cells were eluted in 100 µL of deionized water. From this, 1 µL of elutate was added to the PCR reaction mix. As a biological sample, saliva is significantly less complex than whole blood, as fewer components are present to inhibit the polymerase from functioning. Therefore, we replaced the *Pwo* polymerase used in the whole blood experiments with a more processive *Taq*, *SpeedSTAR™*. Furthermore, the *PrepGEM™* blood buffer was substituted with the saliva buffer and the calcium omitted from the master mix in accordance with manufactures'

protocol. The chemical components of these buffers are proprietary. The negative control for this experiment was a simple no template control, i.e., no epithelial cells were added. With the same microfluidic device used above, and described in **Chapter 4**, this chemistry was applied to achieve successful integration of amplification and detection on a single device. The workflow is the same as above for direct blood: amplification, fluid actuation, then HIA detection with individual magnets. However, due to the use of *SpeedSTAR*™ polymerase, PCR hold times were reduced from 30,30,45 to 2,5,15 seconds for denaturing, annealing and extension respectively. This resulted in PCR being completed in just 35 minutes. Once the amplification, fluid movement and HIA was complete, the aggregates were analyzed using the Mathematica software. Normalizing the maximum aggregation so that the epithelial cells (cheek cells) containing samples' PCR product represent 100% aggregation, the negative control gave 38% aggregation (**Fig. 10**). Successful integration of PCR-HIA for the verification of both human blood and epithelial cells in less than an hour is an important first step towards a universal, accurate preliminary test for forensic science.

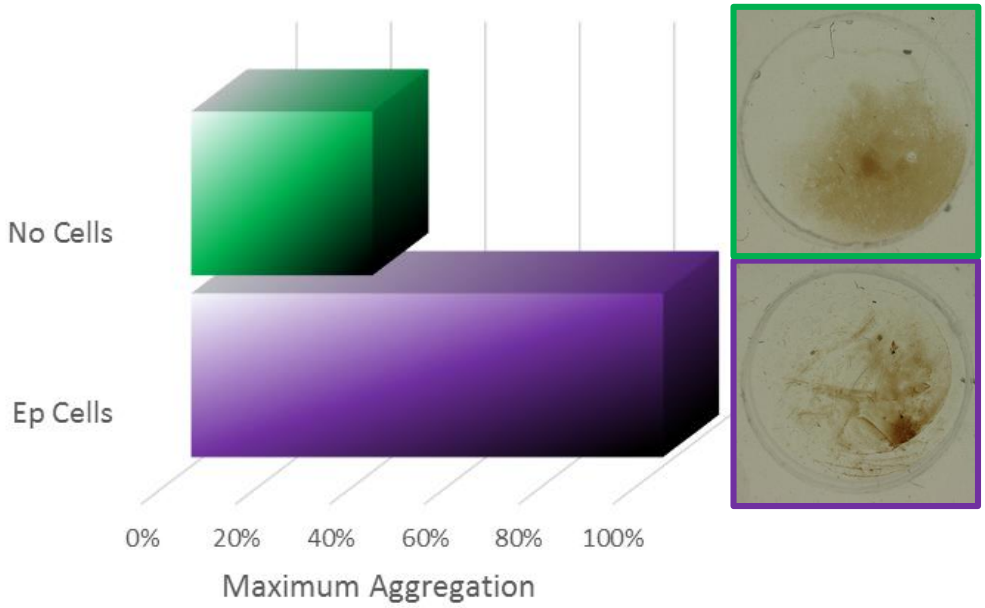

Figure 27: HIA results for the detection of a 63 bp TPOX PCR product on an integrated microfluidic device. Green: The HIA result when no template is added to the PCR reagents. Purple: The result from amplification of human epithelial cells for the 63 bp TPOX product.

5.4 Conclusions

The work presented in this chapter described a novel approach to a forensic confirmatory test for human blood through the amplification and detection of a 63 bp PCR product from the TPOX locus. A PCR protocol was developed using the proteinase EA1 with *Pwo* polymerase for the successful direct amplification of whole blood. This method is preferred to commercial products as non-specific amplification was observed with Phusion®. The versatility of the EA1 and *Pwo* method was demonstrated, with successful direct amplification from a blood stain on 4 common substrates: filter paper, cotton, cotton-polyester blend, and denim. Importantly, the specificity of the protocol was confirmed by analysis of animal blood from pig, rabbit, feline, canine, mouse and monkey, where, in each instance, no 63 bp TPOX PCR amplicon was observed. This direct PCR protocol was then adapted for microdevice amplification, with an 80% reduction in reaction volume to 2 µL as compared to tube-based assays. Further, reduction in volume and amplification through IR-PCR reduced amplification time by ~3-fold to only 56 minutes. This was performed on a multiplex microfluidic device allowing for amplification of positive and negative controls, along with the sample, in a single assay. Following PCR, the product was detected through HIA in only 30 seconds and confirmed through computer software analysis. The same protocol was used to directly amplify epithelial cells from a cheek swab. Since buccal cells have a less complex cellular matrix than whole blood, the cells could be amplified using a different polymerase, which afforded a further reduction in PCR hold times, shortening PCR to only 35 minutes. The fully integrated device, along with the developed assay for direct-PCR from blood, mark the first steps towards a true confirmatory test for serological fluids in forensic science. Future work with this chemistry

would apply to any field of biotechnology requiring amplification of whole blood, e.g., genetic testing.

5.5 References

1. Virkler, K. and I.K. Lednev, *Forensic Science International,* 2009. **188**(1–3): p. 1-17.
2. Fujii, K., et al., *Journal of Forensic Sciences,* 2013: p. n/a-n/a.
3. Hansen, W.J., C. Bruggeman, and P.G. Wolffs, *Pre-analytical Sample Treatment and DNA Extraction Protocols for the Detection of Bacterial Pathogens from Whole Blood,* in *PCR Detection of Microbial Pathogens*, M. Wilks, Editor 2013, Humana Press. p. 81-90.
4. Castelló, A., F. Francés, and F. Verdú, *Journal of Forensic Sciences,* 2012. **57**(2): p. 500-502.
5. de Almeida, J.P., N. Glesse, and C. Bonorino, *Forensic Science International,* 2011. **206**(1–3): p. 58-61.
6. Johnston, S., J. Newman, and R. Frappier, *Canadian Society of Forensic Science Journal,* 2003. **36**(3): p. 173-184.
7. Swander, C.J. and J. Stiles. *Evaluation of the ABAcard HemaTrace™ for the Forensic Identification of Human Blood*. in *Paper submitted to the Michigan Association of Forensic Science Annual Meeting, Michigan USA*. 1998.
8. Hurley, I.P., et al., *Forensic Science International,* 2009. **190**(1): p. 91-97.

9. Monroe, C., C. Grier, and B.M. Kemp, *Forensic Science International,* 2013. **228**(1–3): p. 142-153.

10. Zhang, Z., M.B. Kermekchiev, and W.M. Barnes, *The Journal of Molecular Diagnostics,* 2010. **12**(2): p. 152-161.

11. Kermekchiev, M.B., et al., *Nucleic acids research,* 2009. **37**(5): p. e40.

12. Abu Al-Soud, W. and P. Radstrom, *Appl Environ Microbiol,* 1998. **64**(10): p. 3748-53.

13. Al-Soud, W.A., L.J. Jönsson, and P. Rådström, *Journal of Clinical Microbiology,* 2000. **38**(1): p. 345-350.

14. Alaeddini, R., S.J. Walsh, and A. Abbas, *Forensic Science International: Genetics,* 2010. **4**(3): p. 148-157.

15. Mercier, B., et al., *Nucleic acids research,* 1990. **18**(19): p. 5908.

16. Werle, E., et al., *Nucleic acids research,* 1994. **22**(20): p. 4354.

17. Ivanova, N.V., A.V. Borisenko, and P.D. HEBERT, *Molecular Ecology Resources,* 2009. **9**(s1): p. 35-41.

18. Peeters, S., et al., *Biotechnology progress,* 2010. **26**(6): p. 1678-1684.

19. Verheij, S., J. Harteveld, and T. Sijen, *Forensic Science International: Genetics,* 2012. **6**(2): p. 167-175.

20. Chen, T., et al., *Journal of Forensic Sciences,* 2012. **57**(2): p. 472-477.

21. Manage, D.P., et al., *Microfluidics and nanofluidics,* 2011. **10**(3): p. 697-702.

22. Zeller, K.I., et al., *Genome Biol,* 2003. **4**(10): p. R69.

23. Horsman, K.M., et al., *Journal of Forensic Sciences,* 2006. **51**(4): p. 758-765.

24. Yi Sun, Y.C.K., Nam-Trung Nguyen, *Journal of Micromechanics and Microengineering*, 2006. **16**(8).

25. Leslie, D.C., et al., *Journal of the American Chemical Society*, 2012. **134**(12): p. 5689-5696.

26. Lounsbury, J.A., et al., *Forensic Science International: Genetics*, 2012. **6**(5): p. 607-615.

27. Oda, R., et al., *Analytical Chemistry*, 1998. **70**(20): p. 4361-4368.

6 Conclusions

6.1 Overarching conclusions

The goal of the hybridization-induced aggregation assay was to incorporate the simplistic, rapid pinwheel DNA technology to detect sequence-specific DNA. What is accomplished in this thesis goes far beyond this minimal expectation.

In **chapter two**, the HIA assay was conceptualized and then systematically optimized to enable a limit of detection of 100 fM for a 26-mer sequence of ssDNA. Optimized parameters included buffer chemistry (0.1 M KCl, 10 mM Tris, pH 7.5) and an assay duration of 12 minutes, facilitated by a rotating magnetic field and agitation from a vortexer. The aggregation process was demonstrated to be inert to non-complementary strands of DNA, as well as the cells and protein in whole blood. Further, specificity was demonstrated by introducing point mutations into the target sequence, which destabilized hybridization sufficiently to impact sensitivity to be detectable through aggregation response alone. In fact, the target DNA sequence can be tweaked in composition to alter the sensitivity in a number of ways. The addition of only five non-complementary flanking bases reduce sensitivity from fM to nM, while reducing the number of complementary bases reduces sensitivity further.

In **chapter three**, HIA was developed into an assay which can detect double-stranded DNA in a label-free manner, in only three minutes, enabling HIA to be used for real-world samples. The addition of a thermoelectric Peltier as a heating source, in intimate contact with the microwell, enabled the ability to tune the HIA detection system for a specific sequence, analogous to annealing temperatures for PCR. With these adjustments, HIA was demonstrated with a real-life target for the detection of multi-drug resistant tuberculosis

(MDR-TB). The aim to was to replace qPCR in the diagnosis testing, following amplification of a bacteriophage used to replicate only in viable TB bacteria infected cells. With a sample size of 175 (five antibiotics tested with samples from 35 patients), HIA and qPCR were compared to the gold standard of agar proportion. The HIA assay reuslts gave an 89% correlation while qPCR results gave a 95% correlation, demonstrating that HIA is comparable to qPCR.

Chapter four described taking the detection of dsDNA with HIA on a microdevice further, by defining the design and fabrication of not only an integrated device (IR-PCR and HIA), but a multiplexed device, capable of processing controls as well as sample. Akin to HIA, the device was created keeping simplicity, low cost and ease of use as the key driving forces behind design. The developed device used minimalist techniques for fluid control, including torque-actuated pressure for reproducible fluid movement and a unique capillary burst valve for the prevention of flow. The detection time using HIA was reduced even further to only 30 seconds, by creating individual discrete magnetic fields for each microwell, rather than one large magnetic field. The ubiquity of this microdevice for PCR and HIA detection is shown throughout this work, with detection of clinical TB samples in **chapter three**, an environmental virus, *Salmonella enterica* in **chapter four** and finally a 63 bp fragment of the TPOX locus for forensic investigations in **chapter five**.

In the final chapter, an assay was designed to allow for the direct PCR of whole blood on a microdevice, followed by HIA detection for a forensic application. The assay utilized a neutral proteinase and polymerase combination to create effective chemistry for the amplification of whole blood without any pretreatment. Furthermore, amplification of the 63 bp TPOX human target was successfully accomplished from whole blood on four

substrates: denim, cotton, cotton polyester and filter paper. The purpose was to create an assay to determine if a sample was from a human, thus, was demonstrated for specificity with six other mammals, including feline, canine and monkey. Lastly, this chemistry was successfully applied to the direct amplification from a buccal swab. Conformation of human origin was obtained for blood and buccal cells in 60 and 30 minutes respectively.

6.2 Future Directions

6.2.1 Increased throughput with multiplex IR-PCR-HIA microdevice

The device described in **chapter four** and used in **chapters three** and **five**, had three PCR chambers for sample amplification (with the fourth foir temperature control only). To maximize throughput, making an integrated assay more efficient, it would be wise to increase the number of samples processed simultaneously. A prototype device has been designed and fabricated with seven sample chambers but has yet to tested (**Fig. 1**). The design is based on the that described fully in **chapter four**. Significant alterations had to be made, including increasing the depth of the PCR channels from 0.5 mm to 1.0 mm, which also increase the HIA chamber size from 1.0 mm to 1.5 mm. This changes the

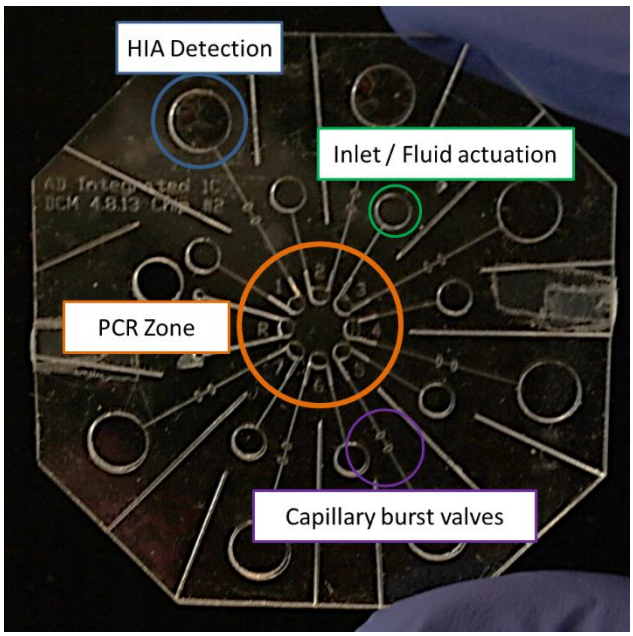

Figure 28: Photograph of a prototype 8-plex, seven sample multiplex IR-PCR HIA microdevice. Three layer device of 0.5, 1.0, 0.5 mm PMMA. PCR zone represents the 1 cm^2 focal spot of the halogen IR bulb. The fluid actuation (10.6 µL) and HIA (30 µL) detection wells are now 50% greater in volume than previously described.

volume required for the HIA assay, from 20 µL to 30 µL, reducing the concentrations of the reagents and target DNA in the assay. Furthermore, the fluid actuation cavity is also 50% greater in volume, now 10.6 µL, and effecting TAP dispensed volumes. Both elements (HIA and TAP) will need to be optimized for these changed dimensions to maintain sensitivity and accuracy.

Once optimized the device can be employed for the multiplex detection of either seven different targets or be used to run seven separate samples simultaneously. Such a device is not suitable to replace high-throughput technologies, such as the 96-well plate qPCR instruments. However, in low sample throughput labs, or in those with reduced monetary supplies, such a device is a useful technique for sample processing. Furthermore, such a device is portable, lightweight and can be deployed in the the field, enableing rapid on-site amplification and detection of DNA.

6.2.2 Apply HIA for detection of single nucleotide polymorphisms

In **chapter two**, it was demonstrated that HIA could successfully detect sequences with point mutations, therefore, this method could be applied to detecting single nucleotide polymorphisms (SNP's). There are two million known SNP's in the human genome[1], many of which are attributed to the causation of disease and phenotyping individual characteristic, e.g. height and hair colour. This open avenues for HIA detection to be applied both diagnostically and in forensic science.

6.2.2.1 Diagnostics

Genetic research accounts for over $7 billon of the annual NIH budget, with $250 million specifically spent on genetic testing (NIH 2013, RCDC report). With genetic sequences no longer patentable[2] any reported mutation can be applied to any suitable detection technique. Therefore, the avenues for applying HIA as the detection modality for these genetic tests are vast, as the system can be honed for a pertinent specific DNA sequence. However, there are limitations; HIA would only be suitable for SNPs that are conserved in the same position for each individual, known as single-gene disorders. Work has already begun in our laboratory applying this methodology to the detection of Kirsten rat sarcoma (KRAS), a cancer biomarker with point mutations found most commonly in codons 12 and 13 of the KRAS gene. Other suitable targets are cystic fibrosis[3], polycystic kidney disease[4] and Huntington's disease[5].

6.2.2.2 Forensics

Chapter 5 described a preliminary method for on-site detection of human DNA, by direct PCR from whole blood, interfaced with HIA on a single microdevice. With the seven-sample microdevice described above, this test can be expanded to not only confirm the DNA is human, but further, gender, eye colour, height and ethnic origin of the individual [6]. Such a multiplexed assay is possible due to the increasing research performed by those in the forensic community to develop multiplex assays to identify SNP's which can parse out such information. Our laboratory collaborates with Dr. Podini, a pioneer in forensic science SNP testing for population somatic traits and is developing a multiplex SNP detection assay[6, 7]. By leveraging the primer sequences his work has developed to create HIA probes, detection of the SNPs can be simplified and dramatically decrease the

processing time six-fold. The HIA method workflow would involve direct PCR from blood, followed by HIA detection. Currently, the workflow includes extraction, amplification, PCR clean-up, single-base extension, and then the results are assessed via fluorescence detection using a CE genetic analyzer. Overall, under ideal conditions, this require take six hours. Providing genotyping knowledge of a suspect (gender, height, eye colour and ethnic origin) to criminal investigators in this hour time-frame, can aid in focusing their resources to arrest the perpetrator earlier and more efficiently.

6.3 Concluding remarks

Hybridization-induced aggregation has been demonstrated to be a highly sensitive and selective assay for sequence-specific DNA detection. This bead-based assay rivals gold nanoparticle hybridization-driven detection with femtomolar detection limits and specificity for SNP detection. However, HIA is more economical. Facilitated by a rotating magnetic field and a vortexer, DNA detection can occur in seconds, requiring nothing other than eyesight for conformation. The applications of this technology are limited only by the scientist's perspective; in this work environmental, clinical and forensic applications were demonstrated.

6.4 References

1. Sachidanandam, R., et al., *Nature,* 2001. **409**(6822): p. 928-933.

2. Kuehn, B.M., *JAMA,* 2013. **310**(4): p. 357-359.

3. Riordan, J.R., et al., *Science,* 1989. **245**(4922): p. 1066-1073.

4. Mochizuki, T., et al., *Science*, 1996. **272**(5266): p. 1339-1342.

5. Lione, L.A., et al., *The Journal of neuroscience*, 1999. **19**(23): p. 10428-10437.

6. Podini, D. and P.M. Vallone, *SNP genotyping using multiplex single base primer extension assays*, in *Single Nucleotide Polymorphisms*2009, Springer. p. 379-391.

7. Budowle, B. and A. van Daal, *Biotechniques*, 2008. **44**(5): p. 603-8.